

2012

Evaluation of Effects of Fire on the I-465 Mainline Bridges—Volume I

Robert J. Connor

Purdue University, rconnor@purdue.edu

Amit H. Varma

Purdue University, ahvarma@purdue.edu

Sorin Marcu

Purdue University

Ryan J. Sherman

Purdue University, rjsherma@purdue.edu

Recommended Citation

Connor, R. J., A. H. Varma, S. Marcu, and R. J. Sherman. *Evaluation of Effects of Fire on the I-465 Mainline Bridges—Volume I*. Publication FHWA/IN/JTRP-2012/12. Joint Transportation Research Program, Indiana Department of Transportation and Purdue University, West Lafayette, Indiana, 2012. doi: 10.5703/1288284314975.

JOINT TRANSPORTATION RESEARCH PROGRAM

INDIANA DEPARTMENT OF TRANSPORTATION
AND PURDUE UNIVERSITY



EVALUATION OF EFFECTS OF FIRE ON THE I-465 MAINLINE BRIDGES—VOLUME I

Robert J. Connor

Associate Professor of Civil Engineering
School of Civil Engineering
Purdue University
Corresponding Author

Amit H. Varma

Associate Professor of Civil Engineering
School of Civil Engineering
Purdue University
Corresponding Author

Sorin Marcu

Graduate Research Assistant
School of Civil Engineering
Purdue University

Ryan J. Sherman

Graduate Research Assistant
School of Civil Engineering
Purdue University

SPR-3474

Report Number: FHWA/IN/JTRP-2012/12

DOI: 10.5703/1288284314975

RECOMMENDED CITATION

Connor, R. J., Varma, A. H., Marcu, S., and Sherman, R. J. *Evaluation of Effects of Fire on the I-465 Mainline Bridges—Volume I*. Publication FHWA/IN/JTRP-2012/12. Joint Transportation Research Program, Indiana Department of Transportation and Purdue University, West Lafayette, Indiana, 2012. doi: 10.5703/1288284314975.

CORRESPONDING AUTHORS

Associate Professor Amit H. Varma
School of Civil Engineering
Purdue University
(765) 496-3419
ahvarma@purdue.edu

Associate Professor Robert J. Connor
School of Civil Engineering
Purdue University
(765) 496-8272
rconnor@purdue.edu

JOINT TRANSPORTATION RESEARCH PROGRAM

The Joint Transportation Research Program serves as a vehicle for INDOT collaboration with higher education institutions and industry in Indiana to facilitate innovation that results in continuous improvement in the planning, design, construction, operation, management and economic efficiency of the Indiana transportation infrastructure.

https://engineering.purdue.edu/JTRP/index_html

Published reports of the Joint Transportation Research Program are available at: <http://docs.lib.purdue.edu/jtrp/>

NOTICE

The contents of this report reflect the views of the authors, who are responsible for the facts and the accuracy of the data presented herein. The contents do not necessarily reflect the official views and policies of the Indiana Department of Transportation or the Federal Highway Administration. The report does not constitute a standard, specification or regulation.

1. Report No. FHWA/IN/JTRP-2012/12		2. Government Accession No.		3. Recipient's Catalog No.	
4. Title and Subtitle Evaluation of Effects of Fire on the I-465 Mainline Bridges—Volume I				5. Report Date June 2012	
				6. Performing Organization Code	
7. Author(s) Robert J. Connor, Amit H. Varma, Sorin Marcu, Ryan J. Sherman				8. Performing Organization Report No. FHWA/IN/JTRP-2012/12	
9. Performing Organization Name and Address Joint Transportation Research Program Purdue University 550 Stadium Mall Drive West Lafayette, IN 47907-2051				10. Work Unit No.	
				11. Contract or Grant No. SPR-3474	
12. Sponsoring Agency Name and Address Indiana Department of Transportation State Office Building 100 North Senate Avenue Indianapolis, IN 46204				13. Type of Report and Period Covered Final Report	
				14. Sponsoring Agency Code	
15. Supplementary Notes Prepared in cooperation with the Indiana Department of Transportation and Federal Highway Administration.					
16. Abstract On October 22, 2009, in Indianapolis, Indiana, a semi tanker carrying liquefied propane lost control on the underpass from I-69 southbound to I-465 eastbound, crashing beneath the east and westbound bridges carrying mainline I-465 traffic. The tanker rolled, causing the tractor to catch fire and the propane tanker to explode. There were concerns the steel superstructure and the high-strength (HS) bolts used in the beam splices were affected by the fire. Also, since the bridge deck was built composite with the steel superstructure, there were concerns the composite action might have been lost or diminished causing the bridge to not behave as it was originally designed. Therefore, the study was focused on identifying any short-term or long-term effects the bridge may have sustained due to the fire exposure. To address the short-term effects, immediately after the accident, several core samples and HS bolts were removed and sent to independent testing laboratories. To establish any long-term effects, field testing was performed over a period of approximately four (4) months. Weldable resistance strain gages were installed at key locations to understand the behavior of the bridge under load and to develop the stress-range histograms. Both controlled load tests, using test trucks of known weight and geometry, and long-term monitoring of random traffic were performed as part of the study. The results presented in this report show the following: <ul style="list-style-type: none"> • The explosion and subsequent fire did not negatively impact the properties of the steel in the main girders, nor the properties of the HS bolts. • The explosion and subsequent fire did not negatively impact the overall load distribution nor adversely alter the behavior of the bridge. • Controlled load testing and long-term monitoring confirmed the steel girders are acting compositely with the concrete deck. • Based on the results of the long-term monitoring, infinite fatigue life is expected at all the monitored locations. 					
17. Key Words fire, bridge, steel, composite action, girder, controlled load tests, fatigue, behavior			18. Distribution Statement No restrictions. This document is available to the public through the National Technical Information Service, Springfield, VA 22161.		
19. Security Classif. (of this report) Unclassified		20. Security Classif. (of this page) Unclassified		21. No. of Pages 93	22. Price

EXECUTIVE SUMMARY

EVALUATION OF EFFECTS OF FIRE ON THE I-465 MAINLINE BRIDGES—VOLUME I

On October 22, 2009, in Indianapolis, Indiana, a semi tanker carrying liquefied propane lost control on the underpass from I-69 southbound to I-465 eastbound, crashing beneath the eastbound and westbound bridges carrying mainline I-465 traffic. The semi rolled, causing the tractor to catch fire and the propane tanker to explode. As a result of the fire, the steel superstructure was subjected to extreme temperatures; however, the duration of exposure and magnitude of these temperatures was not accurately established. Thus, testing was performed to identify and document any short-term or long-term effects that the fire may have had on the steel superstructure. Three primary tasks were performed as part of the study:

1. Quantify the effects of the fire on the properties of the structural steel.
2. Quantify the effects of the fire on the properties of the high strength (HS) bolts.
3. Quantify the effects of the fire on the overall behavior of the bridge.

Immediately after the accident, samples of the structural steel and HS bolts were removed and sent to independent testing laboratories. These results were used to establish any short-term effects the fire had on the structure. To capture any long-term effects, field testing was performed for a period of approximately four months. Weldable resistance strain gages were placed at key locations in an attempt to understand both the response of the bridge to load and to develop the stress-range histograms at critical details. Both controlled load tests, using test trucks of known weight and geometry, and long-term monitoring of random traffic were performed as part of the study.

The remaining fatigue life of the instrumented details was estimated using stress-range histograms from the long-term monitoring data. Since all the stress ranges measured were below the CAFL (constant amplitude fatigue limit) for all monitored details, infinite fatigue life is expected at all of the monitored locations.

CONTENTS

1. INTRODUCTION	1
1.1 Bridge Description	1
1.2. Objective	1
2. SAMPLES TAKEN FOR LABORATORY TESTING	2
2.1 Hardness Tests	2
2.2 Charpy V-Notch Impact Tests (CVN)	2
2.3 Bolt Tests	4
3. INSTRUMENTATION PLAN AND DATA AQUISITION	8
3.1 Strain Gages	8
3.2 Data Acquisition System	9
3.3 Remote Long-term Monitoring	10
4. CONTROLLED LOAD TESTING	10
4.1 Test Trucks	10
4.2 Testing	10
5. RESULTS OF CONTROLLED LOAD TESTING	12
5.1 Single Truck Tests in the Left Lane	12
5.2 Single Truck Tests in the Middle Lane	16
5.3 Single Truck Tests in the Right Lane	18
5.4 Trucks Side-by-Side in the Left and Middle Lanes	20
5.5 Trucks Side-by-Side in the Middle and Right Lanes	22
5.6 Under Bridge Snooper Crawl Test in the Left Lane (SNOOP.DAT)	25
5.7 Composite Action Summary	27
5.8 Load Distribution Summary	27
5.9 Response of Channels near Core Hole Locations	39
5.10 Controlled Load Testing – Summary	39
6. LONG-TERM MONITORING	39
6.1 Triggered Time-History Data	41
6.2 Stress-Range Histograms	41
7. SUMMARY AND CONCLUSION	45
REFERENCES	46
APPENDIX A. Instrumentation Plans	47
APPENDIX B. Development of Stress-Range Histograms Used to Calculate Fatigue Damage	47
APPENDIX C. Report Letters	47
APPENDIX D. Maximum Stress Ranges Figures – Triggered Data Files	47

LIST OF TABLES

Table	Page
Table 2.1 Hardness Test Data and Estimates of Ultimate Strength	3
Table 2.2 CVN Data for the Web Core Samples	4
Table 2.3 CVN Data for the Cover Plate Core Samples	5
Table 2.4 Bolts – Proof Load and Wedge Tension Test Results	7
Table 2.5 Bolts – Hardness Test Results	7
Table 2.6 Nuts – Hardness Test Results	7
Table 3.1 Trigger Channels	10
Table 4.1 Summary of the Controlled Load Tests	12
Table 5.1 Maximum Stresses – Single Truck Tests in the Left Lane	15
Table 5.2 Maximum Stresses – Single Truck Tests in the Middle Lane	19
Table 5.3 Maximum Stresses – Single Truck Tests in the Right Lane	23
Table 5.4 Comparison of Maximum Stresses – CRL_1.DAT and CRL_3.DAT	25
Table 5.5 Maximum Stresses – Trucks Side by Side Tests in the Left and Middle Lanes	27
Table 5.6 Maximum Stresses – Single Truck Tests in the Left Lane	27
Table 5.7 Comparison of Maximum Stresses – CRL_2.DAT and CRL_5.DAT	28
Table 5.8 Maximum Stresses – Trucks Side-by-Side in the Middle and Right Lanes	30
Table 5.9 Comparison of Maximum Stresses – PARK_2C.DAT and PARK_5.DAT	30
Table 5.10 Stresses Recorded in Crawl Tests – SNOOP.DAT and CRL_1.DAT	31
Table 5.11 Neutral Axis Positions	32
Table 5.12 Response of Strain Gages Installed at Midspan (2 nd Span) – <i>Static Tests</i> : Single Truck	32
Table 5.13 Response of Strain Gages installed at Midspan (2 nd Span) – <i>Static Tests</i> : Trucks Side-by-Side	32
Table 5.14 Stresses Measured during the Static Controlled Load Tests and Section Properties of the Composite Section	35
Table 5.15 Moments Determined from the Stresses Measured during the Static Controlled Load Tests	36
Table 5.16 Superposition of Loads Summary – Controlled Load Static Tests	38
Table 5.17 Response of CH_16, CH_17 and CH_18 during the Controlled Load Tests	39
Table 5.18 Stresses in all Channels during the Single Truck and Side-by-Side Trucks Crawl Tests	40
Table 6.1 Summary of the Channels Included in the Long-Term Monitoring	41
Table 6.2 Trigger Channels and the Corresponding Trigger Stress Levels	41
Table 6.3 Maximum Stress Ranges Determined from Triggered Data Files	43
Table 6.4 Stress-Range Histograms for CH_2, CH_4, CH_6, CH_8, CH_10, CH_12 and CH_14 from 01/15/2010 to 05/04/2010	44
Table 6.5 Summary of Fatigue Life Calculations for CH_2, CH_4, CH_6, CH_8, CH_10, CH_12 and CH_14	44
Table 6.6 Stress-Range Histograms for CH_15, CH_16, CH_17 and CH_18	45
Table 6.7 Summary of Fatigue Life Calculations for CH_15, CH_16, CH_17 and CH_18	45

LIST OF FIGURES

Figure	Page
Figure 1.1 View of east and westbound bridges over the south ramp from I-69	1
Figure 1.2 Bearing that fell out during the crash (Beam #12; Bent #3) – Eastbound Bridge	1
Figure 2.1 Cores removed from the web and bottom cover plate (Beam #11) – Westbound Bridge	2
Figure 2.2 CVN specimen obtained from the web core sample	4
Figure 2.3 CVN specimen obtained from the cover plate core sample	5
Figure 2.4 Bolts and nuts removed from Splice #2 – Beams #14 & #15 – Eastbound Bridge	5
Figure 2.5 Bolts and nuts removed from Splice #1 – Beam #12 – Eastbound Bridge	6
Figure 2.6 Bolts and nuts removed from Splice #1 – Beam #11 – Westbound Bridge	6
Figure 2.7 Wedge tension test details	7
Figure 3.1 General view of strain gage locations	8
Figure 3.2 Weldable strain gage	8
Figure 3.3 Strain gage in final installed condition	9
Figure 3.4 Data acquisition system	9
Figure 3.5 Weather-tight enclosure containing data acquisition system	9
Figure 4.1 Test truck #63480 used in the control load testing	10
Figure 4.2 Geometry and tire load data for test truck #63480	11
Figure 4.3 Geometry and tire load data for test truck #63701	11
Figure 5.1 Response of strain gages installed at midspan (2 nd span) – <i>Crawl test</i> : single truck in the left lane	13
Figure 5.2 Response of strain gages installed at midspan (2 nd Span) as the test truck passes over the 2 nd span	14
Figure 5.3 Response of strain gages installed at midspan (2 nd Span) – <i>Static test</i> : single truck in the left lane	15
Figure 5.4 Strain variation in composite beams	16
Figure 5.5 Neutral axis of the composite section – AASHTO 2010	16
Figure 5.6 Neutral axis of the composite section – from stresses recorded in PARK_1.DAT	17
Figure 5.7 Response of strain gages installed at midspan (2 nd Span) – <i>Crawl test</i> : single truck in the middle lane	18
Figure 5.8 Response of strain gages installed at midspan (2 nd Span) – <i>Static test</i> : single truck in the middle lane	19
Figure 5.9 Response of CH_11 indicates semis passing in the right lane during the single truck static test in the middle lane	20
Figure 5.10 Neutral axis of the composite section – from stresses recorded in PARK_2C.DAT	21
Figure 5.11 Response of strain gages installed at midspan (2 nd Span) – <i>Crawl test</i> : single truck in the right lane	22
Figure 5.12 Response of strain gages installed at midspan (2 nd Span) – <i>Static test</i> : single truck in the right lane	23
Figure 5.13 Neutral axis of the composite section – from stresses recorded in PARK_4.DAT	24
Figure 5.14 Response of strain gages installed at midspan (2 nd Span) – <i>Crawl test</i> : trucks side-by-side in the left and middle lanes	25
Figure 5.15 Response of strain gages installed at midspan (2 nd Span) – <i>Static test</i> : trucks side-by-side in the left and middle lanes	26
Figure 5.16 Neutral axis of the composite section – from stresses recorded in PARK_3.DAT	27
Figure 5.17 Response of strain gages installed at midspan (2 nd Span) – <i>Crawl test</i> : trucks side-by-side in the middle and right lanes	28
Figure 5.18 Response of strain gages installed at midspan (2 nd Span) – <i>Static test</i> : trucks side-by-side in the middle and right lanes	29
Figure 5.19 Neutral axis of the composite section – from stresses recorded in PARK_5.DAT	30
Figure 5.20 Response of strain gages installed at midspan (2 nd Span) – <i>Crawl test</i> : under bridge snoopers in the left lane	31
Figure 5.21 Sketch for determination of the longitudinal stiffness parameter K_g	33
Figure 5.22 Distribution load factor – exterior longitudinal beam – Lever Rule	33

Figure 5.23 Section properties – composite section (interior beam case)	35
Figure 5.24 Section properties – composite section (exterior beam case)	36
Figure 5.25 Moments determined from stresses recorded during single truck static tests	36
Figure 5.26 Load distribution between girders – single truck static tests	37
Figure 5.27 Moments determined from stresses recorded during side-by-side trucks static tests	38
Figure 5.28 Load distribution between girders – trucks side-by-side static tests	38
Figure 5.29 Response of CH_16, CH_17 and CH_18 – Crawl test: trucks side-by-side in left and middle lanes	40
Figure 6.1 Typical trigger event: Two semi tractor trailers side-by-side in the middle and right lanes	42
Figure 6.2 Typical trigger event: Semi tractor trailer in the middle lane	42
Figure 6.3 Maximum stress range recorded in CH_2 from triggered data	43
Appendix D Figures	
Figure D.1 Maximum stress range recorded in CH_4 from triggered data	
Figure D.2 Maximum stress range recorded in CH_6 from triggered data	
Figure D.3 Maximum stress range recorded in CH_8 from triggered data	
Figure D.4 Maximum stress range recorded in CH_10 from triggered data	
Figure D.5 Maximum stress range recorded in CH_12 from triggered data	
Figure D.6 Maximum stress range recorded in CH_14 from triggered data	
Figure D.7 Maximum stress range recorded in CH_16 from triggered data	
Figure D.8 Maximum stress range recorded in CH_17 & CH_18 from triggered data	

1. INTRODUCTION

1.1 Bridge Description

Built in 1968, Bridge I-465-125-2377 JBSB (eastbound) and Bridge I-465-125-2377 BNBL (westbound) are located in the northeast corner of Indianapolis, IN. Both bridges are four span continuous composite steel girder structures which carry mainline I-465 over the ramp from I-69 southbound to I-465 eastbound. The steel girders are rolled shapes and utilize welded cover plates as needed. Bridge I-465-125-2377 JBSB (eastbound) carries three lanes of mainline I-465 traffic as well as an exit lane. In total, the eastbound bridge is 199'-0" long made up two 44'-0" end spans and two 55'-6" middle spans. Due to the exit lane, the width varies from 70'-0" to 78'-0" west to east. Bridge I-465-125-2377 BNBL (westbound) is similar, but not identical, as it carries three lanes of mainline I-465 and no exit lane. The westbound structure is 210'-0" long made up of two 44'-0" end spans and two 61'-0" middle spans and has a constant width of 67'-5". In 1992 the decks of both bridges were substantially reconstructed. The westbound bridge had a 24'-2" widening obtaining the constant width of 67'-5". This widening resulted in a width of 24'-0" for the right lane. The wider right lane accommodates the traffic merging onto I-465 westbound from the Binford Blvd./I-69 on-ramp. Figure 1.1 shows an aerial view of both east and westbound bridges over the south ramp from Interstate 69.

1.2. Objective

On October 22, 2009 a tanker truck carrying liquefied propane lost control and crashed beneath both I-465 bridges. The propane tanker was punctured during the crash, resulting in an explosion and fire. As a result of the fire, the steel superstructure was subjected to extreme temperatures; however, the duration of exposure and magnitude of these temperatures was not accurately established. Hence, the amount and extent of damage, if any, was unknown. To identify and document any short-term and long-term negative effects the fire may have had on the bridge a study was undertaken with the following three tasks described.



Figure 1.1 View of east and westbound bridges over the south ramp from I-69 (Microsoft 2010).

Effects of Fire on Properties of Structural Steel

If steel is exposed to temperatures exceeding approximately 1,100°F (600°C) for extended periods, or if the steel is sprayed with cold water by firefighters while at elevated temperatures the potential exists to alter the metallurgy of the steel. In the absence of any visual damage such as the distortion of the steel, the most common concerns are: (1) decreases in toughness of the steel; and (2) increases in the strength of steel due to uncontrolled quenching. Neither of which would be desirable.

Effects of Fire on Properties of High Strength Bolts

High strength (HS) bolts are also susceptible to damage if exposed to temperatures of about 750°F (450°C) for extended periods. The bolts used in the I-465 bridges are high strength ASTM A325 bolts. Since A325 bolts obtain their increased strength through a heat treatment process, they are generally more susceptible to fire than other constructional steels.

Effects of Fire on the Overall Behavior of the Bridge

If large differences in thermal strains developed between the steel and concrete, the composite action may be reduced or compromised. Should composite action be lost or reduced, then the load distribution among the girders will not be as originally designed. In addition, the live load stresses would also increase.

It is also noted that due to the damage to the west pier on the eastbound structure (Bent #3), the bearing of the exterior girder (Beam #12) on the north side of the bridge fell out (see Figure 1.2). As a result, the span length of this girder was significantly increased. Although the bearing was replaced when the pier was repaired, the amount of dead load that was put back into the exterior girder is unknown. Thus, the proportion of live load carried by this girder may not be as



Figure 1.2 Bearing that fell out during the crash (Beam #12; Bent #3) – Eastbound Bridge.

originally assumed in design if the repaired bearing is not operating as originally built.

Cores were taken from several girders in regions of high stress range in order to obtain steel samples for CVN specimens. At these regions, the condition at the cored hole could be classified as an AASHTO Category D fatigue detail (CAFL = 7.0 ksi). Since the original fatigue detail category at these locations was most likely Category B (CAFL = 16.0 ksi), the fatigue resistance of the detail has been significantly reduced. However, this reduction in fatigue category may not be significant if the actual in-service live load stress ranges are low. In the absence of field measured stress ranges, the effect of the cored holes on the fatigue performance of the bridge is unknown.

Samples of the structural steel and HS bolts were removed from the bridge and sent to independent testing facilities shortly after the crash. All field instrumentation and monitoring was conducted over the period between December 2009 and May 2010 by the Research Team from the Bowen Laboratory at Purdue University, West Lafayette, IN.

2. SAMPLES TAKEN FOR LABORATORY TESTING

Immediately following the fire, steel samples were removed from both bridges for metallurgical investigation to determine if the extreme temperature exposure had any negative effects on the steel properties. Steel samples were cored from the web and cover plate of the girders to create Charpy V-Notch (CVN) impact specimens and perform hardness testing. Figure 2.1 is a photograph of cores removed from Beam #11 (Westbound Bridge). Additionally, bolts were removed from the web and flange splices at selected locations for specific tests: proof load, wedge tension and hardness. These tests were used to determine if the material properties of the fasteners were degraded due to uncontrolled heating and cooling, such as may have

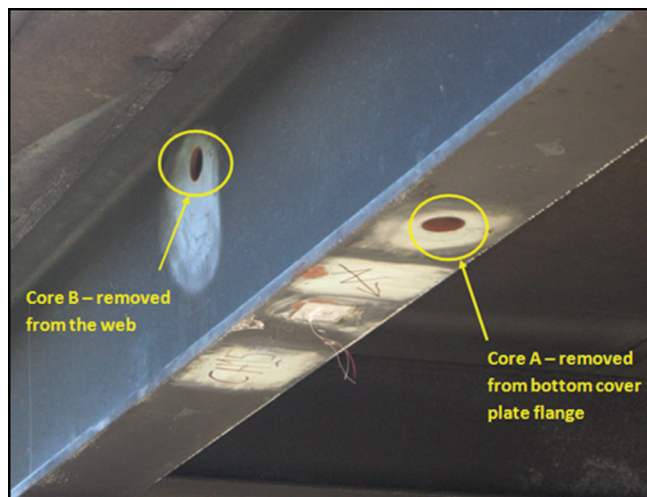


Figure 2.1 Cores removed from the web and bottom cover plate (Beam #11) – Westbound Bridge.

occurred during the fire. All metallurgical testing occurred in the days immediately following the accident.

2.1 Hardness Tests

2.1.1 Hardness Test Background

A total of fourteen (14) cores were removed from the girders of both bridges: seven (7) from the web and seven (7) from the bottom cover plate. Six (6) of the fourteen (14) cores removed were taken from an area of the westbound bridge least exposed to the explosion and fire: three (3) from the web and three (3) from the bottom flange cover plate. These six (6) specimens were used as control samples for the CVN and hardness tests. The remaining eight (8) specimens were taken from both bridges from exposed areas to explosion and fire. Drawings located in Appendix A specify the exact locations for all cores removed.

2.1.2 Hardness Test Results

The original design drawings indicated the steel girders were made from ASTM A36 steel. Based on the current ASTM specifications the ultimate strength (F_u) of A36 steel is permitted to be between 58 ksi and 80 ksi. To establish if the fire had any impact on the ultimate strength (F_u) of the steel, hardness tests were performed to verify that the material still fell within acceptable limits. Testing was done using an Instron automated testing machine and Rockwell Hardness Scale 'B' (HRB). From the hardness data, estimates of the ultimate strength (F_u) of the steel were made according to ASTM A370. Hardness test results along with the estimated ultimate strength (F_u) values are summarized in Table 2.1.

2.1.3 Hardness Test Conclusions

The hardness test data along with the estimates of ultimate strength were submitted to INDOT in a report letter dated October 30, 2009 (see Appendix C). As discussed in that report, two primary observations were made from the hardness data presented:

1. The estimated ultimate strength (F_u) of the steel is well within the limits of the ASTM specification.
2. There is no statistical difference between the control data set and the data obtained from samples that were exposed to fire.

Based on these results from the hardness testing, it is the opinion of the Purdue Research Team that the fire did not have any effect on the ultimate strength (F_u) of the structural steel in the bridge.

2.2 Charpy V-Notch Impact Tests (CVN)

2.2.1 Core Removal and Background Information

The same steel cores removed by INDOT from locations in the web and bottom cover plate on the east

TABLE 2.1
Hardness Test Data and Estimates of Ultimate Strength

SPECIMEN TYPE	AS MARKED	LAB ID	WEB OR CP*	EB OR WB BRIDGE/SPAN	ROCKWELL B (HRB)				ESTIMATED F _U (KSI)
					TEST 1	TEST 2	TEST 3	AVG	
CONTROL	1	AA	WEB	WB/D	67.5	66.5	70.0	68.0	59.0
	2	BB	CP	WB/D	65.5	66.5	72.7	68.2	59.0
	3	CC	WEB	WB/D	66.7	71.5	75.0	71.1	62.0
	4	DD	CP	WB/D	X	70.5	71.5	71.0	62.0
	5	EE	WEB	WB/D	X	70.7	73.5	72.1	63.0
	6	FF	CP	WB/D	74.5	84.5	80.5	79.8	72.0
					AVG CONTROL DATA			71.7	63.0
EXPOSED TO FIRE	A	A	CP	WB/B	73.5	68.5	76.5	72.8	64.0
	B	B	WEB	WB/B	X	65.0	68.5	66.8	58.0
	C	C	CP	EB/B	78.5	75.0	80.0	77.8	69.0
	D	D	CP	EB/B	80.0	80.0	79.5	79.8	72.0
	E	E	WEB	EB/B	X	66.5	70.0	68.3	59.0
	F	F	WEB	EB/B	71.5	73.0	69.0	71.2	62.0
	G	G	CP	EB/B	75.5	78.5	80.0	78.0	69.0
	H	H	WEB	EB/B	70.0	71.5	74.0	71.8	63.0
					AVG EXPOSED DATA			73.3	64.0

X – Denotes invalid data; CP – cover plate.

and westbound bridges for the hardness tests were used to make CVN specimens. Specimen preparation and testing was performed by Steel Dynamics on October 23, 2009 at no cost to INDOT or the project. Also, Mr. Scott Newbolds with INDOT witnessed the CVN specimen preparation and testing. Test results were then submitted to the Purdue Research Team for review and interpretation.

Prior to discussing any results it is important to mention a few things about the CVN requirements from the period these bridges were built. Since these bridges were built in late 1960's, the AASHTO Bridge Design Specifications and INDOT Bridge Design Manual did not specify any minimum CVN requirements. Thus, it would not necessarily be appropriate to compare these bridge steels to the modern specifications and requirements. The current AASHTO Bridge Design Specification requires 15 ft-lbs @ 40F for specimens oriented in the longitudinal direction (i.e., Zone II, Non-fracture critical).

One other important thing to note is that it is well known in the steel community that the mechanical properties (CVN, yield strength, etc.) of steel plates and rolled beams vary with the rolling direction. Data obtained from specimens in the *longitudinal direction* (*direction of rolling and, in this case, the direction of traffic*) will be higher than those obtained in the *transverse direction* from the same plates or beam. Hence, data obtained from specimens in the transverse direction will be conservative, estimating the lower bound of the actual material properties, including CVN.

2.2.2 Core Test Results: Web Cores

The CVN specimens obtained from the web core samples were oriented in the *longitudinal direction*.

Thus, the notch was oriented transverse to the longitudinal axis of the beam and parallel with the surface of the web. Figure 2.2 is a diagram showing the orientation of the web core samples.

A total of seven (7) web samples were tested. Four (4) samples were from regions exposed to fire and three (3) samples were from a region of the bridge nominally protected from the fire near the embankment. All measured data were well above modern AASHTO requirements for Zone II non-fracture critical applications as specified in ASTM A709. As stated above, the modern specification requires 15 ft-lbs @ 40F. For comparison, the *lowest* value measured from the samples removed was 94 ft-lbs. The data obtained are summarized in Table 2.2.

2.2.3 Core Test Results: Bottom Flange Cover Plate Cores

The CVN specimens obtained from the cores removed from the bottom flange cover plate were oriented in the transverse direction; thus, the notch was oriented parallel to the longitudinal axis of the beam. Normally, the specimens would have been oriented longitudinally, as required by the AASHTO Specifications. However, in the hours immediately following the fire and in the urgency to obtain data, the samples were mislabeled and the CVN specimens oriented transversely. As previously stated, these data provide a conservative lower-bound estimate of the longitudinal mechanical properties. Figure 2.3 is a diagram showing the orientation of the bottom flange cover plate core samples.

Like the web, seven (7) cover plate samples were tested: four (4) from the region exposed to fire and three (3) from the region nominally protected from the fire. The data obtained are tabulated in Table 2.3.

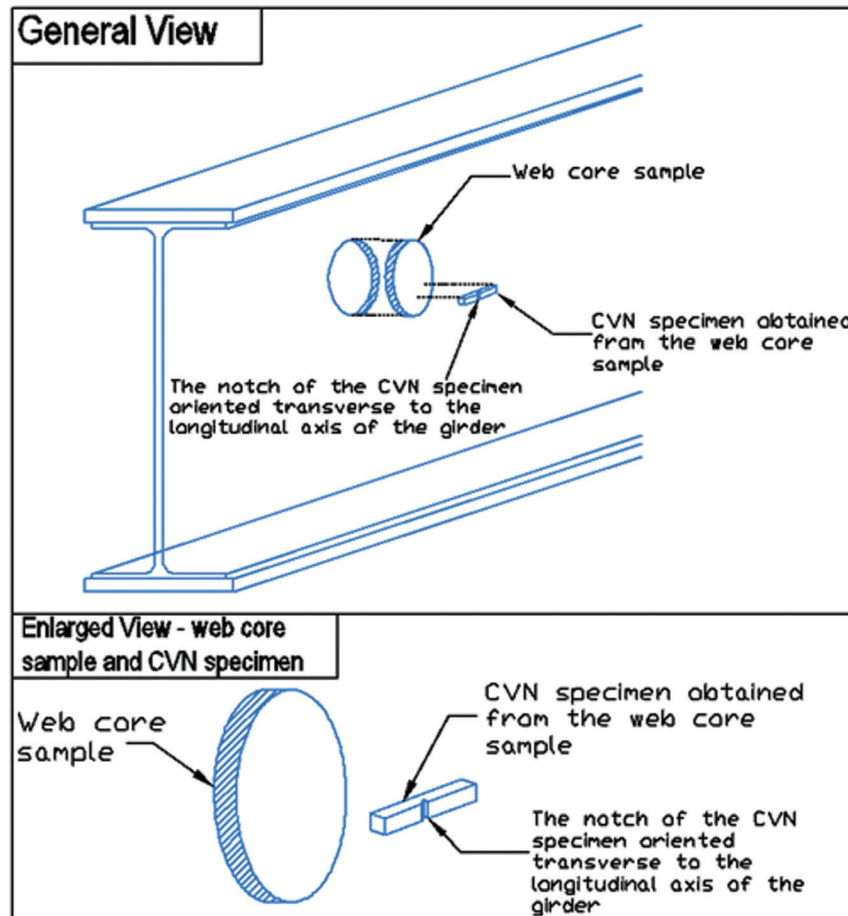


Figure 2.2 CVN specimen obtained from the web core sample.

From Table 2.3 it can be observed that both sets of data contain results that are below the modern AASHTO Zone II non-fracture critical requirements for the *longitudinal* direction. However, these data were obtained from specimens oriented *transversely* and lower energy values would thus be expected. The longitudinal CVN impact energy values will be substantially greater than the transverse values measured. It should be noted that no specifications, modern or older, have ever had any transverse CVN requirements specified. Although the data are somewhat lower

than presently specified, they are considered acceptable since the CVN values would be significantly greater had the specimen been oriented longitudinally.

2.2.4 Core Sample Conclusions

Based on the measured data and the orientation of the specimens, it is the opinion of the Purdue Research Team that the CVN impact energy data are adequate for this bridge. It is also the opinion of the Research Team that the longitudinal CVN impact energies will be substantially greater than the transverse values obtained from the bottom flange cover plate cores.

TABLE 2.2
CVN Data for the Web Core Samples

1 st set - Control Samples	CVN (ft-lbs)
1	139
3	104
5	142
2 nd set - Samples from Regions Exposed to Fire	CVN (ft-lbs)
B	157
E	168
F	133
H	94

2.3 Bolt Tests

2.3.1 Bolt Removal and Background Information

A total of eight (8) bolts and eight (8) nuts were removed from various web and flange splices for hardness, proof load, and wedge tension testing. In all the locations where bolts and nuts were removed for testing new galvanized fasteners were installed. Two (2) bolts and two (2) nuts were removed from the westbound bridge (Beam #11) and the remaining samples were taken from the eastbound bridge

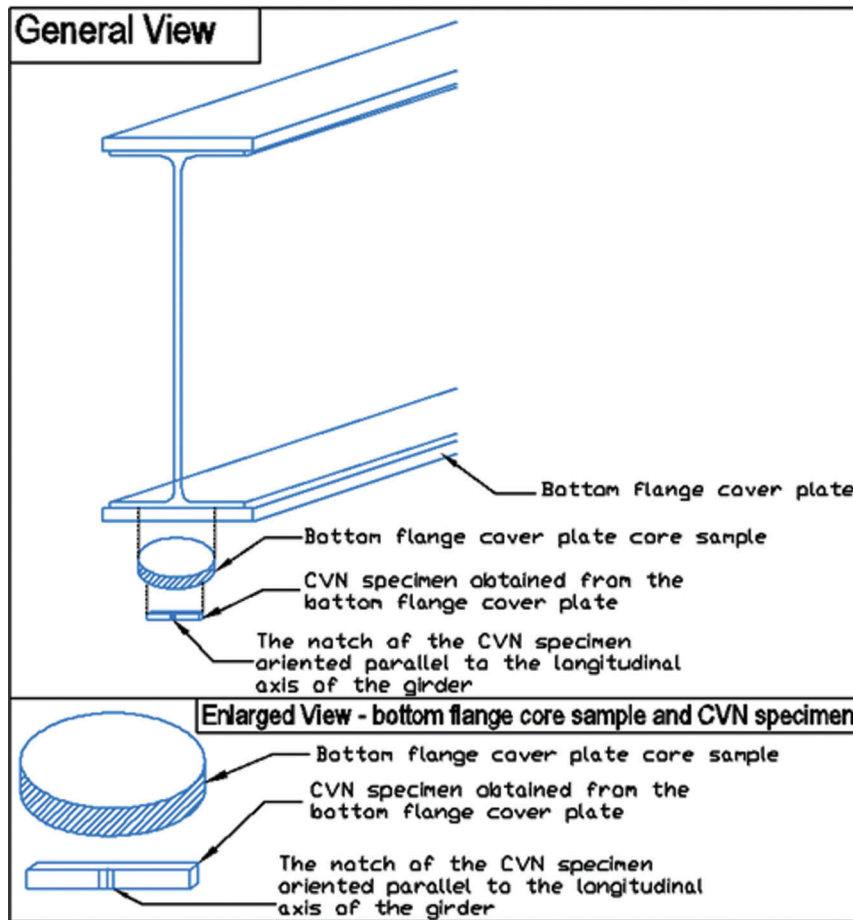


Figure 2.3 CVN specimen obtained from the cover plate core sample.

(Beams #12, 14 and 15). Drawings of the exact splice locations where the bolts and nuts were removed can be found in Appendix A.

All bolts removed are 3/4" diameter ASTM A325 HS bolts with ASTM A563 Grade C nuts. These bolts obtain their strength from a heat treatment procedure known as the quenching and tempering process (Q/T). Materials that obtain their properties (i.e. strength) through the Q/T process are more susceptible to

degradation due to uncontrolled heating and cooling, such as may have occurred during the fire.

Figure 2.4, Figure 2.5, and Figure 2.6 are photographs of the replaced HS bolts and nuts on both bridges.

TABLE 2.3
CVN Data for the Cover Plate Core Samples

1 st set - Control Samples	CVN (ft-lbs)
2	11
4	40
6	19
2 nd set - Samples from Regions Exposed to Fire	CVN (ft-lbs)
A	21
C	12
D	16
G	8



Figure 2.4 Bolts and nuts removed from Splice #2 - Beams #14 & #15 - Eastbound Bridge.

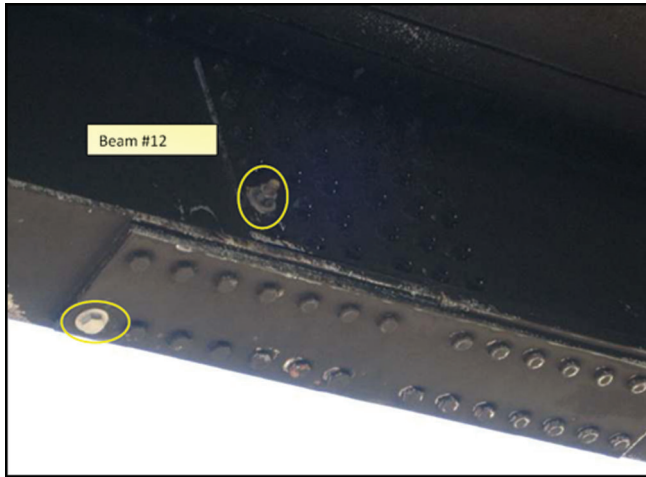


Figure 2.5 Bolts and nuts removed from Splice #1 – Beam #12 – Eastbound Bridge.

2.3.2 Bolt Test Results: Proof Load and Wedge Tension Test

All fasteners were tested as a courtesy to INDOT by NUCOR Steel in Indiana. Dr. Victor Hong of INDOT Research witnessed the tests. The bolt test results are summarized in Table 2.4 and Table 2.5. The tests revealed that only one (1) bolt (Bolt #7) did not pass the proof load test requirements per ASTM A325. It should be noted that Bolt #8 failed the first proof load test but passed the second test with a 3% increased proof load. All other bolts passed the proof load tests.

ASTM F606 describes the proof load test procedures. The test consists of maintaining a load specified by ASTM A325 over a ten (10) second period without causing permanent elongation of the bolt. In the event that the bolt shows deformation outside the allowable limits of ± 0.0005 inches (*note: this range is **only** given for possible measurement error*); a second test is allowed by ASTM F606. However, the second test has a 3%



Figure 2.6 Bolts and nuts removed from Splice #1 – Beam #11 – Westbound Bridge.

increased proof load. It is also worth mentioning that the proof load test is an indicator of axial elongation and not load carrying capacity in tension.

All bolts passed the wedge tension test. The wedge tension test consists of testing the bolt in tension to fracture using a wedge under the head of the bolt. To meet the requirements of this test, the bolt must support a load prior to fracture not less than the minimum tensile strength specified in ASTM A325 for the applicable bolt size, grade, and thread series. In this case, the minimum load that the bolt must support prior fracture is 40,100 lbs. ASTM F606 describes the wedge tension test procedures. The wedge used under the head of the bolt must meet certain criteria described in ASTM F606 that depend on the bolt size being tested. Figure 2.7 shows the wedge test details.

2.3.3 Bolt Test Results: Hardness Test

The hardness test results are tabulated in Table 2.5. According to ASTM A325, to pass the hardness test all the bolts needed Rockwell Hardness C (HRC) values between 25 and 34. None of the bolts exceeded the maximum hardness limit of 34 HRC given in ASTM A325. However, Bolts #7 and #8 did not meet the minimum hardness requirement of 25 HRC specified in ASTM A325. These two bolts had average hardness values of 22 HRC and 23 HRC respectively.

2.3.4 Nut Test Results: Hardness Test

Hardness testing was also performed on all eight (8) nuts removed (see Table 2.6). The hardness requirements for grade C nuts per ASTM A563 have a rather broad range and are set between 78 HRB and 38 HRC. Since all results from the hardness tests were given in Rockwell C scale, these values must be converted to Rockwell B scale for comparison to the minimum acceptable value. The minimum hardness value obtained on Rockwell scale C was 4 HRC which corresponds on the Rockwell B scale to a hardness value of 84 HRB. This value is greater than the minimum requirement of 78 HRB and is therefore satisfactory. None of the nuts exceeded the maximum hardness limit of 38 HRC. Therefore, all the nuts had hardness values within the acceptable range given in ASTM A563.

2.3.5 Fastener Conclusions

Considering there was no physical damage/evidence of fire on the bolts (i.e. no heat or damaged paint), all the bolts passed the wedge tension test, and all the bolts passed the proof load test (with the exception of Bolt #7), it is the opinion of the Purdue Research Team that there was no fire damage to the bolts. Bolts #7 and #8 do not meet the current specifications; however, it is not unreasonable for some bolts to be slightly out of the tolerance given the vintage of the bolts. ASTM F1470 provides guidelines regarding fastener sampling for

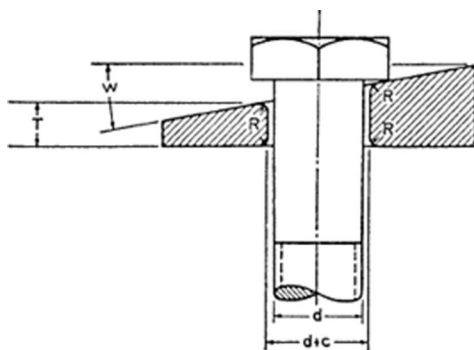
TABLE 2.4
Bolts - Proof Load and Wedge Tension Test Results

Bolt Label	Location	Proof Load Test		Wedge tension test	
		(1) 28,400 lb	(2) 29,350 lb = Test (1) + 3%	40,100 lb to pass	
1	BNBL - Beam #11-Flange Splice	PASS	N/A	50,660 lb	PASS
5	BNBL - Beam #11 - Web Splice	PASS	N/A	49,540 lb	PASS
2	JBSB - Beam #15 - Flange Splice	PASS	N/A	48,220 lb	PASS
6	JBSB - Beam #15 - Web Splice	PASS	N/A	49,750 lb	PASS
3	JBSB - Beam #14 - Flange Splice	PASS	N/A	50,800 lb	PASS
8	JBSB - Beam #14 - Web Splice	FAIL	PASS	44,720 lb	PASS
4	JBSB - Beam #12 - Flange Splice	PASS	N/A	52,030 lb	PASS
7	JBSB - Beam #12 - Web Splice	FAIL	FAIL	42,640 lb	PASS

NOTE: All the bolts tested were 3/4" HS ASTM A325.

TABLE 2.5
Bolts - Hardness Test Results

Bolt Label	Location	Hardness Test					Average	
		#1	#2	#3	#4			
1	BNBL - Beam #11 - Flange Splice	27.9	27.2	29.9	30.3	28.825	PASS	
5	BNBL - Beam #11 - Web Splice	25.7	26.6	25.6	24.6	25.625	PASS	
2	JBSB - Beam #15 - Flange Splice	21.9	28.9	27.4	24.4	25.65	PASS	
6	JBSB - Beam #15 - Web Splice	28.4	31.5	29.3	29.7	29.725	PASS	
3	JBSB - Beam #14 - Flange Splice	29.8	30.2	31.2	31	30.55	PASS	
8	JBSB - Beam #14 - Web Splice	24.7	23.1	22.1	22.6	23.125	FAIL	
4	JBSB - Beam #12 - Flange Splice	28.9	31.5	31.6	27	29.75	PASS	
7	JBSB - Beam #12 - Web Splice	23	21.8	21.9	21.9	22.15	FAIL	



Where:

- c = clearance of hole
- d = diameter of bolt or screw
- R = radius or chamfer
- T = reference thickness of wedge at thin side of hole equals one half diameter of bolt or screw
- W = wedge angle

Figure 2.7 Wedge tension test details.

TABLE 2.6
Nuts - Hardness Test Results

Nut Label	Location	Hardness Test - HRC		Strength Test
		Reading 1	Reading 2	
1	BNBL - Beam #11 - Flange Splice	12.4	12.2	Could not perform the strength test (threads were damaged)
5	BNBL - Beam #11 - Web Splice	4.1	4.5	
2	JBSB - Beam #15 - Flange Splice	15.7	14.4	
6	JBSB - Beam #15 - Web Splice	14.6	14	
3	JBSB - Beam #14 - Flange Splice	15.5	8.8	
8	JBSB - Beam #14 - Web Splice	14.6	12.8	
4	JBSB - Beam #12 - Flange Splice	14.1	15.6	
7	JBSB - Beam #12 - Web Splice	11.3	11	

specified mechanical properties and performance inspection in the manufacturing process. For example, for a lot size of 35,000 fasteners according to ASTM F1470, four (4) randomly selected fasteners should be tested for hardness (approximately 0.012% fasteners tested from the considered lot) and three (3) randomly selected fasteners should be tested for proof load and tensile strength (approximately 0.009% fasteners tested from the considered lot). If any of the samples fails the test, the entire lot is rejected.

Additionally, hardness test results of the nuts also suggest the fire did not have any negative effect on the integrity of the nuts.

3. INSTRUMENTATION PLAN AND DATA ACQUISITION

On December 16 and 17, 2009 long-term monitoring instrumentation was installed by the Purdue Research Team on the I-465 bridges. Instrumentation was primarily focused on the eastbound structure with limited instrumentation on the westbound bridge. The primary intent of the monitoring was to capture live load stress ranges in predetermined areas of interest. These areas included the location of maximum moment as well as the locations where core samples were removed for metallurgical testing. Using the live load stress ranges it could be determined if or to what extent the composite action was compromised. Additionally, the stress ranges were used to evaluate the fatigue performance of the structure; specifically, in those areas where cores were removed and subsequently reduced the fatigue resistance.

Two types of tests were performed over the four month monitoring period: controlled truck load testing and in-service long-term monitoring. Identical instrumentation plans were used for both of these tests. As-built instrumentation drawings that contain the specific location of all strain gages can be found in Appendix A.

A total of eighteen (18) uniaxial resistance-type strain gages were installed on the two bridges: seventeen (17) strain gages on the eastbound structure and only one (1) strain gage on the westbound structure. Seven beam lines of the eastbound bridge had strain gages installed on the top and bottom flange near midspan, totaling fourteen (14) gages. The remaining four (4) strain gages were placed near three (3) core holes in the bottom flange cover plate of both bridges. Figure 3.1 shows the fourteen (14) strain gages installed at midspan of the eastbound bridge.

3.1 Strain Gages

Strain gages were installed to capture the local response of particular details, for example where core samples were removed from the bottom flange cover plate of the girders. Strain gages were also used to establish the global response of the bridge as a system. The particular strain gages installed on the steel girders of the I-465 bridges were produced by Vishay



Figure 3.1 General view of strain gage locations.

Micro-Measurements model LWK-06-W250B-350 with an active grid length of 0.25 inches. These are uniaxial weldable resistance-type strain gages and were selected to be used at this site for their easy installation techniques in the field. Additionally, the selected strain gages have proven to produce accurate strain measurements over long periods of time (anywhere from months to years). Other notable specifications for this particular strain gage type include that they are temperature-compensated for use on structural steel and have a resistance of 350 ohms. An excitation voltage of 10 volts was used for the strain gages.

The strain gages come pre-bonded to a metal strip by the manufacturer. To attach them to the bridge in the field, multiple pinprick sized resistance spot welds are used as shown in Figure 3.2. The spot welds pose no concern with respect to fatigue. To prepare the surface for installation the metal is simply ground smooth and cleaned with degreaser. The final step in the installation process involves covering the strain gage with a proven multi-layer weatherproofing system to protect it against the extreme outdoor conditions. Figure 3.3 shows the

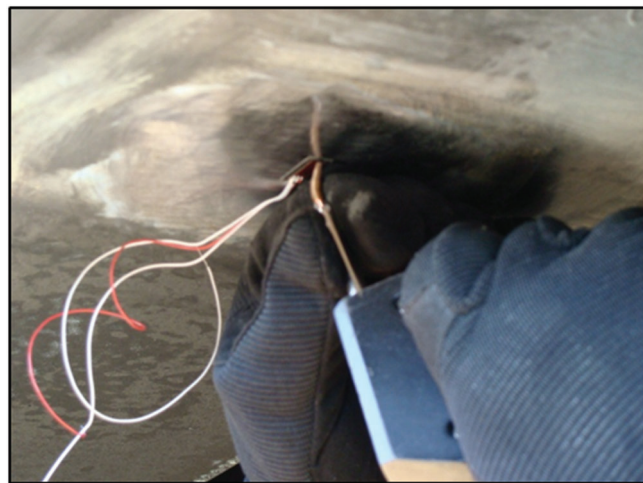


Figure 3.2 Weldable strain gage.

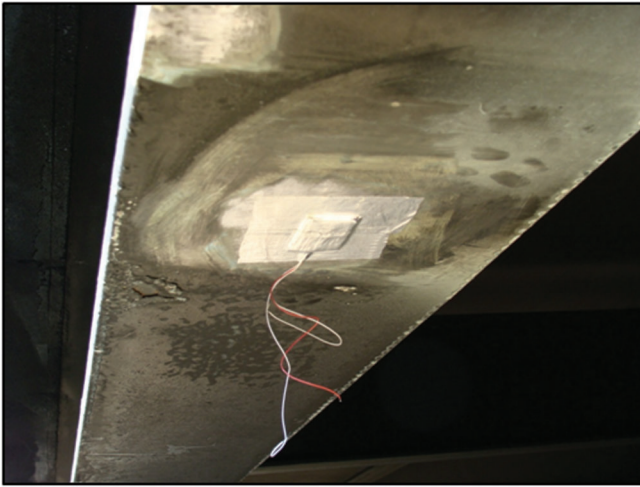


Figure 3.3 Strain gage in final installed condition.

final condition of the strain gage after installation and sealing.

3.2 Data Acquisition System

A data logger, cellular modem and antenna were installed to collect and transmit data. A battery back-up was provided should there be a loss of power on-site. Additional equipment including battery chargers, marine batteries, a charge controller, and power inverter were also required at the site for monitoring. What follows is a brief description of notable equipment used as part of the monitoring system. Also, Figure 3.4 is a photograph of the complete data acquisition system.

A Campbell Scientific CR9000X data logger was used for data collection for the duration of testing. The CR9000X is a high-speed, multi-channel, 16-bit system configured with digital and analog filters to assure noise-free signals. Other notable features of the CR9000X include its ease of programming, ability to develop stress-range histograms using the rainfall cycle counting method, and capability for live data viewing.

The cellular modem used onsite was an 882-EVDO CDMA Data Modem and IP Router, manufactured by CalAmp/LandCell. The 882-EVDO Cellular Data Modem is an external 3G cellular broadband router with integrated DHCP server, port forwarding and port mapping capabilities providing wireless data connectivity through public cellular networks.

The high-speed cellular modem installed serves several purposes. The first of which is to retrieve data remotely. Data is initially collected locally and stored onsite. Then using specialized software installed on a server residing at Purdue University the data are automatically downloaded at a predefined interval. Secondly, the cellular modem makes it possible to view live data in real time allowing the Research Team to verify the monitoring system is still functional without being onsite. One final attractive feature of the cellular modem is the ability to reprogram the data logger remotely through the cellular connection. This allows

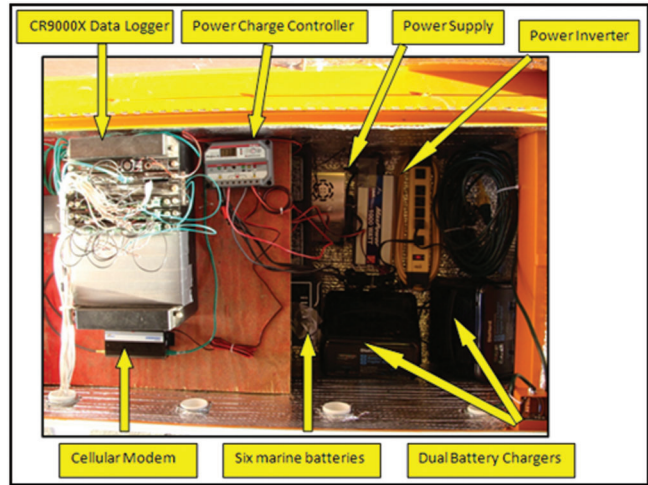


Figure 3.4 Data acquisition system.

the Research Team to update and change the program based on the review of prior data.

The monitoring equipment (data logger, cellular modem, charge controller, etc.) were enclosed in a weather-tight steel box as shown in Figure 3.5. This box was located under the eastbound bridge behind Bent #2. The instrumentation box was locked and chained to the bent to help deter anyone from tampering with the equipment.

Power was provided from an electrical outlet installed near Bent #2 where the instrumentation box was placed. Power from the outlet was run to the box and connected to a surge protector powering two battery chargers. The two battery chargers were connected to a charge controller. A charge controller was used to ensure the six marine batteries maintained an optimal charge level. The charge controller also powered the cellular modem. Connecting the



Figure 3.5 Weather-tight enclosure containing data acquisition system.

instrumentation in this fashion insured the monitoring system would have power for approximately three days should external power be lost.

3.3 Remote Long-term Monitoring

3.3.1 Triggered Data

To minimize the volume of data collected during the monitoring period, time-history data were not recorded continuously. Rather, trigger events were used to start and stop data collection. The trigger events were based on predefined stress levels measured in the bottom flange of the girders located in the left, center, and rightmost lanes of mainline I-465. When the stress produced by heavy trucks exceeded predefined levels the data logger ‘triggered’ and recorded time-history data from all strain gages for a defined period of time before and after the event. For the duration of monitoring, the time interval was set at six seconds (three seconds before and three seconds after an event). This time period was chosen to ensure the entire loading event was captured. The strain gages used to trigger the recording of data were selected so that eastbound traffic in each lane could be identified and stored in separate files. All the trigger channels were located on the eastbound bridge. Table 3.1 explains the trigger channels and levels used for data collection. The duration of the trigger event and all trigger stress levels were established by the Research Team based on a review of data collected over the first month of monitoring (December 17, 2009 through January 15, 2010).

3.3.2 Stress-Range Histograms

In addition to the recorded triggered events, stress-range histograms for selected channels were generated by the data logger using the rainflow cycle counting algorithm. Not all channels were included in the analysis of the stress-range histograms. Based on the data from the first month of monitoring (December 17, 2009 through January 14, 2010), specific channels of interest were chosen to be included in the analysis. The rainflow cycle counting algorithm was programmed to place all cycles in equally divided 0.5 ksi bins. The exception to the 0.5 ksi bin size is the first bin which holds cycles between 0.25 ksi and 0.5 ksi. Cycles less

TABLE 3.1
Trigger Channels

Trigger Channel	Lane	Trigger Stress Level(ksi)
CH_4	Left	1.75
CH_8	Middle	2.5
CH_12	Right	2.5

than the 0.25 ksi threshold are neglected in the bin counts.

4. CONTROLLED LOAD TESTING

A series of controlled tests were conducted to verify the measurements obtained during in-service testing. The controlled tests were performed using two similar test trucks of known load and geometry, provided by INDOT. These tests were conducted on March 25, 2010 between 12:30 AM and 2:30 AM. Night testing was chosen to reduce the impact on interstate traffic in the area as multiple lanes of I-465 were closed for the testing. All control testing was performed on the eastbound bridge where the majority of strain gages were installed (seventeen (17) out of eighteen (18) channels).

4.1 Test Trucks

As mentioned above, the two trucks used for testing were similar but had slightly different axle spacing. The first truck (ID #63480) was a tandem axle plow truck with a gross weight of 48,000 pounds. Likewise, the second truck (ID #63701) was also a tandem axle plow truck with a gross weight of 47,180 pounds. Figure 4.1 is a photograph of truck #63480. While onsite the Research Team obtained accurate measurements of each truck and INDOT provided individual tire weights. Figure 4.2 and Figure 4.3 show the geometry and tire load data for truck #63480 and truck #63701 respectively.

4.2 Testing

Testing consisted of a series of five (5) static tests and five (5) crawl tests. The static tests involved parking one or both trucks at midspan between Piers #2 and #3 in



Figure 4.1 Test truck #63480 used in the control load testing.

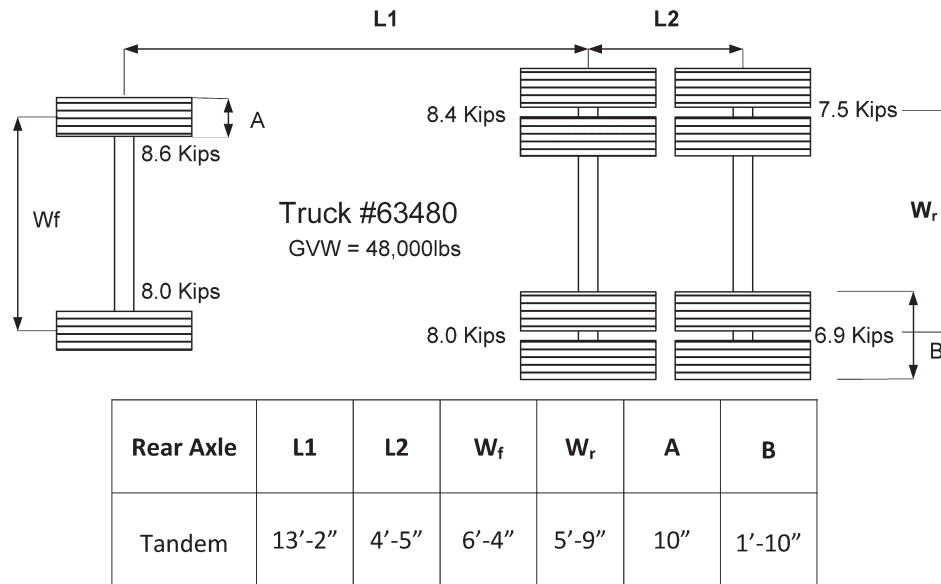


Figure 4.2 Geometry and tire load data for test truck #63480.

predetermined transverse locations. Likewise, the crawl tests consisted of driving either one or two trucks across the bridge at approximately five miles per hour in predetermined transverse locations. A summary of the controlled load tests performed is presented in Table 4.1.

As mentioned above, testing was conducted transversely across the bridge. The transverse locations were determined by the bridge lanes. In the first three static tests, Truck #63480 was parked at midspan between Piers #2 and #3, in each of the three lanes of mainline I-465 (no tests were performed on the exit lane/ramp). During the fourth and fifth static tests both trucks were

used. The trucks were parked side-by-side, again at midspan between Piers #2 and #3, with the heavier truck (#63480) located on the north side in both tests. Transverse locations for these tests included left/middle lanes and middle/right lanes. The five (5) crawl tests used approximate transverse locations and the same truck(s) as the five static tests. Note that during the crawl tests only approximate transverse locations to the static tests could be achieved depending on the skills of the driver(s).

The night of the controlled testing INDOT was performing an inspection of the bridge with their under bridge snooper vehicle. Thus, one crawl test was

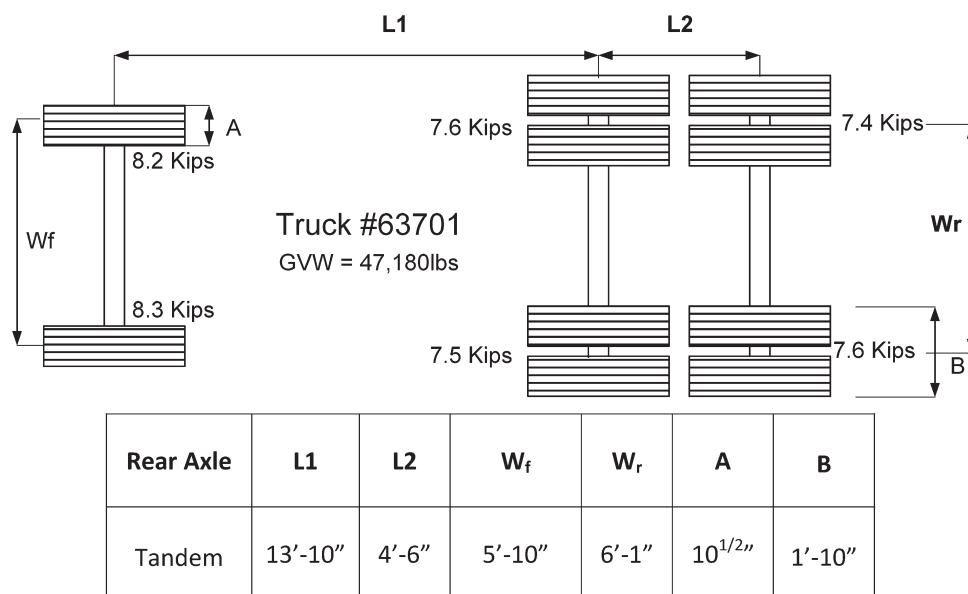


Figure 4.3 Geometry and tire load data for test truck #63701.

TABLE 4.1
Summary of the Controlled Load Tests

Test			
File Name	Description	Lane(s)	Truck(s)
PARK_1.DAT	Single <i>parked</i>	Left Lane	Truck #63480
CRL_1.DAT	Single <i>crawl</i>	Left Lane	Truck #63480
PARK_2C.DAT	Single <i>parked</i>	Middle Lane	Truck #63480
CRL_2.DAT	Single <i>crawl</i>	Middle Lane	Truck #63480
PARK_3.DAT	Double <i>parked</i>	Left Lane 2	Truck #63480
		Middle Lane	Truck # 63701
CRL_3.DAT	Double <i>crawl</i>	Left Lane	Truck #63480
		Middle Lane	Truck # 63701
PARK_4.DAT	Single <i>parked</i>	Right Lane	Truck #63480
CRL_4.DAT	Single <i>crawl</i>	Right Lane	Truck #63480
PARK_5.DAT	Double <i>parked</i>	Middle Lane	Truck # 63480
		Right Lane	Truck # 63701
CRL_5.DAT	Double <i>crawl</i>	Middle Lane	Truck # 63480
		Right Lane	Truck # 63701
SNOOP.DAT	Single <i>crawl</i>	Left Lane	Under Bridge SNOOPER

performed in the left lane using the snoopers (estimated GVW = 64,000 lbs) in order to compare the test results obtained with the test trucks.

5. RESULTS OF CONTROLLED LOAD TESTING

As previously discussed, the controlled load testing consisted of five (5) crawl tests and five (5) static tests, using either a single truck or two trucks side-by-side of known load and geometry. All the tests were performed on the eastbound bridge, where the majority of the strain gages were installed in the second span. As-built instrumentation drawings that contain the specific location of all strain gages can be found in Appendix A. The results of the controlled load tests are discussed in this section and are summarized in the five (5) cases shown below. Each case is based on the truck(s) position(s):

- **Case 1: Single truck** – static and crawl tests in the left lane (PARK_1.DAT & CRL_1.DAT)
- **Case 2: Single truck** – static and crawl tests in the middle lane (PARK_2C.DAT & CRL_2.DAT)
- **Case 3: Single truck** – static and crawl tests in the right lane (PARK_4.DAT & CRL_4.DAT)
- **Case 4: Two trucks side-by-side** – static and crawl tests in the left and middle lanes (PARK_3.DAT and CRL_3.DAT)
- **Case 5: Two trucks side-by-side** – static and crawl tests in the middle and right lanes (PARK_4.DAT & CRL_4.DAT)

The response of channels installed near core hole locations during controlled load testing along with results from the snoopers crawl test in the left lane are also presented in this section. A summary of the controlled load testing can be found at the conclusion of this section.

5.1 Single Truck Tests in the Left Lane

5.1.1 Single Truck Crawl Test in the Left Lane (CRL_1.DAT)

In general, the response of the bridge was as expected and typical of a continuous multi-span steel bridge. Figure 5.1 presents the response of CH_2, CH_3, CH_4, CH_6, CH_8, CH_10, CH_12 and CH_14 as the test truck (#63480) passed over the left lane. All channels mentioned above were installed at midspan of the second span (Span B) of the Eastbound Bridge. All but one of the channels were installed on the bottom flange cover plate of Beams #12 through #16. Only CH_3 was installed on the top flange of Beam #13 (under left lane). As expected, the response in all eight (8) channels is positive and maximum as the test truck passed over the middle of the second span (where the strain gages were installed) and then becomes negative as it passes into the adjacent third span. Likewise, a negative moment response was also observed as the truck crossed span one. It is also important to note that the positive response of CH_10, CH_12 & CH_14 before and after the maximum response of the test truck is due to the light traffic in the right lane. The right lane was open to traffic during testing. Some of responses due to traffic in the right lane are highlighted in Figure 5.1.

Figure 5.1 also shows good load distribution between the girders. The maximum response was observed in the girders closer to the test truck (CH_4 & CH_6) and a smaller response was observed in the girders further away from the test truck (CH_2, CH_8, CH_10, CH_12 & CH_14). This observation is very clear as the test truck passed over the second span as shown in Figure 5.1. As the truck passed over the other spans the load distribution becomes less clear. This is a

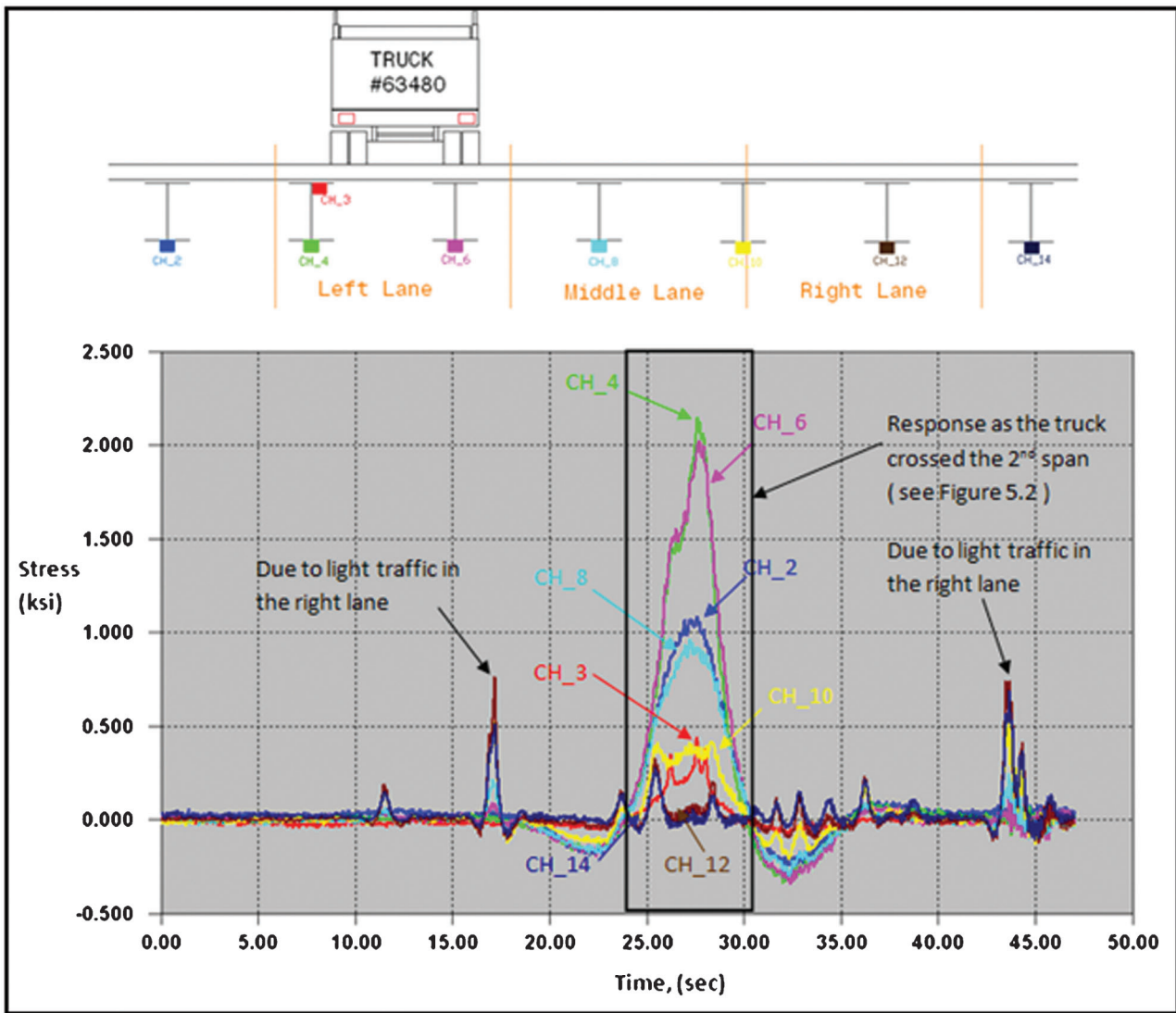


Figure 5.1 Response of strain gages installed at midspan (2nd span) – Crawl test: single truck in the left lane.

typical behavior expected in a continuous bridge due to the substantial transverse and longitudinal load distribution which occurs as loads move further away from the instrumented section (2nd Span at midspan).

Often times the strain gages can also help to identify the number and type of vehicle(s) (i.e., number of axles) that cross the bridge. Figure 5.2 presents a zoomed in image of the boxed section of Figure 5.1. Using the response from strain gages installed on the top flanges of the girders, local bending effects can be observed that help identify the vehicle. For example, CH_3 in Figure 5.2 (red trace) clearly shows a vehicle having three (3) axles (i.e., a test truck). This is best exemplified with data collected from the controlled load test where the truck configuration was known; however, this same concept was used to identify vehicles in triggered time-history data.

5.1.2 Single Truck Static Test in the Left Lane (PARK_1.DAT)

The single truck static test consisted of a single test truck being parked at midspan (2nd Span) in the left lane for a short period of time as measurements were taken. Figure 5.3 shows the response during the static test (PARK_1.DAT) of the same channels considered in test (CRL_1.DAT). Maximum stress values obtained during both left lane single truck tests are summarized in Table 5.1.

As it can be seen, the response of the static test (PARK_1.DAT) was relatively similar to that of the crawl test (CRL_1.DAT). The small difference between the two tests can be explained by the transverse location of the truck. During the crawl test (CRL_1.DAT) the truck did not pass through the exact transverse position as it was parked during the static test (PARK_1.DAT).

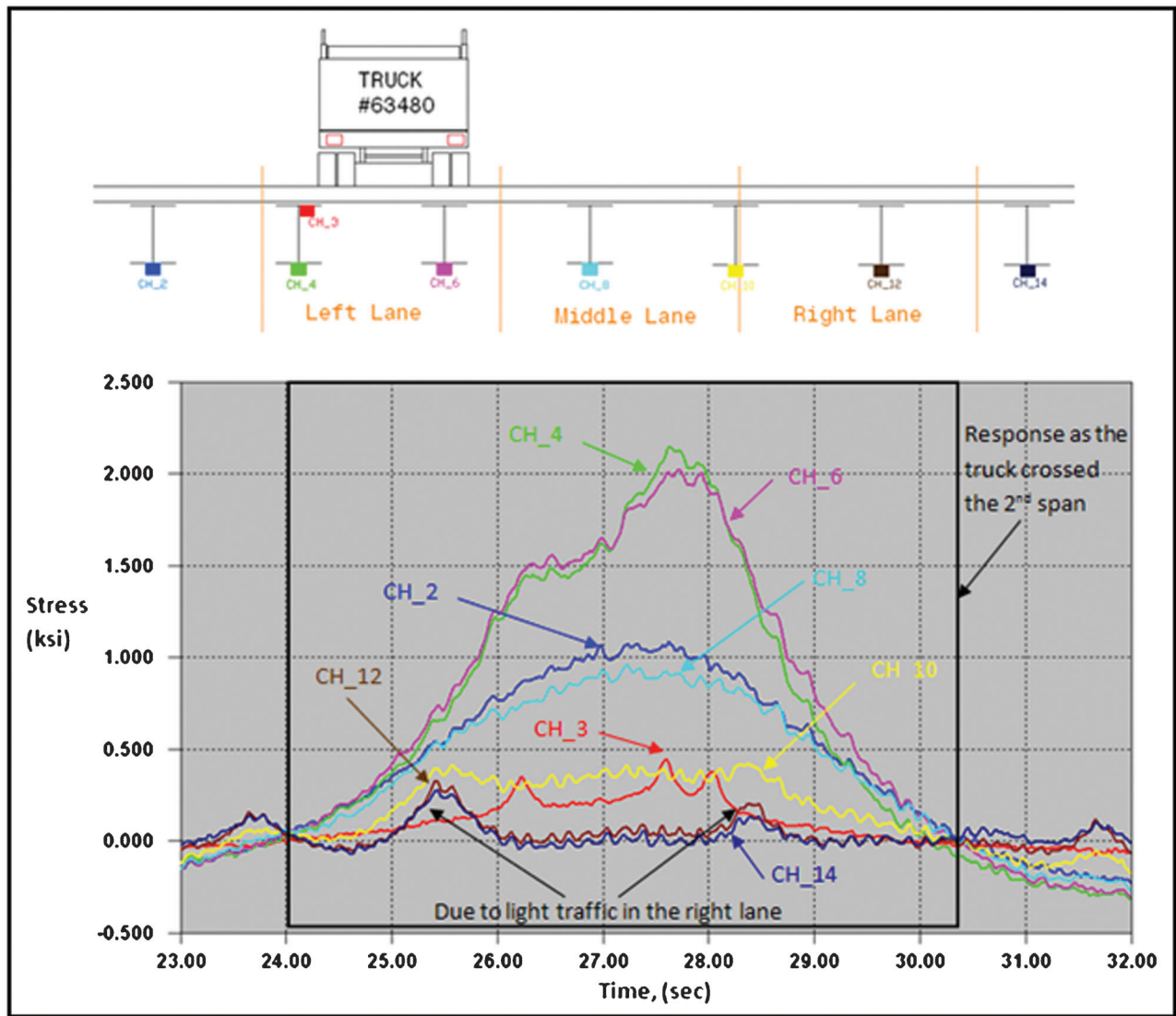


Figure 5.2 Response of strain gages installed at midspan (2nd Span), as the test truck passes over the 2nd span.

5.1.3 Composite Action

Composite action is developed when two load carrying structural members such as a concrete deck system and the supporting steel beam, are integrally connected and deflect as a single unit. When a system acts compositely no relative slip occurs between the slab and beam, resulting in a single neutral axis in a strain diagram. This resulting neutral axis is located between the neutral axis of the slab and that of the beam. Figure 5.4 illustrates the strain variation in composite beams.

The effective width of the slab, according to AASHTO 2010 (2) - Article 4.6.2.6.1, can be taken as one-half the distance to the adjacent stringer or girder on each side of the component. Thus, in this case the effective width of the slab is 7'-4" for an interior beam. Using the stresses recorded in the field during the controlled load testing, the position of the neutral axis of

the composite section will be determined using a linear stress diagram. Following is a summary of calculations for locating the neutral axis of the composite section. Two sets of calculations are included. First, the neutral axis is calculated according to AASHTO 2010 (2). Then it is determined from the stresses recorded during the PARK_1.DAT controlled load test. It is also important to note, that the distances to the centroid of individual elements were all taken from the bottom of the cover plate when calculating the position of the neutral axis. Also, the position of the neutral axis is always referenced from the *bottom of the cover plate*.

Calculations – Summary

1. Neutral axis of the composite section - AASHTO 2010 (2) (Figure 5.5)

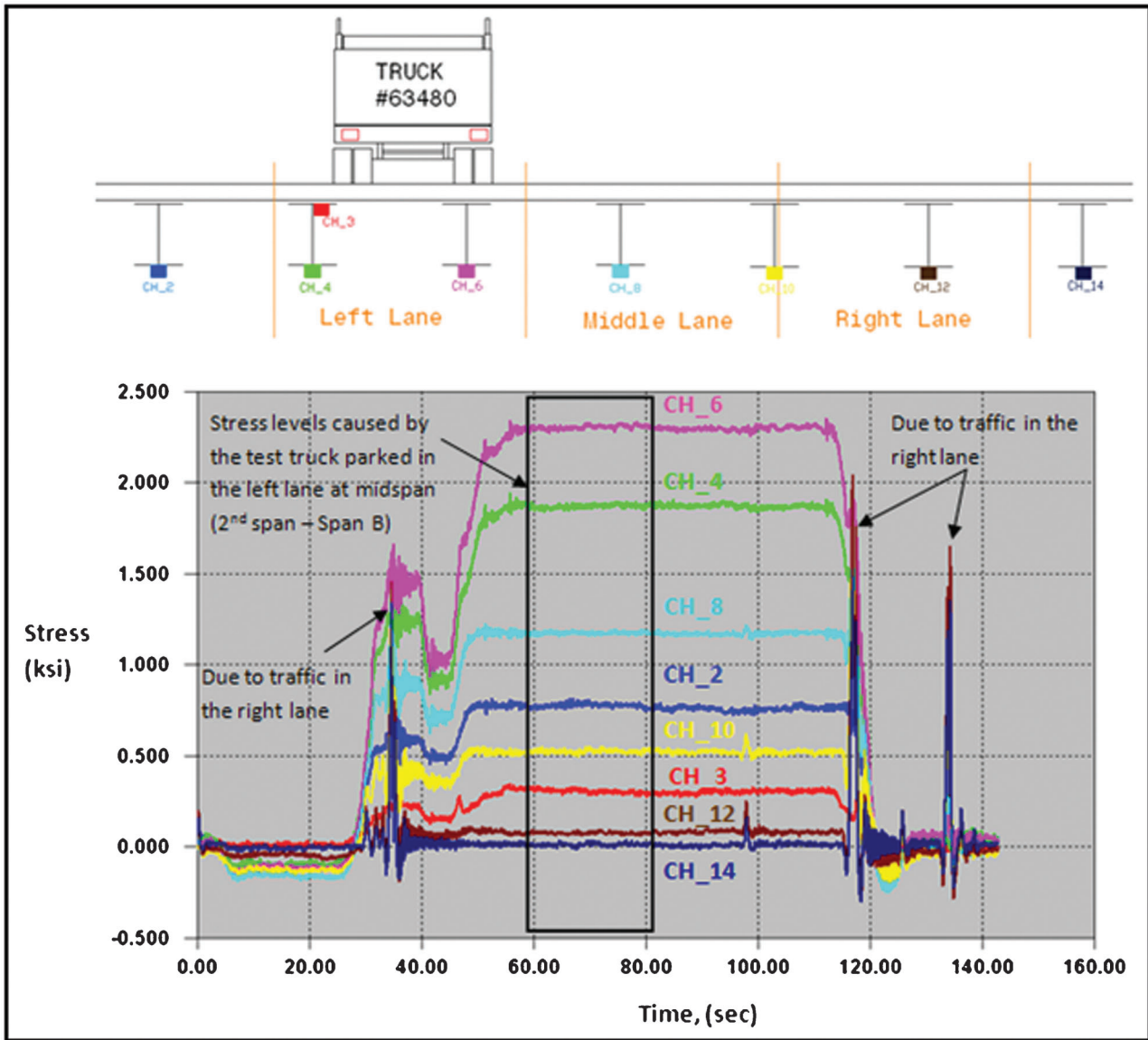


Figure 5.3 Response of strain gages installed at midspan (2nd Span) – Static test: single truck in the left lane.

TABLE 5.1
Maximum Stresses - Single Truck Tests in the Left Lane

Channel	CRL_1.DAT Max. Stress (ksi)	PARK_1.DAT Max. Stress (ksi)
CH_2	1.1	0.8
CH_3	0.4	0.3
CH_4	2.1	1.9
CH_6	2.0	2.3
CH_8	0.9	1.2
CH_10	0.4	0.5
CH_12	0.1	0.1
CH_14	0.0	0.0

Neutral axis of the beam and cover plate only:

$$A_{cvr-plate} = 10in \times 0.5in = 5in^2$$

$$A_{beam24W76} = 22.4in^2$$

$$A_{total} = 22.4in^2 + 5in^2 = 27.4in^2$$

$$y_{beam-cvrplate} = \frac{(11.95in + 0.5in) \times 22.4in^2 + 0.25in \times 5in^2}{27.4in^2}$$

$$= 10.23in$$

Neutral axis of the concrete deck only (includes the haunch detail):

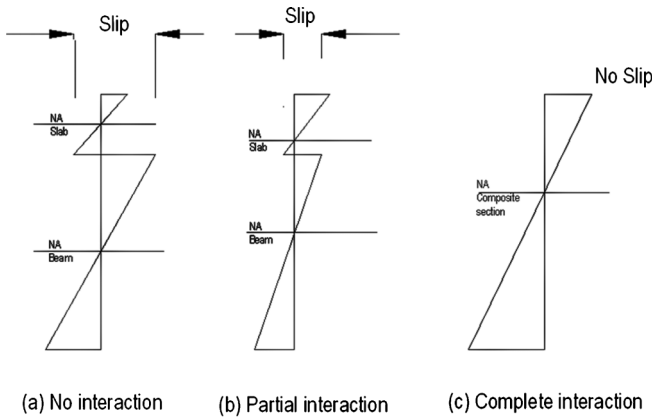


Figure 5.4 Strain variation in composite beams.

$$A_{total-conc.deck} = 88in \times 7.5in + 2 \times 4in \times 1in = 668in^2$$

$$y_{conc.deck} = \frac{(0.5in + 23.9in + 0.32in + 3.75in) \times (88in \times 7.5in) + (0.5in + 23.9in - 0.68in + 0.25in) \times 8in^2}{668in^2}$$

$$y_{conc.deck} = 28.42in$$

Neutral axis of the composite section:

$$E_{concrete} = 1820\sqrt{f'_c} = 1820\sqrt{3ksi} = 3,152ksi$$

$$n = \frac{E_{steel}}{E_{concrete}} = \frac{29,000ksi}{3,152ksi} = 9.2 \cong 9.00$$

$$y_{comp.section} = \frac{(27.4in^2 \times 10.23in) + \left(7.5in \times \frac{88in}{9}\right) \times 28.42in}{\left(27.4in^2 + 7.5in \times \frac{88in}{9}\right)}$$

$$= 23.47in$$

- Neutral axis of the composite section—from stresses recorded in PARK_1.DAT

From Table 5.1 the stresses recorded by CH_3 (bottom face of top flange) and CH_4 (bottom flange cover plate) are 0.3 ksi and 1.9 ksi, respectively. Using these values and considering elastic section properties (linear stress-strain diagram) the position of the neutral axis of the composite section can then be determined from similar triangles (geometry). Figure 5.6 shows the position of the neutral axis of the composite section determined from the stresses recorded in PARK_1.DAT.

Using elastic section properties (linear stress-strain diagram) and similar triangles (Figure 5.6) the position of the neutral axis of the composite section is determined:

$$\frac{1.9 - 0.3}{23.72} = \frac{1.9}{N.A.}$$

$$N.A. = \frac{23.72 \times 1.9}{1.9 - 0.3} = 28.17in$$

The location of the neutral axis of the composite section determined from the field measured stresses is above the location predicted by AASHTO 2010 (2) (see Figure 5.5). Hence, full-composite behavior is developed. This difference is not unusual since AASHTO 2010 (2) does not take into consideration the influence of the parapets and the overlay surface which all contribute to the actual load distribution and composite behavior.

5.2 Single Truck Tests in the Middle Lane

5.2.1 Single Truck Crawl Test in the Middle Lane (CRL_2.DAT)

Figure 5.7 presents the response of CH_2, CH_4, CH_6, CH_7, CH_8, CH_10, CH_12 and CH_14 as the test truck (#63480) passed over the middle lane. The

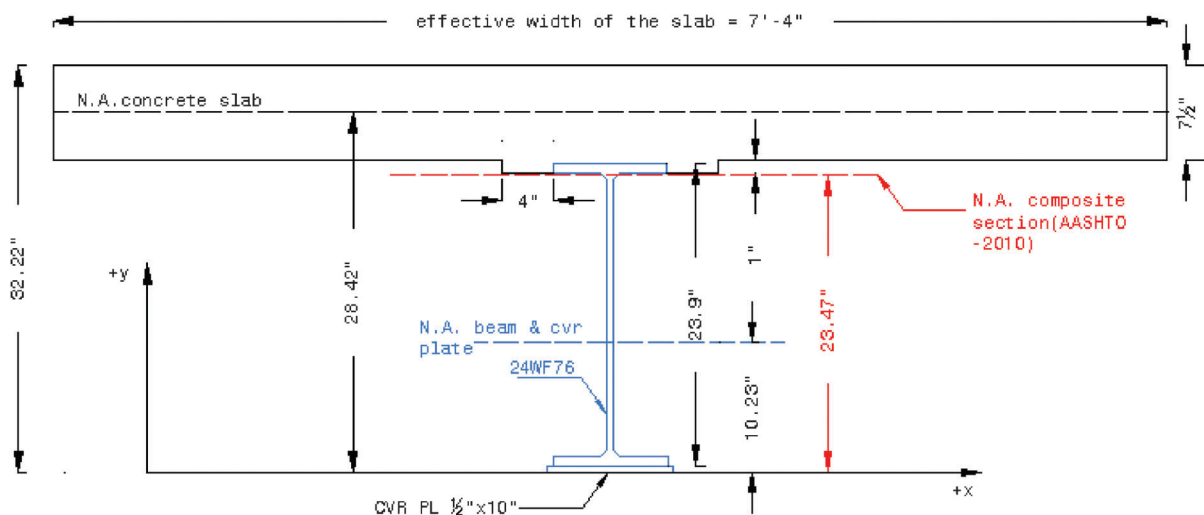


Figure 5.5 Neutral axis of the composite section – AASHTO 2010 (2).

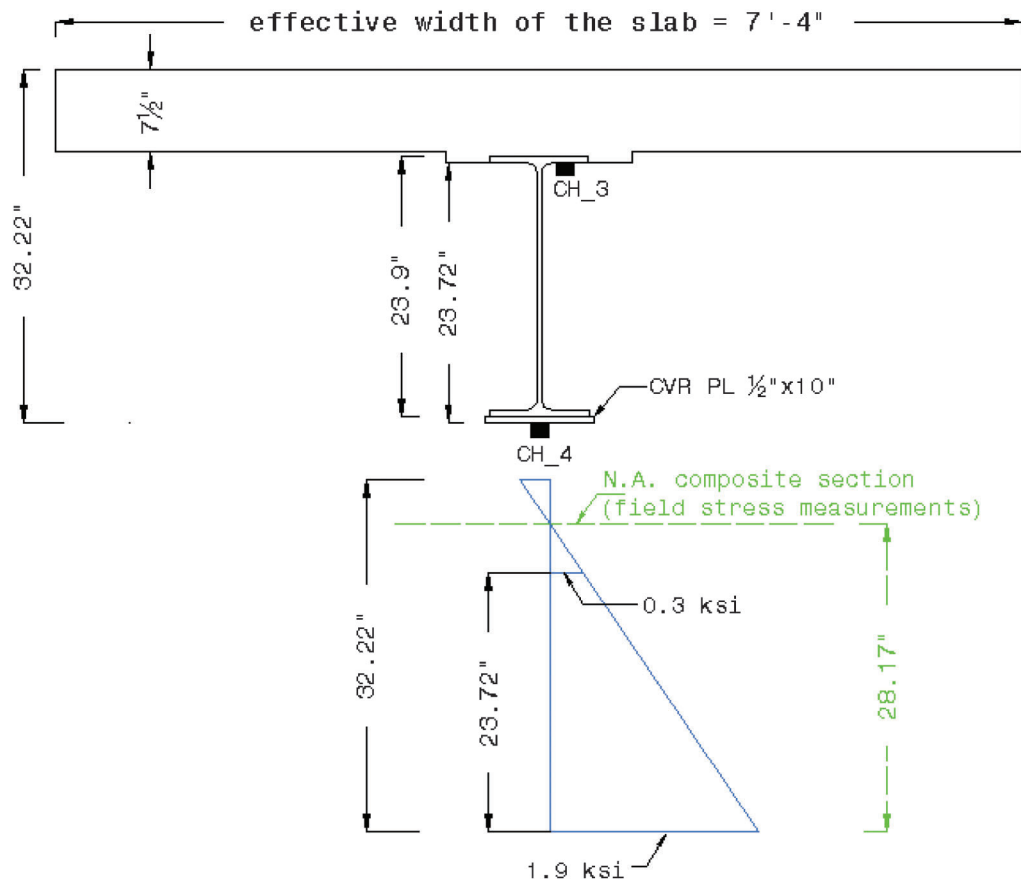


Figure 5.6 Neutral axis of the composite section – from stresses recorded in PARK_1.DAT.

response in all eight (8) channels is positive as the test truck passed over the second span (where the channels were installed). Negative moments were observed as the truck passed through the first and third spans. Also, as previously discussed in section 5.1.1, using the response from strain gages installed on the top flange of the girders, the type (number of axles) and number of vehicle(s) can be identified. This can be seen in CH_7 (pink trace) of Figure 5.7 where a tandem axle truck can be observed.

5.2.2 Single Truck Static Test in the Middle Lane (PARK_2C.DAT)

The single truck static test consisted of the test truck being parked at midspan (2nd span) for a short period of time while measurements were made. Figure 5.8 shows the response during the static test PARK_2C.DAT of the same channels considered in Figure 5.7. Maximum stress values obtained during the single truck tests in the middle lane are summarized in Table 5.2. The response of the static test was relatively similar to the response from the crawl test (CRL_2.DAT). Again, the small difference in stresses between these two tests is explained by the transverse positioning.

Heavy traffic was noted in the right lane during the static test (PARK_2C.DAT). Figure 5.9 shows the response of the strain gages to this heavy traffic. In the figure, CH_11 indicates three (3) semi-trailers passed back-to-back in the right lane. The semis were identified by the top flange response to the axles. An expanded view of the response to one of the semis exemplifies how they were identified.

5.2.3 Composite Action

As presented in section 5.1.3, to determine if full composite action is being developed between the concrete deck and the steel girder, the neutral axis of the composite section determined from field stress measurements must be located above the position indicated by AASHTO 2010 (2). From Table 5.2, the stresses recorded in test PARK_2C.DAT by CH_7 (bottom face of top flange) and CH_8 (bottom flange cover plate) are 0.3 ksi and 2.2 ksi, respectively. Figure 5.10 shows the position of the neutral axis of the composite section using the stresses recorded in PARK_2C.DAT.

Using elastic section properties (linear stress-strain diagram) and similar triangles (Figure 5.10) the

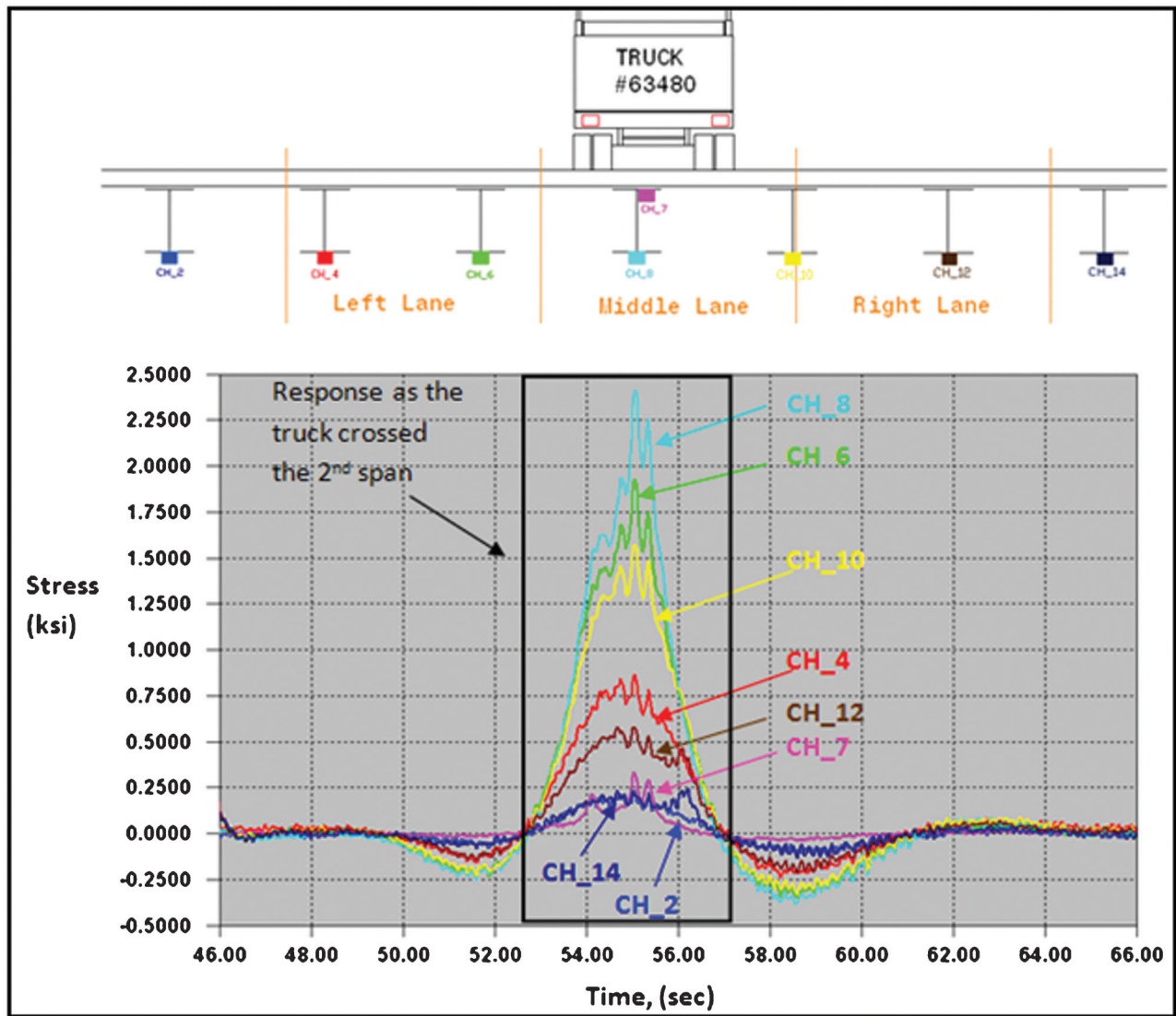


Figure 5.7 Response of strain gages installed at midspan (2nd Span) – Crawl test: single truck in the middle lane.

position of the neutral axis of the composite section is determined:

$$\frac{2.2 - 0.3}{23.72} = \frac{2.2}{N.A.}$$

$$N.A. = \frac{23.72 \times 2.2}{2.2 - 0.3} = 27.47 \text{ in}$$

The position of the neutral axis of the composite section determined from the field measured stresses is above the position indicated by AASHTO 2010 (2) (see Figure 5.5). Hence, full composite-behavior is developed. As previously explained in section 5.1.3, this difference is not unusual since there are other factors (parapets and overlay surface) that contribute to the load distribution and composite action in turn influencing the position of neutral axis.

5.3 Single Truck Tests in the Right Lane

5.3.1 Single Truck Crawl Test in the Right Lane (CRL_4.DAT)

When the controlled tests were performed in the right lane, the traffic on I-465 was stopped; thus, only the test truck was on the bridge. Figure 5.11 presents the response of CH_2, CH_4, CH_6, CH_8, CH_10, CH_11, CH_12 and CH_14 as the test truck (#63480) passed the bridge in the right lane. The response in all eight (8) channels is the same as in the previous single truck crawl tests: positive as the test truck passed over the second span (where the channels were installed) and negative as it passes through the first and third spans. Also, as for the previous two single truck positions, the

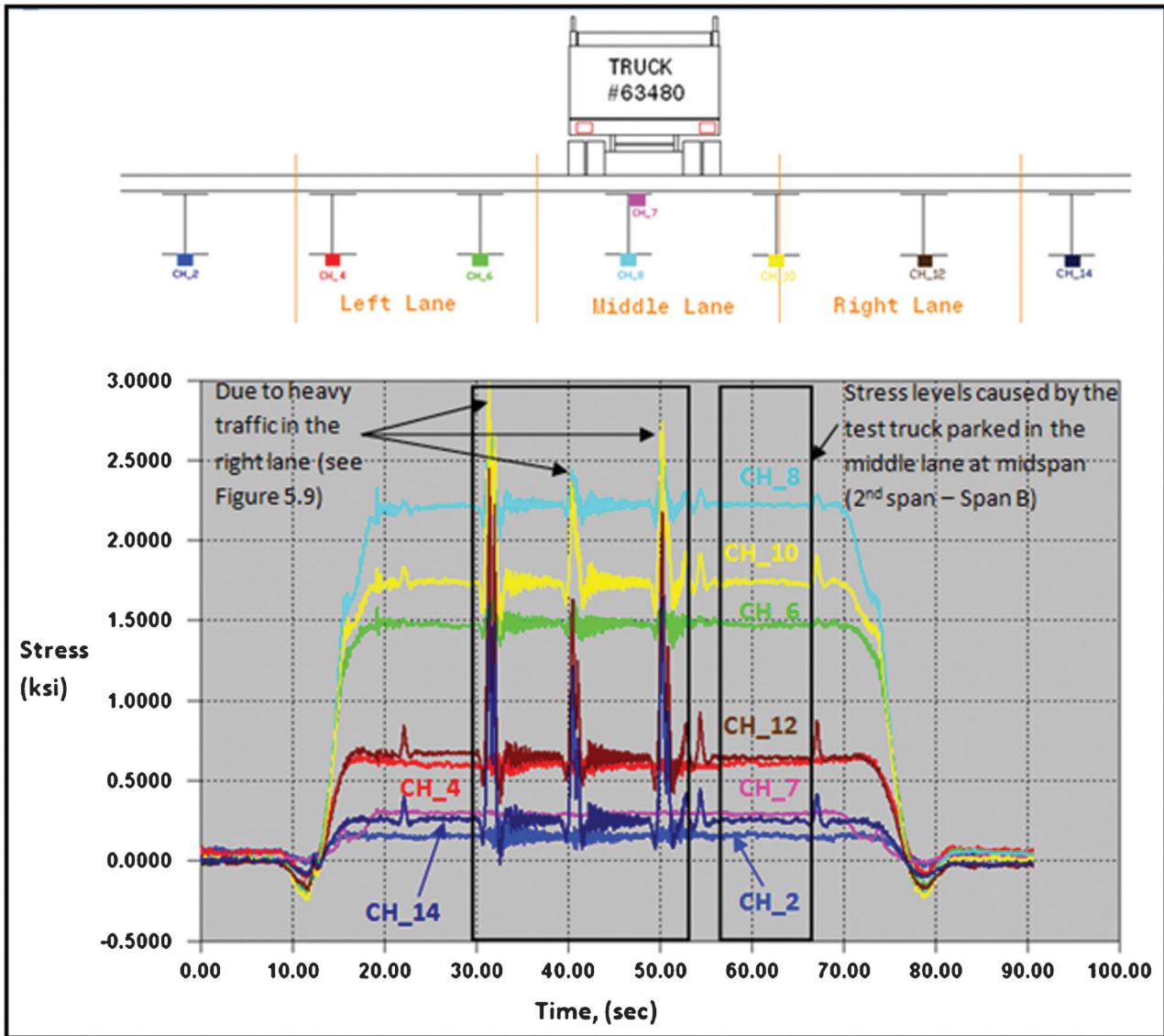


Figure 5.8 Response of strain gages installed at midspan (2nd Span) – Static test: single truck in the middle lane.

TABLE 5.2
Maximum Stresses - Single Truck Tests in the Middle Lane

Channel	CRL_2.DAT Max. Stress (ksi)	PARK_2C.DAT Max. Stress (ksi)
CH_2	0.2	0.2
CH_4	0.9	0.6
CH_6	1.9	1.5
CH_7	0.3	0.3
CH_8	2.4	2.2
CH_10	1.6	1.7
CH_12	0.6	0.6
CH_14	0.2	0.3

response from strain gages installed on the top flange of the girders can identify the type (number of axles) and number of vehicle(s). In Figure 5.11, CH_11 (yellow trace) shows a tandem axle truck crossing the bridge.

5.3.2 Single Truck Static Test in the Right Lane (PARK_4.DAT)

The single truck right lane static test consisted of the test truck being parked at midspan (2nd Span) of the right lane for a short period of time while measurements were made. Figure 5.12 shows the response of the same channels considered in Figure 5.11 during the static test PARK_4.DAT. Maximum stress values obtained during the single truck tests in the middle lane are summarized in Table 5.3.

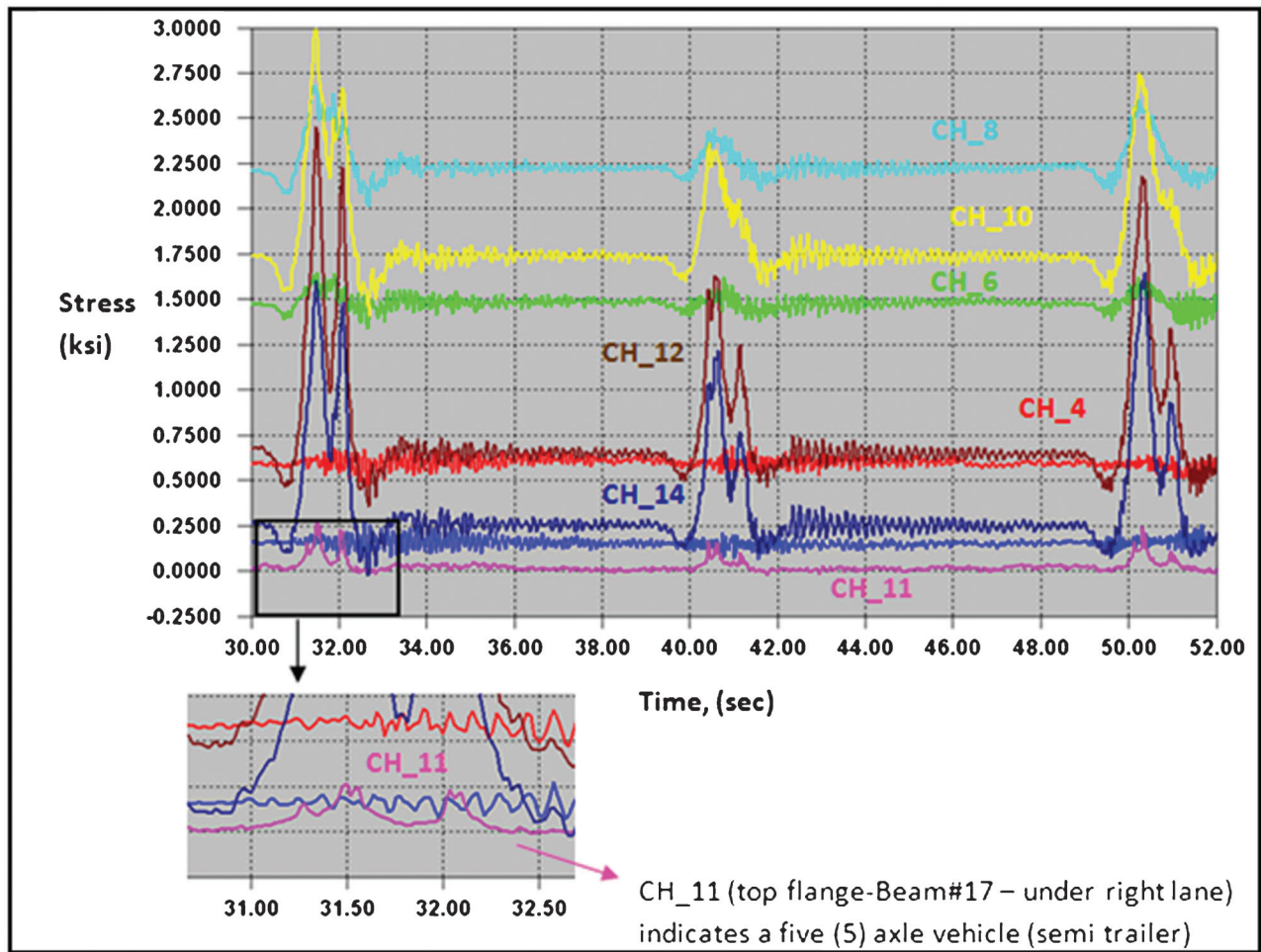


Figure 5.9 Response of CH_11 indicates semis passing in the right lane during the single truck static test in the middle lane.

The response of the channels was relatively similar to the response from the crawl test (CRL_4.DAT). As previously discussed, the small difference between the static and crawl tests can be explained by difference in transverse position between the two tests.

$$\frac{2.1 - 0.2}{23.72} = \frac{2.1}{N.A.}$$

$$N.A. = \frac{23.72 \times 2.1}{2.1 - 0.2} = 26.22in$$

5.3.3 Composite Action

As discussed in section 5.1.3, to determine if full composite action is being developed between the concrete deck and the steel girder, the neutral axis of the composite section determined from field stress measurements must be located above the position indicated by AASHTO 2010 (2). From Table 5.3 the stresses recorded in test PARK_4.DAT by CH_11 (bottom face of top flange) and CH_12 (bottom flange cover plate) are 0.2 ksi and 2.1 ksi, respectively. Figure 5.13 shows the position of the neutral axis of the composite section determined from the stresses recorded in PARK_4.DAT.

Using elastic section properties (linear stress-strain diagram) and similar triangles (Figure 5.13) the position of the neutral axis of the composite section is determined:

The position of the neutral axis of the composite section determined from the field measured stresses is above the position indicated by AASHTO 2010 (2) (see Figure 5.5). Hence, full-composite behavior is developed. As previously explained in section 5.1.3, this difference is not unusual since there are other factors (parapets and overlay surface) that contribute in the load distribution and composite action in turn influencing the position of neutral axis.

5.4 Trucks Side-by-Side in the Left and Middle Lanes

5.4.1 Trucks Side-by-Side in the Left and Middle Lanes – Crawl Test (CRL_3.DAT)

Figure 5.14 presents the response of CH_2, CH_3, CH_4, CH_6, CH_8, CH_10, CH_12 and CH_14 as both test trucks passed side-by-side over the bridge

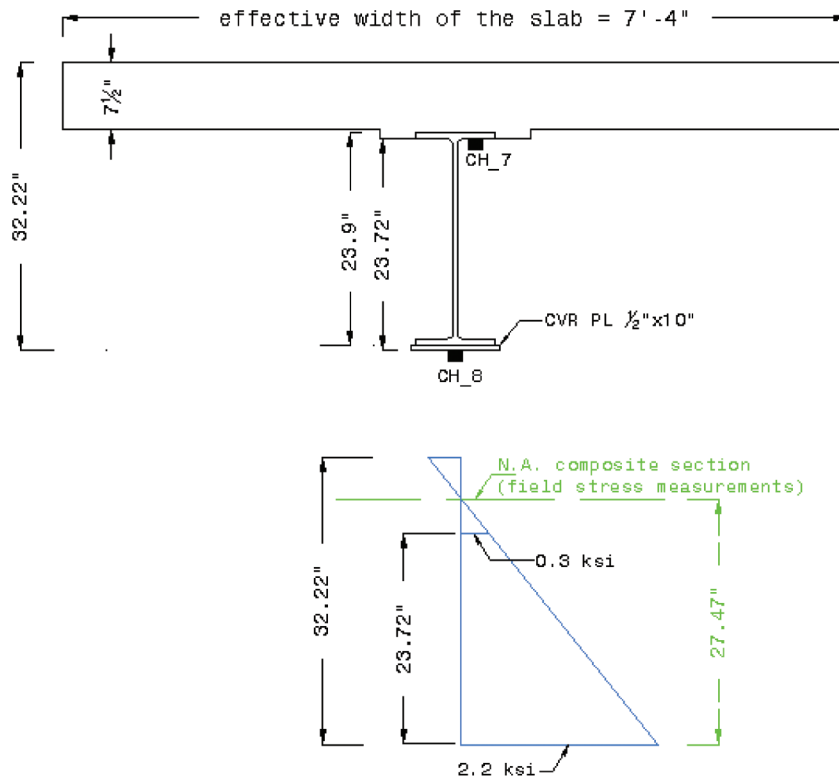


Figure 5.10 Neutral axis of the composite section – from stresses recorded in PARK_2C.DAT.

in the left and middle lanes during crawl test CRL_3.DAT. The figure shows very good load distribution between the girders. Comparing the results of the double truck test to those from the single truck crawl test in left lane (CRL_1.DAT – see section 5.1.1) the responses of CH_6 (Beam #14) and CH_8 (Beam #15) are much greater in the second test (CRL_3.DAT). These channels have a greater response because both trucks load these girders heavily. In the first test (CRL_1.DAT), CH_6 and CH_8 recorded stresses of 2.0 ksi and 0.9 ksi respectively, while in the second test (CRL_3.DAT) these channels recorded stresses of 3.6 ksi and 3.1 ksi respectively.

However, the effect of the second truck has little impact on the exterior girder. Comparing Figure 5.1 and Figure 5.14, the effect of a second truck in the middle lane has little influence on the stress in Beam #12 (CH_2). In other words, all the load of the truck in the middle lane was distributed out among the girders near the middle lane. This is best observed when comparing the stresses recorded during these two tests. In the first test (CRL_1.DAT), CH_2 recorded a maximum stress of approximately 1.1 ksi while in the second test (CRL_3.DAT) a maximum stress of 1.0 ksi was recorded. A similar response is also seen when looking at the first interior girder (Beam #13). Comparing the response of CH_4 for both truck configurations, only a small increase of approximately 0.5 ksi is observed when the second truck is added in the middle lane. A comparison of the maximum bottom flange cover plate stresses recorded for each of these

crawl tests (CRL_1.DAT & CRL_3.DAT) is presented in Table 5.4.

5.4.2 Trucks Side-by-Side in the Left and Middle Lanes – Static Test (PARK_3.DAT)

The double truck static test consisted of both test trucks being parked side-by-side in the left and middle lanes at midspan (2nd Span) for a short period of time while measurements were recorded. Figure 5.15 shows the response during the static test PARK_3.DAT of the same channels considered in Figure 5.14.

The maximum stresses recorded during the side-by-side trucks tests (crawl and static tests) in the left and middle lanes are summarized in Table 5.5. As discussed in section 5.1.2, there are some small differences between the static and crawl tests responses accounted for by the transverse position of the trucks during each test. A comparison of maximum stresses recorded in the single truck static test (PARK_1.DAT) and the trucks side-by-side static test (PARK_3.DAT) is presented in Table 5.6.

5.4.3 Composite Action

As presented in section 5.1.3, to determine if full composite action is being developed between the concrete deck and the steel girder, the neutral axis of the composite section determined from field stress measurements must be located above the position indicated by AASHTO 2010 (2). From Table 5.5 the

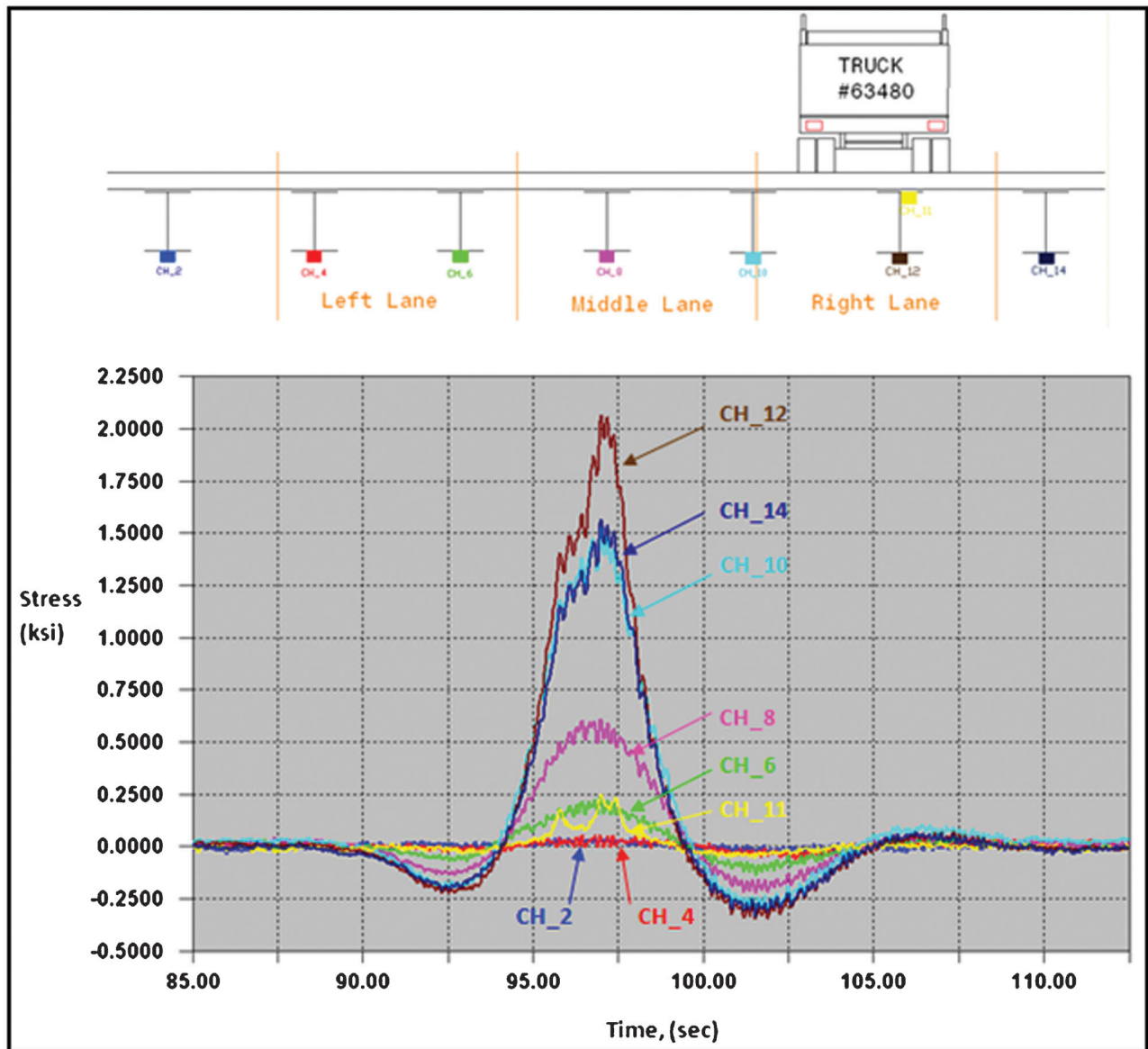


Figure 5.11 Response of strain gages installed at midspan (2nd Span) – Crawl test: single truck in the right lane.

stresses recorded in test PARK_3.DAT by CH_3 (bottom face of top flange) and CH_4 (bottom flange cover plate) are 0.4 ksi and 2.7 ksi, respectively. Figure 5.16 shows the position of the neutral axis of the composite section using the stresses recorded in static test PARK_3.DAT.

Using elastic section properties (linear stress-strain diagram) and similar triangles (Figure 5.16) the position of the neutral axis of the composite section is determined:

$$\frac{2.7 - 0.4}{23.72} = \frac{2.7}{N.A.}$$

$$N.A. = \frac{23.72 \times 2.7}{2.7 - 0.4} = 27.85 \text{ in}$$

The position of the neutral axis of the composite section determined from the field measured stresses is above the position indicated by AASHTO 2010 (2) (see Figure 5.5). Hence, full-composite behavior is developed. As previously discussed in section 5.1.3, this difference is not unusual since there are other factors (parapets and overlay surface) that contribute to the load distribution and composite action in turn influencing the position of neutral axis.

5.5 Trucks Side-by-Side in the Middle and Right Lanes

5.5.1 Trucks Side-by-Side in the Middle and Right Lanes – Crawl Test (CRL_5.DAT)

Figure 5.17 presents the response of CH_2, CH_4, CH_6, CH_7, CH_8, CH_10, CH_12 and CH_14 as

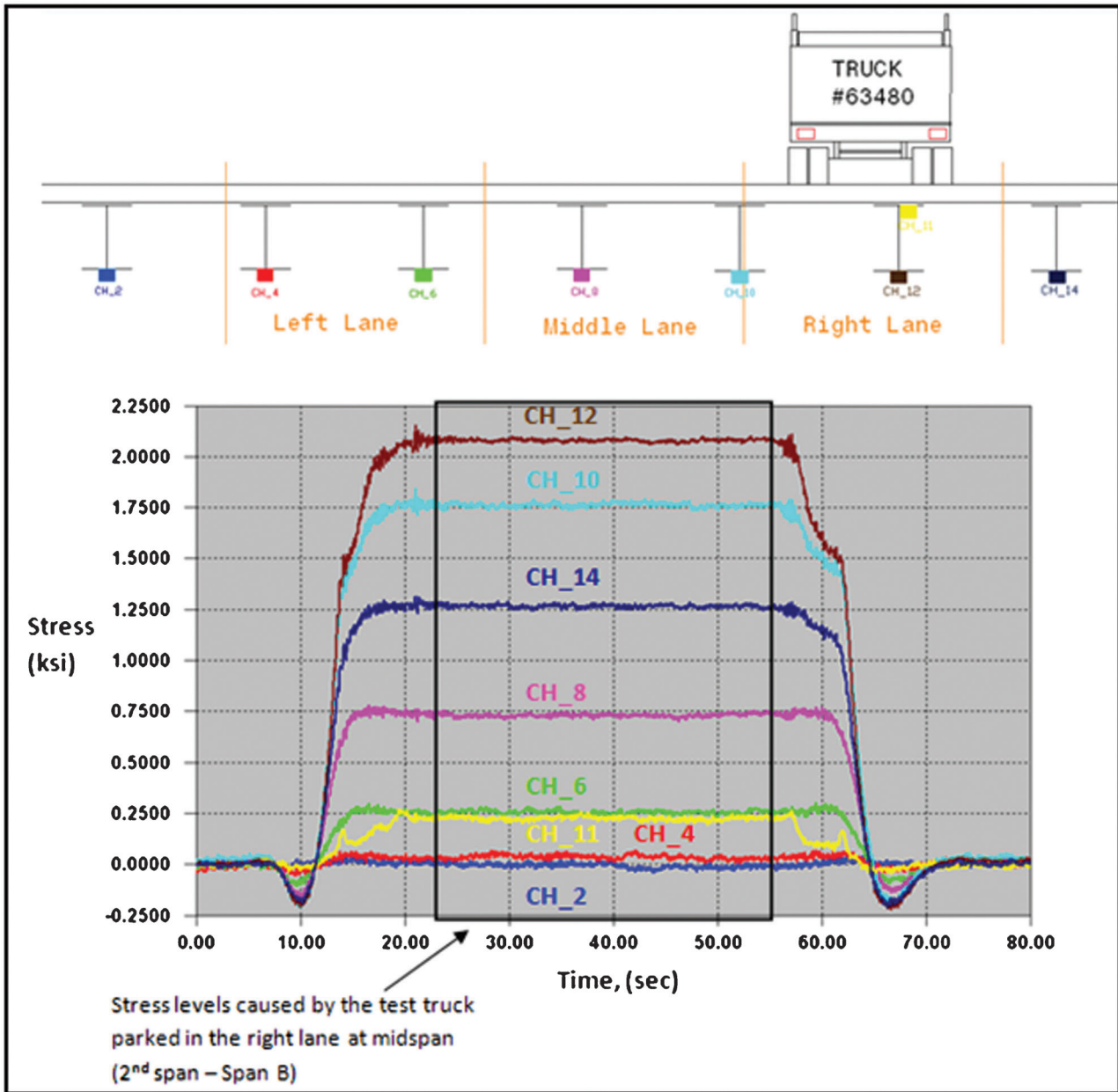


Figure 5.12 Response of strain gages installed at midspan (2nd Span) – *Static test*: single truck in the right lane.

TABLE 5.3
Maximum Stresses – Single Truck Tests in the Right Lane

Channel	CRL_4.DAT Max. Stress (ksi)	PARK_4.DAT Max. Stress (ksi)
CH_2	0.0	0.0
CH_4	0.0	0.1
CH_6	0.2	0.3
CH_8	0.6	0.7
CH_10	1.5	1.8
CH_11	0.2	0.2
CH_12	2.0	2.1
CH_14	1.5	1.3

both test trucks passed side-by-side in the middle and right lanes in crawl test CRL_5.DAT. The same type of behavior (load distribution between the girders) is encountered in this crawl test (CRL_5.DAT) as presented in section 5.4.1. Maximum stresses were recorded in channels located on the girders nearest to the load. In this case CH_8, CH_10 and CH_12 recorded stresses of 2.8 ksi, 3.2 ksi and 2.6 ksi, respectively. Again, as seen in section 5.4.1, by comparing the response of CH_2 (Beam #12) and CH_4 (Beam #13) in both truck configurations (CRL_2.DAT & CRL_5.DAT) it is observed that the presence of a second truck in the right lane has little to no influence on these two (2) girders.

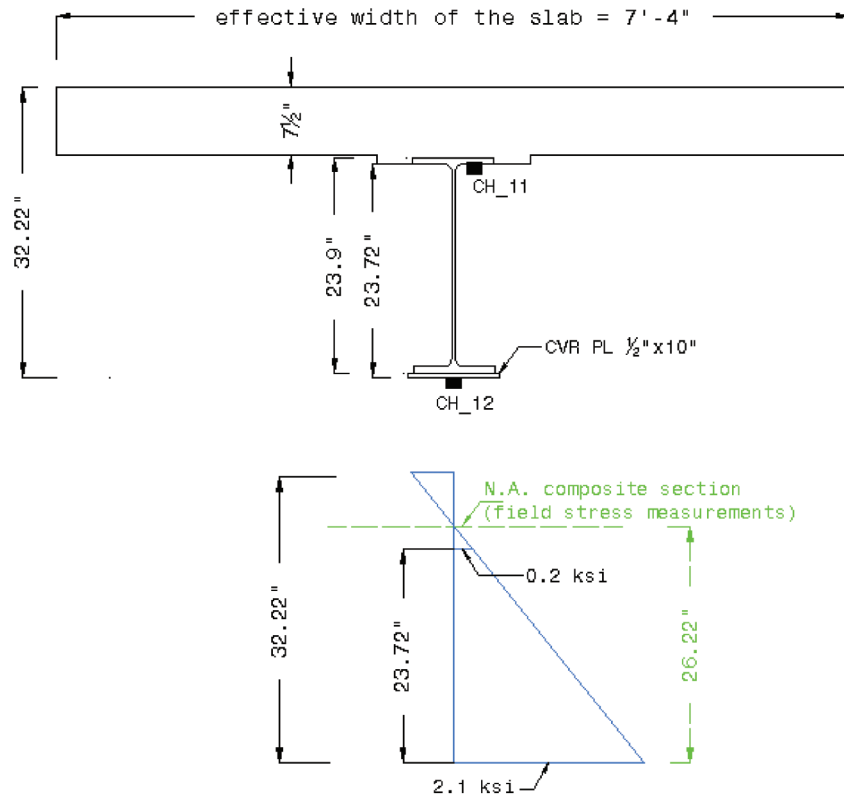


Figure 5.13 Neutral axis of the composite section – from stresses recorded in PARK_4.DAT.

A comparison of stresses recorded in these two crawl tests (CRL_2.DAT & CRL_5.DAT) is presented in Table 5.7.

5.5.2 Trucks Side-by-Side in the Middle and Right Lanes – Static Test (PARK_5.DAT)

The double truck static test consisted of both test trucks being parked side-by-side in the middle and left lanes at midspan (2nd Span) for a short period of time while measurements were recorded. Traffic on I-465 was stopped during the test. Figure 5.18 shows the response during the static test PARK_5.DAT of the same channels considered in Figure 5.17. As discussed in section 5.1.2, there are some small differences between the static and crawl tests response. These differences are attributed to the transverse position of the trucks. The maximum stresses recorded during both side-by-side trucks tests are summarized in Table 5.8. A comparison of maximum stresses recorded during the single truck static test in the middle lane (PARK_2C.DAT) and the two trucks side-by-side static test in the middle and right lanes (PARK_5.DAT) is presented in Table 5.9.

5.5.3 Composite Action

As discussed in section 5.1.3, to determine if full composite action is being developed between the

concrete deck and the steel girder, the neutral axis of the composite section determined from field stress measurements must be located above the position indicated by AASHTO 2010 (2). From Table 5.9 the stresses recorded in test PARK_5.DAT by CH_7 (bottom face of top flange) and CH_8 (bottom flange cover plate) are 0.3 ksi and 2.7 ksi, respectively. Figure 5.19 shows the position of the neutral axis of the composite section using the stresses recorded in static test PARK_5.DAT.

Using elastic section properties (linear stress-strain diagram) and similar triangles (Figure 5.19) the position of the neutral axis of the composite section is determined:

$$\frac{2.7 - 0.3}{23.72} = \frac{2.7}{N.A.}$$

$$N.A. = \frac{23.72 \times 2.7}{(2.7 - 0.3)} = 26.69 \text{ in}$$

The position of the neutral axis of composite section determined from the field measured stresses is above the position indicated by AASHTO 2010 (2) (see Figure 5.5), hence full-composite behavior is developed. As previously explained in section 5.1.3, this difference is not unusual since there are other factors (parapets and overlay surface) that contribute in the load distribution and composite action in turn influencing the position of neutral axis.

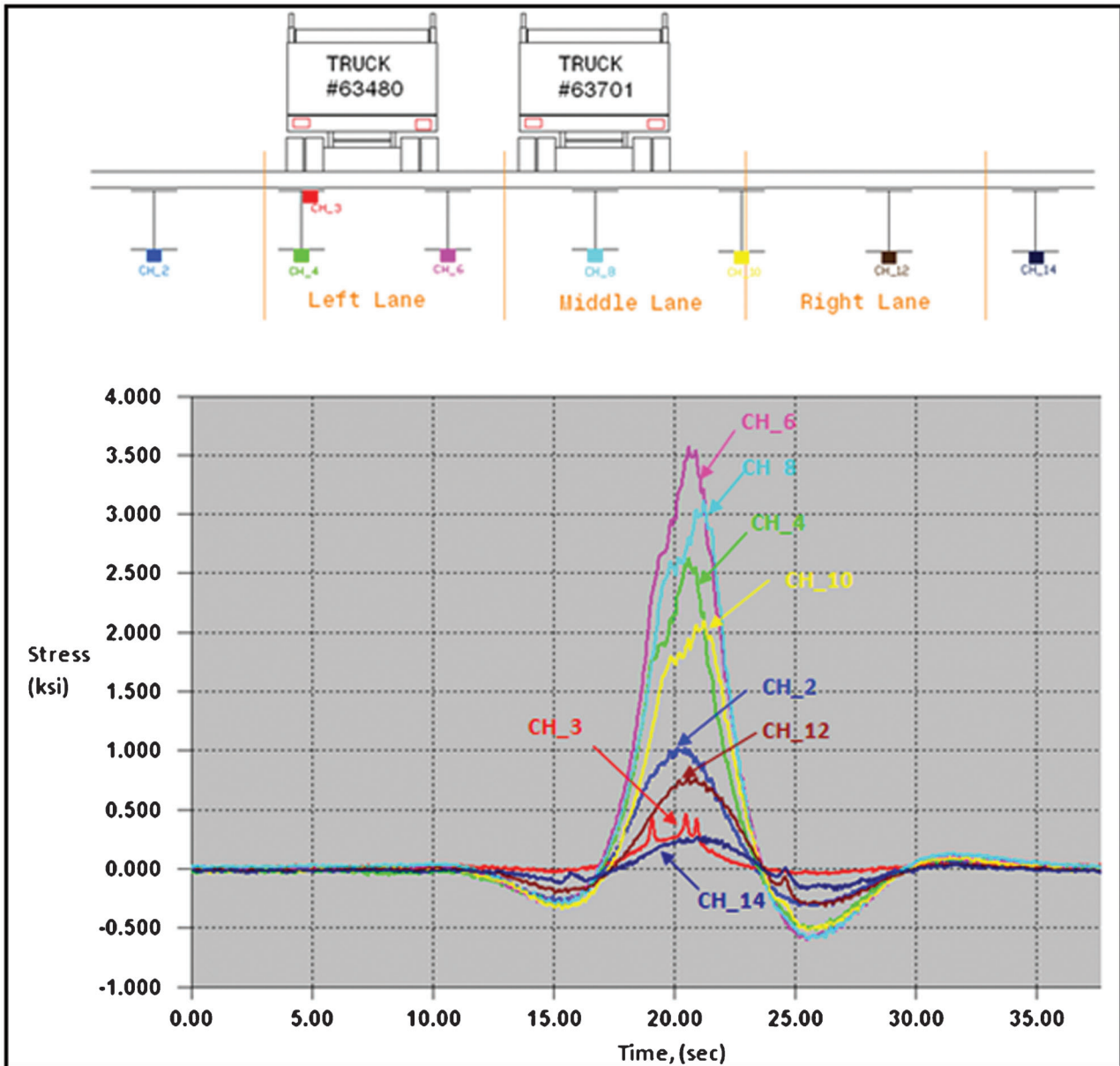


Figure 5.14 Response of strain gages installed at midspan (2nd Span) – Crawl test: trucks side-by-side in the left and middle lanes.

5.6 Under Bridge Snooper Crawl Test in the Left Lane (SNOOP.DAT)

TABLE 5.4
Comparison of Maximum Stresses – CRL_1.DAT and CRL_3.DAT

Channel	CRL_1.DAT Max. Stress (ksi)	CRL_3.DAT Max. Stress (ksi)
CH_2	1.1	1.0
CH_4	2.1	2.6
CH_6	2.0	3.6
CH_8	0.9	3.0
CH_10	0.4	2.0
CH_12	0.1	0.8
CH_14	0.0	0.3

Figure 5.20 presents the response of CH_2, CH_3, CH_4, CH_6, CH_8, CH_10, CH_12 and CH_14 as the under bridge snooper passed over the left lane in crawl test SNOOP.DAT. This test was performed in order to compare the results with those obtained from the single truck crawl test in the left lane (CRL_1.DAT). As expected, the response of the channels was higher in SNOOP.DAT than CRL_1.DAT, as the under bridge snooper weighs approximately 16,000 lbs more than the test truck.

The greatest stress values were recorded in CH_4 and CH_6 for both crawl tests (CRL_1.DAT and SNOOP.DAT). This was because the load was directly

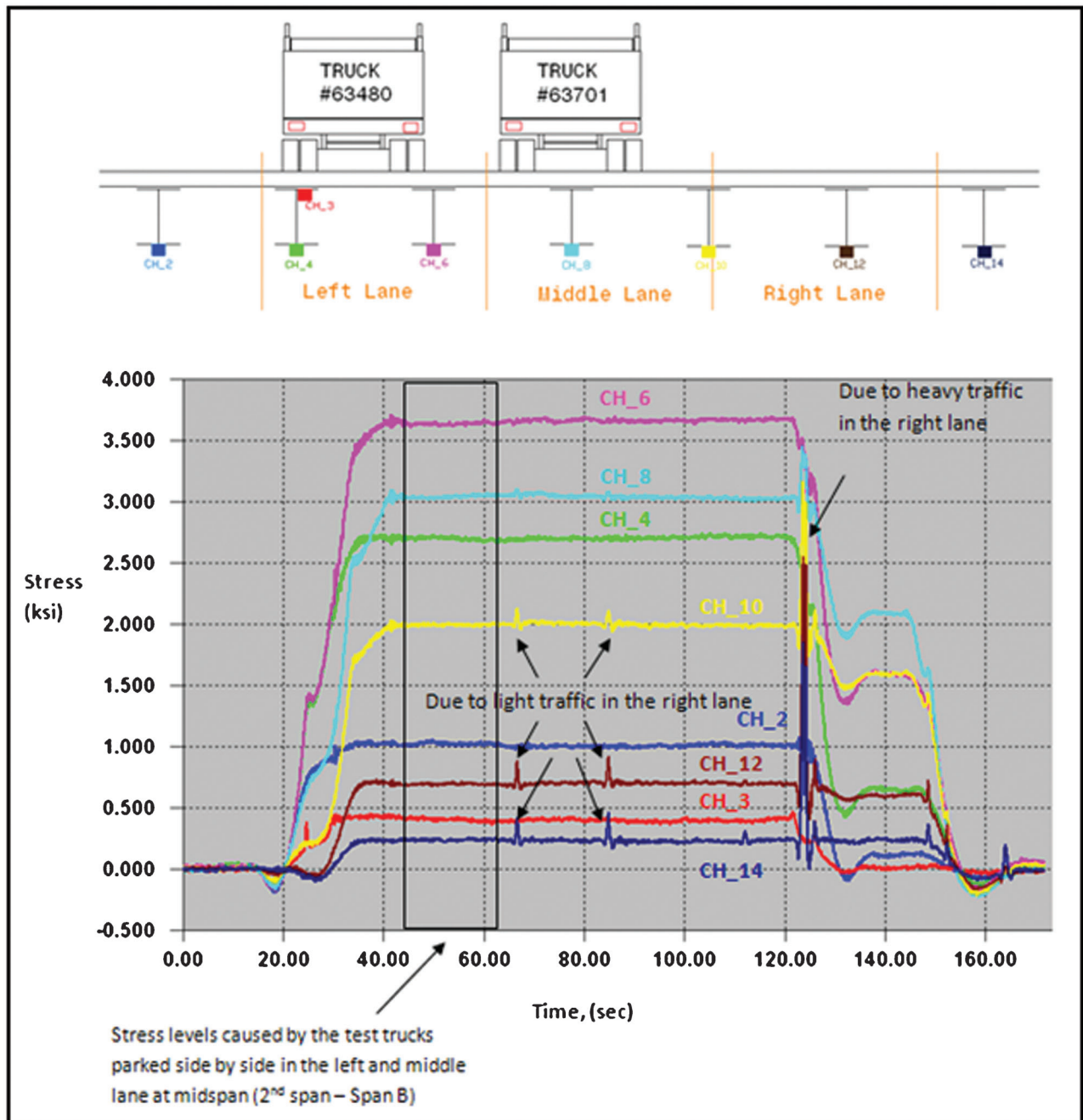


Figure 5.15 Response of strain gages installed at midspan (2nd Span) – *Static test*: trucks side-by-side in the left and middle lanes.

above these channels. For the single truck test (CRL_1.DAT), the maximum recorded values in CH_4 and CH_6 were approximately 2.3 ksi and 2.0 ksi respectively; while, for the snoop test (SNOOP.DAT), the maximum recorded values in these channels were approximately 3.1 ksi and 2.9 ksi respectively. Although the gross weight of the under bridge snoop was approximately 16,000 lbs more than that of the test truck (33% increase), due to a greater axle spacing of the snoop, the load was more longitudinally distributed.

This resulted in moderately higher stresses than in the first test (CRL_1.DAT). Also, it must be taken into consideration that during the tests these vehicles did not pass through the exact same transverse location. A summary of stresses recorded by channels installed at midspan in these two tests is presented in Table 5.10. As presented in sections 4.1 and 4.2, the GVW for Truck #63480 was 48,000 lbs while for the under bridge snoop GVW was estimated at 64,000 lbs, resulting in an approximate GVW ratio of 1.33.

TABLE 5.5
Maximum Stresses – Trucks Side-by-Side Tests in the Left and Middle Lanes

Channel	CRL_3.DAT Max. Stress (ksi)	PARK_3.DAT Max. Stress (ksi)
CH_2	1.0	1.0
CH_3	0.5	0.4
CH_4	2.6	2.7
CH_6	3.6	3.6
CH_8	3.1	3.0
CH_10	2.1	2.0
CH_12	0.8	0.7
CH_14	0.3	0.2

TABLE 5.6
Maximum Stresses – Single Truck Tests in the Left Lane

Channel	PARK_1.DAT Max. Stress (ksi)	PARK_3.DAT Max. Stress (ksi)
CH_2	0.8	1.0
CH_3	0.3	0.4
CH_4	1.9	2.7
CH_6	2.3	3.6
CH_8	1.2	3.0
CH_10	0.5	2.0
CH_12	0.1	0.7
CH_14	0.0	0.2

5.7 Composite Action Summary

As discussed in previous sections, composite action is developed when two load carrying structural members, such as a concrete deck system and the supporting steel beams, are integrally connected and deflect as a single unit. Stresses measured during the controlled load tests were used to construct stress diagrams and calculate the position of neutral axis of the composite section. Table 5.11 summarizes the positions of the neutral axis of the composite section during the controlled load tests.

From Table 5.11 it is observed that the position of the neutral axis of composite section determined from the field measured stresses (stress diagrams) is located above the neutral axis position indicated by AASHTO 2010 (2). This indicates full composite action behavior. As stated, this difference is not unusual since AASHTO 2010 (2) does not take into consideration the influence of the parapets and the overlay surface which all contributes in the load distribution and composite action in turn influencing the position of the neutral axis of the composite section.

5.8 Load Distribution Summary

This section will reveal that the fire did not have any negative effects on the steel superstructure by demonstrating that a good load distribution between the girders is present. Data collected during the controlled

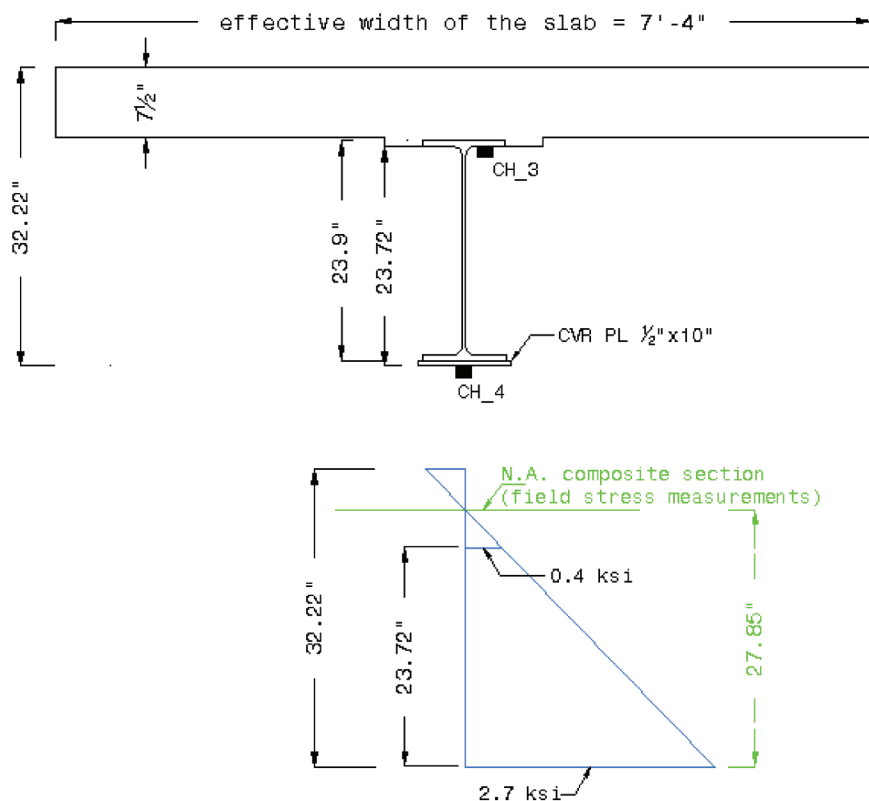


Figure 5.16 Neutral axis of the composite section – from stresses recorded in PARK_3.DAT.

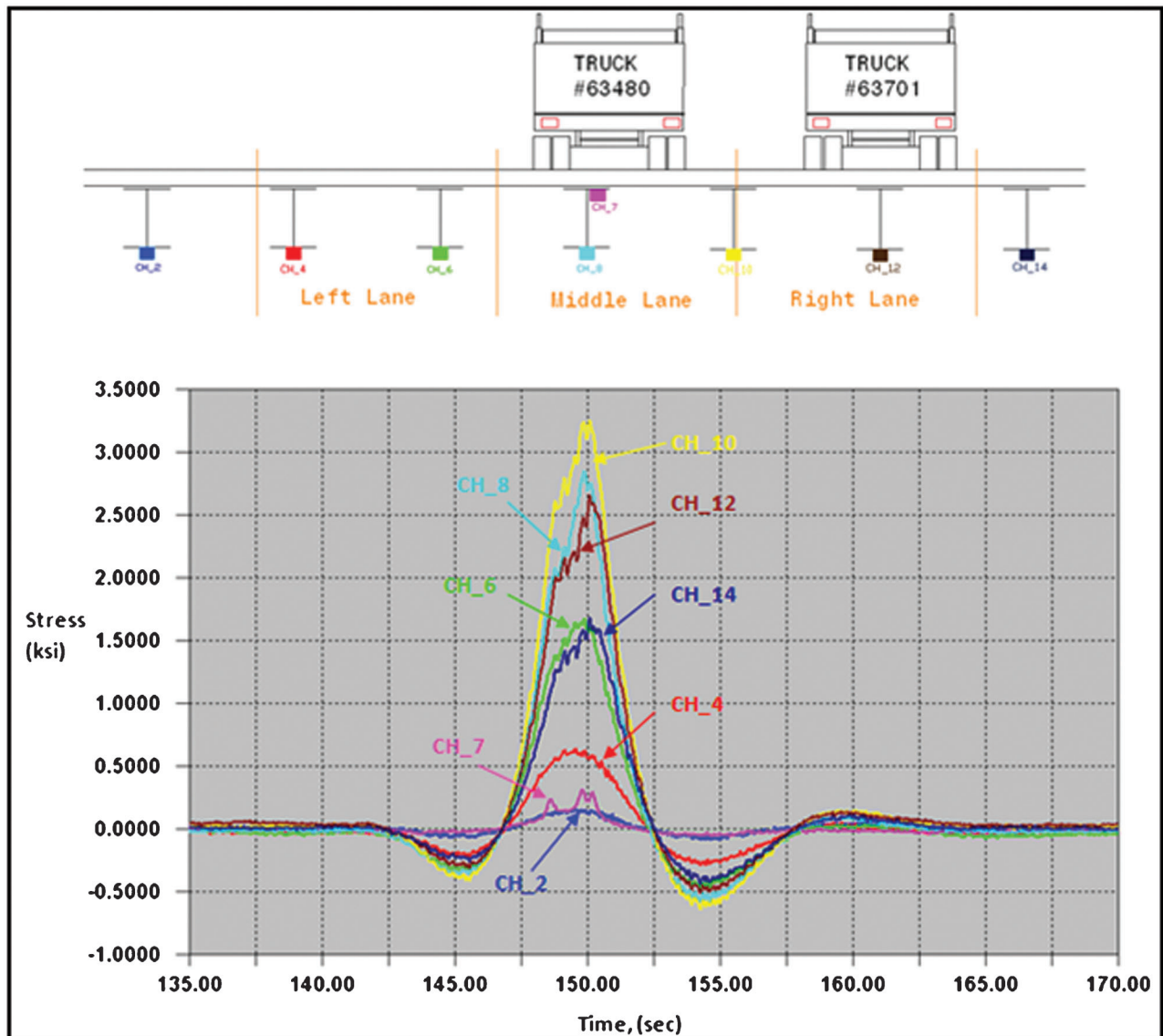


Figure 5.17 Response of strain gages installed at midspan (2nd Span) – Crawl test: trucks side-by-side in the middle and right lanes.

TABLE 5.7
Comparison of Maximum Stresses – CRL_2.DAT and CRL_5.DAT

Channel	CRL_2.DAT Max. Stress (ksi)	CRL_5.DAT Max. Stress (ksi)
CH_2	0.2	0.2
CH_4	0.9	0.6
CH_6	1.9	1.6
CH_7	0.3	0.3
CH_8	2.4	2.8
CH_10	1.6	3.2
CH_12	0.6	2.6
CH_14	0.2	1.6

load testing (static tests) will be used in the load distribution assessment. Distribution load factors will be determined according to AASHO 1965 (1) (the specification used in the original design) and AASHTO 2010 (2) (current specification). These values will then be compared to the distribution load factors obtained from the stress measurements during the controlled load tests (see Table 5.12 and Table 5.13).

5.8.1 Distribution Load Factors – AASHO 1965

Distribution of wheel loads is covered in Section 3 of AASHO 1965 (1). For a bridge with two (2) or more traffic lanes, the distribution load factor for bending moment for interior longitudinal beams is calculated as follows:

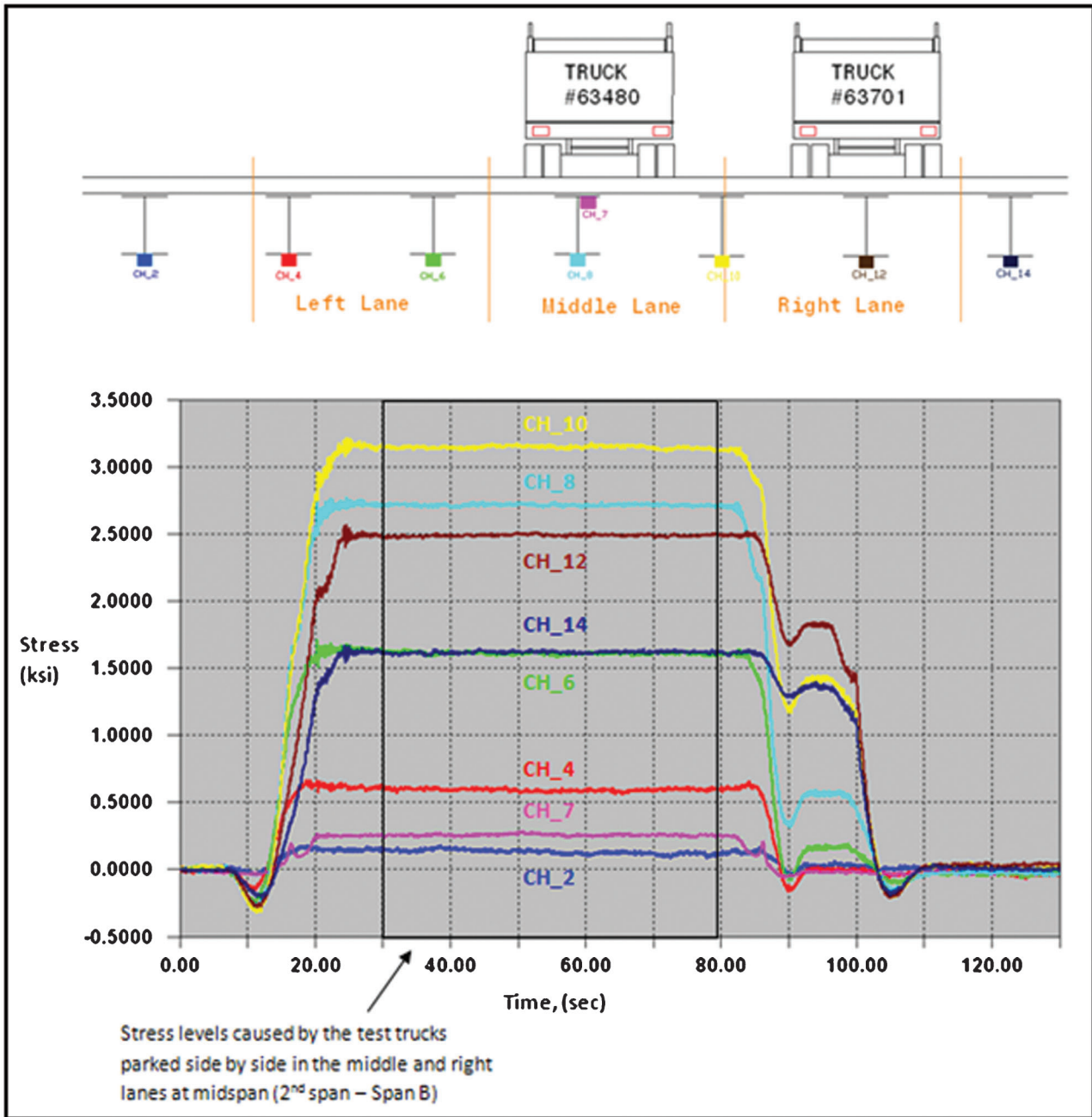


Figure 5.18 Response of strain gages installed at midspan (2nd Span) – *Static test*: trucks side-by-side in the middle and right lanes.

$$DF = \frac{S}{5.5} = \frac{7' - 4''}{5.5} = \frac{7.33'}{5.5} = 1.33$$

Where:

S = distance in feet between outside and adjacent interior stringers (S < 14')

For *exterior longitudinal beams*, the distribution load factor for bending moment is determined as follows:

$$DF = \frac{S}{4.0 + 0.25S} = \frac{7.33'}{4.0 + 0.25 \times 7.33'} = 1.26$$

Where:

S = distance in feet between outside and adjacent interior stringers (6' < S < 14')

It is important to note that these distribution factors (*DF*) are applied to wheel loads (one set of wheels – front and rear). Thus, the distribution factors obtained

TABLE 5.8
Maximum Stresses – Trucks Side-by-Side in the Middle and Right Lanes

Channel	CRL_5.DAT Max. Stress (ksi)	PARK_5.DAT Max. Stress (ksi)
CH_2	0.2	0.1
CH_3	0.6	0.6
CH_4	1.6	1.6
CH_6	0.3	0.3
CH_8	2.8	2.7
CH_10	3.2	3.1
CH_12	2.6	2.5
CH_14	1.6	1.6

TABLE 5.9
Comparison of Maximum Stresses – PARK_2C.DAT and PARK_5.DAT

Channel	PARK_2C.DAT Max. Stress (ksi)	PARK_5.DAT Max. Stress (ksi)
CH_2	0.2	0.1
CH_4	0.9	0.6
CH_6	1.9	1.6
CH_7	0.3	0.3
CH_8	2.4	2.7
CH_10	1.6	3.1
CH_12	0.6	2.5
CH_14	0.2	1.6

from AASHTO 2010 (2) and field measured stress values need to be multiplied by two (2) when compared to these values.

5.8.2 Distribution Load Factors – AASHTO 2010

The distribution factors for AASHTO 2010 (2) are covered in Section 4: Structural Analysis and Evaluation. Distribution factors per lane for moment in the interior longitudinal beams are determined according to Table 4.6.2.2b-1 as follows:

Case I: One Design Lane Loaded

$$DF = 0.06 + \left(\frac{S}{14}\right)^{0.4} \cdot \left(\frac{S}{L}\right)^{0.3} \cdot \left(\frac{K_g}{12.0 \cdot L \cdot t_s^3}\right)^{0.1}$$

Case II: Two or More Design Lanes Loaded

$$DF = 0.075 + \left(\frac{S}{9.5}\right)^{0.6} \cdot \left(\frac{S}{L}\right)^{0.2} \cdot \left(\frac{K_g}{12.0 \cdot L \cdot t_s^3}\right)^{0.1}$$

Where:

S = spacing of beams or webs – ft – ($3.5 \leq S \leq 16.0$)

L = span of beam – ft – ($20 \leq L \leq 240$)

t_s = depth of concrete slab – in – ($4.5 \leq t_s \leq 12.0$)

K_g = longitudinal stiffness parameter – in^4 – ($10000 \leq K_g \leq 7000000$)

Also, for the above equations to apply for the distribution load factors, the minimum number of beams is four (4). All of the above conditions are met by the I-465 bridges.

The longitudinal stiffness parameter K_g is determined as follows:

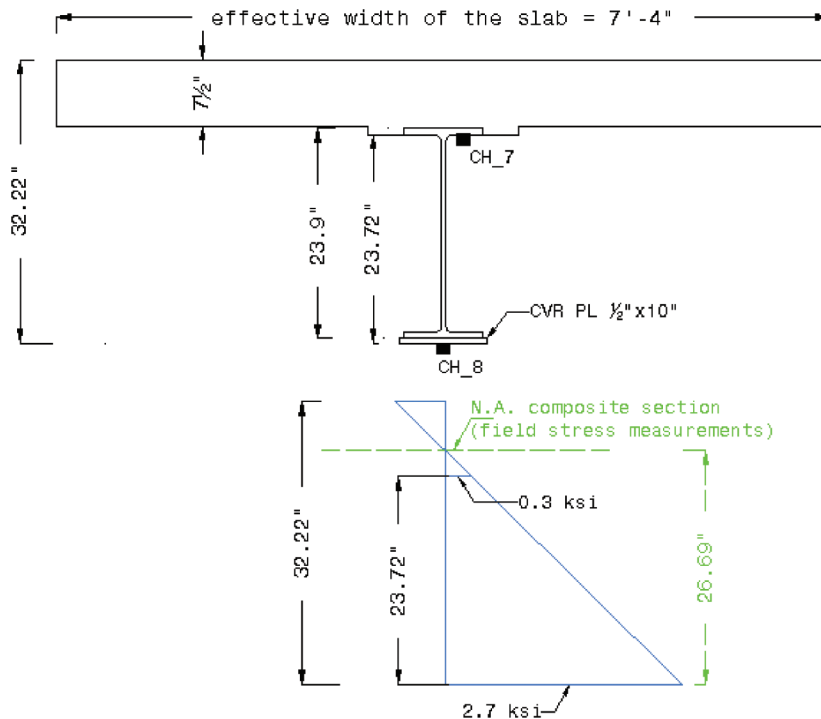


Figure 5.19 Neutral axis of the composite section – from stresses recorded in PARK_5.DAT.

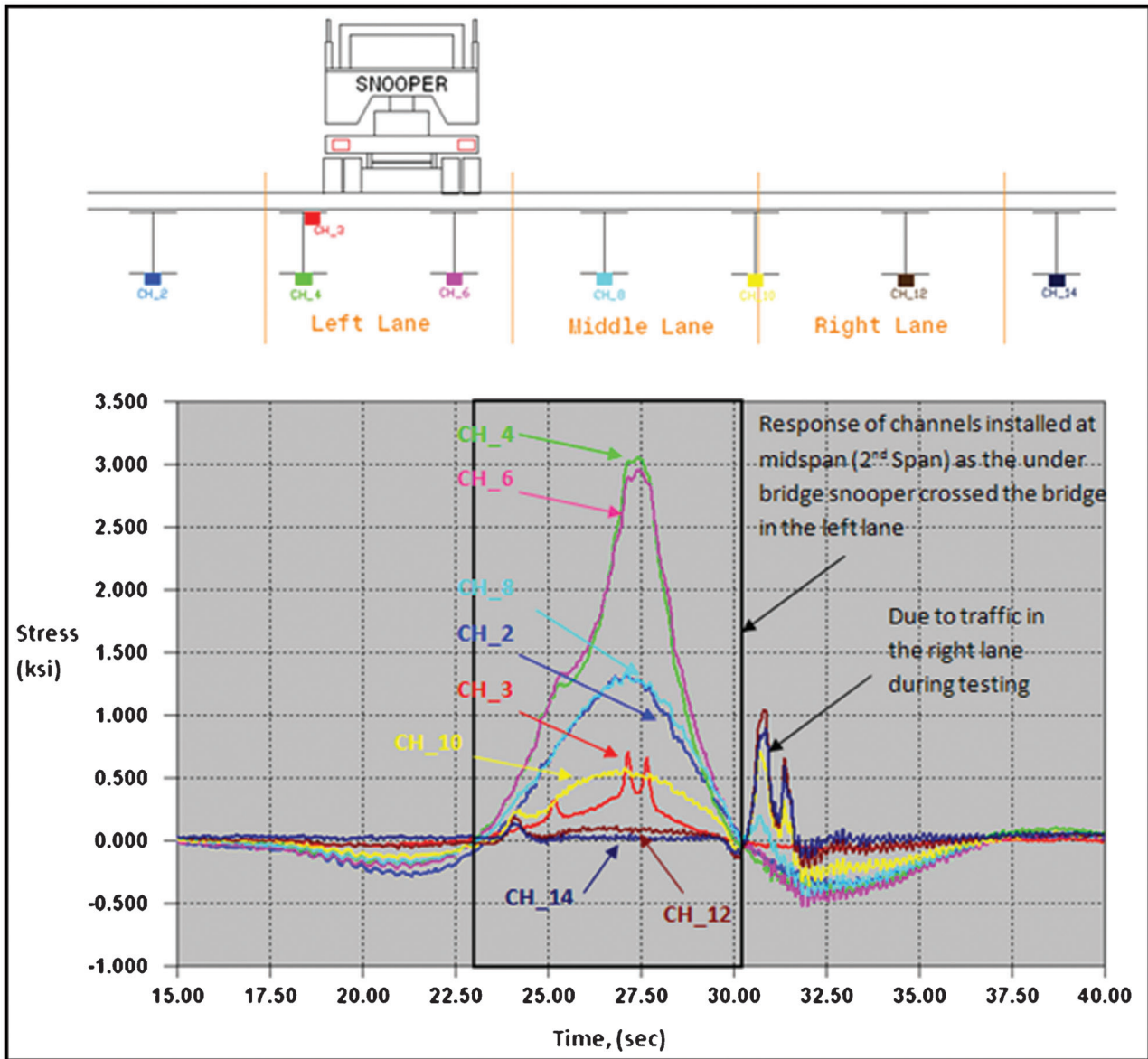


Figure 5.20 Response of strain gages installed at midspan (2nd Span) – Crawl test: under bridge snooper in the left lane.

$$K_g = n(I + A \cdot e_g^2)$$

Where:

n= modulus ratio;

$$n = \frac{E_B}{E_D}$$

E_B = modulus of elasticity of beam material (ksi)

E_D = modulus of elasticity of deck material (ksi)

I = moment of inertia of beam (in.⁴)

A = area of beam (in.²)

e_g = distance between the centers of gravity of the basic beam and deck (in.)

Determine the longitudinal stiffness parameter (K_g) (see Figure 5.21):

TABLE 5.10
Stresses Recorded in Crawl Tests: SNOOP.DAT and CRL_1.DAT

Channel	SNOOP.DAT Max. Stress (ksi)	CRL_1.DAT Max. Stress (ksi)	Ratio of Stresses
CH_2	1.3	1.1	1.18
CH_3	0.7	0.4	1.75
CH_4	3.1	2.1	1.48
CH_6	2.9	2.0	1.45
CH_8	1.3	0.9	1.44
CH_10	0.6	0.4	1.50
CH_12	0.1	0.1	1.00
CH_14	0.0	0.0	1.00

TABLE 5.11
Neutral Axis Positions

Controlled Load Test	N.A. of Girder & Cover Plate* (Only)	N.A. of Concrete Deck* (Only)	N.A. of Composite Section (AASHTO 2010)*	N.A. of Composite Section (Stress Diagrams)*
PARK_1.DAT	10.23"	28.42"	23.47"	28.17"
PARK_2C.DAT	10.23"	28.42"	23.47"	27.47"
PARK_4.DAT	10.23"	28.42"	23.47"	26.22"
PARK_3.DAT	10.23"	28.42"	23.47"	27.85"
PARK_5.DAT	10.23"	28.42"	23.47"	26.69"

*N.A. = neutral axis.

NOTE: Distances are referenced from the bottom face of the cover plate – see Figure 5.5.

TABLE 5.12
Response of Strain Gages Installed at Midspan (2nd Span) – Static tests: Single Truck

Channel	(PARK_1.DAT)	(PARK_2C.DAT)	(PARK_4.DAT)
	Max. Stress (ksi)	Max. Stress (ksi)	Max. Stress (ksi)
CH_2	0.8	0.2	0.0
CH_4	1.9	0.6	0.1
CH_6	2.3	1.5	0.3
CH_8	1.2	2.2	0.7
CH_10	0.5	1.7	1.8
CH_12	0.1	0.6	2.1
CH_14	0.0	0.3	1.3

$$E_{concrete} = 1820\sqrt{f'_c} = 1820\sqrt{3ksi} = 3,152ksi$$

$$n = \frac{E_{steel}}{E_{concrete}} = \frac{29,000ksi}{3,152ksi} = 9.2 \cong 9.00$$

Determine the moment of inertia of the beam (I):

$$A_1 = 22.4in^2$$

$$I_1 = 2100in^4$$

$$A_2 = 0.5in \times 10in = 5in^2$$

$$A = A_1 + A_2 = 22.4in^2 + 5in^2 = 27.4in^2$$

$$I_2 = \frac{bh^3}{12} = \frac{10 \times 0.5^3}{12} = 0.104in^2$$

$$y_{cog} = \frac{y_1A_1 + y_2A_2}{A_1 + A_2} = \frac{(0.5in + 11.95in) \times 22.4in^2 + 0.25in \times 5in^2}{22.4in^2 + 5in^2} = 10.23in$$

$$I = I_1 + A_1d_1^2 + I_2 + A_2d_2^2$$

$$I = 2100in^4 + 22.4in^2(0.5in + 11.95in - 10.23in)^2 + 0.104in^4 + 5in^2(10.23in - 0.25in)^2$$

$$I = 2708.5in^4$$

Determine the distance between the centers of gravity (e_g):

$$A_{total-conc.deck} = 88in \times 7.5in + 2 \times 4in \times 1in = 668in^2$$

$$y_{conc.deck} =$$

$$\frac{(0.5in + 23.9in + 0.32in + 3.75in) \times (88in \times 7.5in) + (0.5in + 23.9in - 0.68in + 0.25in) \times 8in^2}{668in^2}$$

$$y_{conc.deck} = 28.42in$$

$$e_g = 28.42in - 10.23in = 18.19in$$

Then:

$$K_g = 90 \times \left[2708.5in^4 + 27.4in^2 \times (18.19in)^2 \right] = 105,971in^4$$

TABLE 5.13
Response of Strain Gages Installed at Midspan (2nd Span) – Static tests: Trucks Side-by-Side

Channel	(PARK_3.DAT)	(PARK_5.DAT)
	Max. Stress (ksi)	Max. Stress (ksi)
CH_2	1.0	0.1
CH_4	2.7	0.6
CH_6	3.6	1.6
CH_8	3.0	2.7
CH_10	2.0	3.1
CH_12	0.7	2.5
CH_14	0.2	1.6

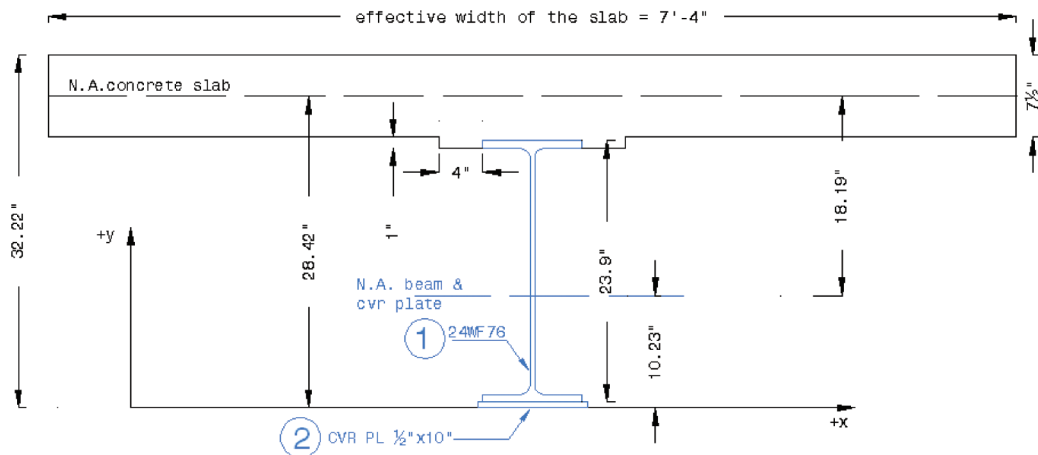


Figure 5.21 Sketch for determination of the longitudinal stiffness parameter K_g .

Finally, the distribution factors (per lane) for moment in *interior longitudinal beams* can be calculated:

Case I: One Design Lane Loaded

$$DF = 0.06 + \left(\frac{7.33}{14}\right)^{0.4} \cdot \left(\frac{7.33}{55.5}\right)^{0.3} \cdot \left(\frac{105,971}{12.0 \cdot 55.5 \cdot 7.5^3}\right)^{0.1}$$

$$DF = 0.06 + (0.77 \cdot 0.55 \cdot 0.91) = 0.45$$

Case II: Two or More Design Lanes Loaded

$$DF = 0.075 + \left(\frac{7.33}{9.5}\right)^{0.6} \cdot \left(\frac{7.33}{55.5}\right)^{0.2} \cdot \left(\frac{105,971}{12.0 \cdot 55.5 \cdot 7.5^3}\right)^{0.1}$$

$$DF = 0.075 + (0.86 \cdot 0.67 \cdot 0.91) = 0.6$$

The distribution factors (per lane) for moment in *exterior longitudinal beams* are determined according to Table 4.6.2.2d-1 as follows:

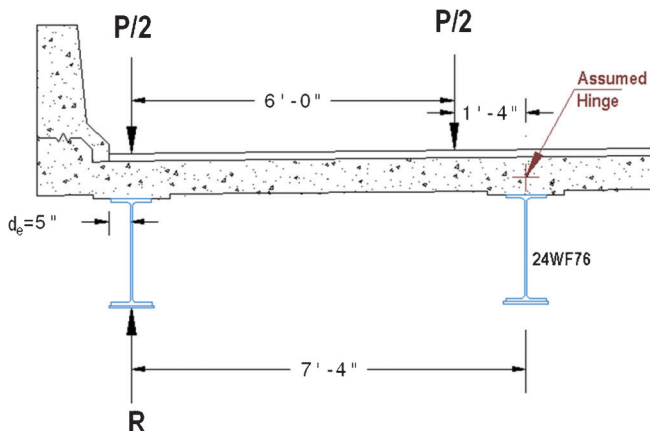


Figure 5.22 Distribution load factor – exterior longitudinal beam – Lever Rule.

Case I: One Design Lane Loaded

DF - determined with Lever Rule (see Figure 5.22) From Figure 5.22:

$$R \times 88in - \frac{P}{2} \times 88in - \frac{P}{2} \times 16in = 0$$

$$R \times 88in = \frac{P}{2} \times 104in$$

$$R = 0.59P$$

$$DF = 0.59$$

Case II: Two or More Design Lanes Loaded

In this case the distribution factor is obtained from the equation presented in Case II for *interior longitudinal beam* modified by the following factor:

$$0.77 + \frac{d_e}{9.1}$$

Where:

d_e = distance between the exterior web of exterior girder to the face of traffic barrier (ft.) ($d_e = 5'$, see Figure 5.22)

Then:

$$DF = \left(0.77 + \frac{d_e}{9.1}\right) \times 0.6 = \left(0.77 + \frac{0.42}{9.1}\right) \times 0.6 = 0.49$$

5.8.3 Distribution Factors Determined from Stress Measurements – Controlled Load Tests

In order to determine the distribution factors, the section properties of the composite section need to be determined first. Following is a summary, showing the calculations for both cases: interior and exterior beam.

Neutral axis of the beam and cover plate:

$$A_{cvr-plate} = 10in \times 0.5in = 5in^2$$

$$A_{beam24W76} = 22.4in^2$$

$$A_{total} = 22.4in^2 + 5in^2 = 27.4in^2$$

$$y_{beam-cvrplate} = \frac{(11.95in + 0.5in) \times 22.4in^2 + 0.25in \times 5in^2}{27.4in^2}$$

$$= 10.23in$$

Neutral axis of the concrete deck (includes the haunch detail):

$$A_{total-conc.deck} = 88in \times 7.5in + 2 \times 4in \times 1in = 668in^2$$

$$y_{conc.deck} =$$

$$\frac{(0.5in + 23.9in + 0.32in + 3.75in) \times (88in \times 7.5in) + (0.5in + 23.9in - 0.68in + 0.25in) \times 8in^2}{668in^2}$$

$$y_{conc.deck} = 28.42in$$

Neutral axis of the composite section:

$$E_{concrete} = 1820\sqrt{f'_c} = 1820\sqrt{3ksi} = 3,152ksi$$

$$n = \frac{E_{steel}}{E_{concrete}} = \frac{29,000ksi}{3,152ksi} = 9.2 \cong 9.00$$

$$y_{comp.sec t} = \frac{(27.4in^2 \times 10.23in) + \left(7.5in \times \frac{88in}{9}\right) \times 28.42in}{\left(27.4in^2 + 7.5in \times \frac{88in}{9}\right)}$$

$$= 23.47in$$

Determine the moment of inertia (I) for the composite section:

$$I_{comp.sec t} = I_1 + A_1 \cdot d_1^2 + I_2 + A_2 \cdot d_2^2$$

Determine the moment of inertia of the beam and cover plate (I_1):

$$A_{beam} = 22.4in^2$$

$$A_{cvr.plate} = 0.5in \times 10in = 5in^2$$

$$I_{beam} = 2100in^4$$

$$I_{cvr.plate} = \frac{b \cdot h^3}{12} = \frac{10 \cdot 0.5^3}{12} = 0.104in^2$$

$$I_1 = I_{beam} + A_{beam} \cdot d_{beam}^2 + I_{cvr.plate} + A_{cvr.plate} \cdot d_{cvr.plate}^2$$

$$I_1 = 2100in^4 + 22.4in^2 \cdot (0.5in + 11.95in - 10.23in)^2 + 0.104in^2 + 5in^2 \cdot (10.23in - 0.25in)^2$$

$$I_1 = 2708.5in^4$$

$$A_1 = A_{beam} + A_{cvr.plate} = 22.4in^2 + 5in^2 = 27.4in^2$$

Determine the moment of inertia of the concrete deck (I_2):

$$A_2 = A_{total-conc.deck} = 668in^2$$

$$y_{conc.deck} = 28.42in$$

$$I_2 = I_{conc.deck} = \frac{b \cdot h^3}{12} = \frac{88in \cdot (7.5in)^3}{12} = 3094in^4$$

Then:

$$I_{comp.sec t} = I_1 + A_1 \cdot d_1^2 + I_2 + A_2 \cdot d_2^2$$

$$I_{comp.sec t} = 2708.5in^4 + 27.4in^2 \cdot (23.47in - 10.23in)^2 + 3094in^4 + 668in^2 \cdot (28.42in - 23.47in)^2$$

$$I_{comp.sec t} = 26,973in^4$$

Neutral axis of the beam and cover plate:

$$A_{cvr-plate} = 10in \times 0.5in = 5in^2$$

$$A_{beam24W76} = 22.4in^2$$

$$A_{total} = 22.4in^2 + 5in^2 = 27.4in^2$$

$$y_{beam-cvrplate} = \frac{(11.95in + 0.5in) \times 22.4in^2 + 0.25in \times 5in^2}{27.4in^2}$$

$$= 10.23in$$

Neutral axis of the concrete deck (includes the haunch detail):

$$A_{total-conc.deck} = 65in \times 7.5in + 2 \cdot 4in \cdot 1in = 495.5in^2$$

$$y_{conc.deck} =$$

$$\frac{(65in + 7.5in) \times (0.5in + 23.9in + 0.32in + 3.75in) + 8in^2 \times (0.5 + 23.9in - 0.68in + 0.25in)}{495.5in^2}$$

$$y_{conc.deck} = 28.40in$$

Neutral axis of the composite section:

$$E_{concrete} = 1820\sqrt{f'_c} = 1820\sqrt{3ksi} = 3,152ksi$$

$$n = \frac{E_{steel}}{E_{concrete}} = \frac{29,000ksi}{3,152ksi} = 9.2 \cong 9.00$$

$$y_{comp.sec t} = \frac{(27.4in \times 10.23in) + \left(7.5in \times \frac{65in}{9}\right) \times 28.40in}{\left(27.4in^2 + 7.5in \times \frac{65in}{9}\right)}$$

$$= 22.30in$$

The moment of inertia of the beam and cover plate (I_1) was determined previously:

$$I_1 = 2708.5in^4$$

$$A_1 = A_{beam} + A_{cvr.plate} = 22.4in^2 + 5in^2 = 27.4in^2$$

Determine the moment of inertia of the concrete deck (I_2):

TABLE 5.14
Stresses Measured during the Static Controlled Load Tests and Section Properties of the Composite Section

Channel	Max. Stresses Measured during the Static (Parked) Controlled Load Tests (ksi)					Section Properties (Composite Section)*	
	PARK_1.DAT	PARK_2C.DAT	PARK_4.DAT	PARK_3.DAT	PARK_5.DAT	I (in^4)	c (in)
CH_2	0.8	0.2	0.0	1.0	0.1	27,423	22.30
CH_4	1.9	0.6	0.1	2.7	0.6	26,973	23.47
CH_6	2.3	1.5	0.3	3.6	1.6	26,973	23.47
CH_8	1.2	2.2	0.7	3.0	2.7	26,973	23.47
CH_10	0.5	1.7	1.8	2.0	3.1	26,973	23.47
CH_12	0.1	0.6	2.1	0.7	2.5	26,973	23.47
CH_14	0.0	0.3	1.3	0.2	1.6	26,973	23.47

* I and c were determined for the composite section (see Figure 5.23 and Figure 5.24).

$$A_2 = A_{total - conc. deck} = 495.5 in^2$$

$$y_{conc. deck} = 28.40 in$$

$$I_2 = I_{conc. deck} = \frac{b \cdot h^3}{12} = \frac{65 in \cdot (7.5 in)^3}{12} = 2285 in^4$$

Determine the moment of inertia (I) for the composite section:

$$I_{comp. sect} = I_1 + A_1 \cdot d_1^2 + I_2 + A_2 \cdot d_2^2$$

$$I_{comp. sect} = 2708.5 in^4 + 27.4 in^2 \cdot (22.30 in - 10.23 in)^2 + 2285 in^4 + 495.5 in^2 \cdot (28.40 in - 22.30 in)^2$$

$$I_{comp. sect} = 27,423 in^4$$

Now that the section properties of the composite section are known, the moments can be determined from the stresses recorded during the controlled load tests. Table 5.14 and Table 5.15 summarize the

section properties along with the moments calculated from the stresses recorded during the controlled load tests.

The data presented in Figure 5.25, show the moments determined from measured stresses during the single truck controlled load tests (see Table 5.15 for raw values).

The data presented in Figure 5.26 show how the load was distributed among the girders during the single truck controlled load tests. When the test truck is parked in the left lane, the maximum percentage of the total load received by an interior girder, in this case Beam #14 - CH_6, is 34% (DF = 0.34). The maximum percentage of the total load received by the exterior girder, in this case Beam #12 - CH_2, is only 12 % (DF = 0.12). A comparison of these values with those obtained from AASHTO 1965 (1) and AASHTO 2010 (2) (see sections 5.8.1 and 5.8.2) shows the specification values being higher. This is expected since the load is also distributed longitudinally, while the specifications do not take this into consideration, offering a more conservative estimate of the portion of the load distributed to one of the

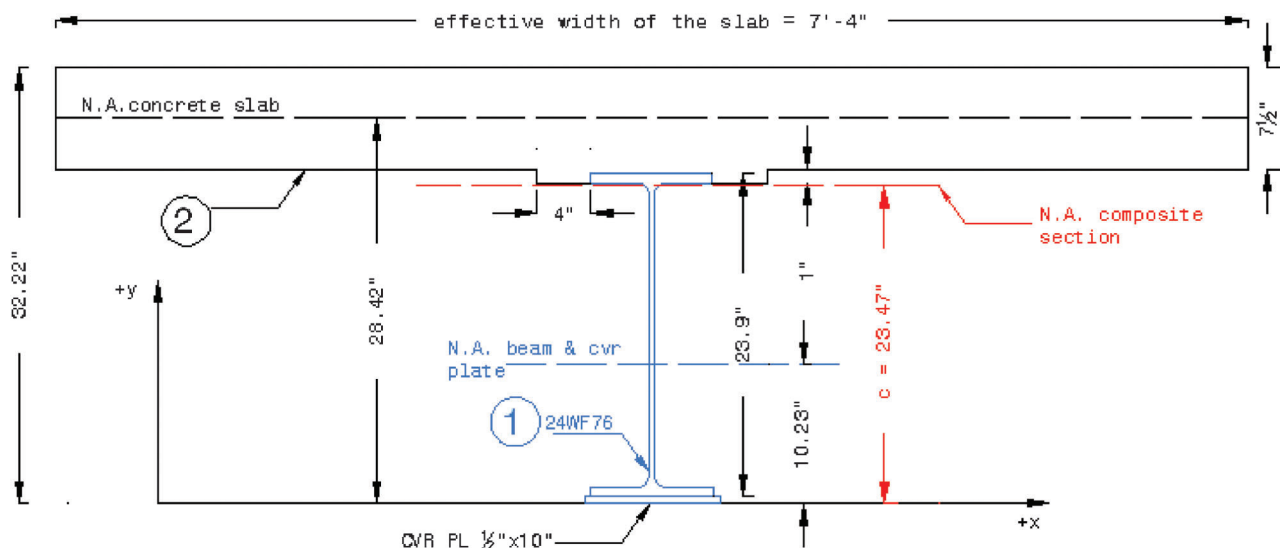


Figure 5.23 Section properties – composite section (interior beam case).

girders. It is also worth noting that the AASHTO equations for distribution factor need to account for minor skews, many types of girders, and different section properties (*i.e., estimated vs. actual effective width*). Hence, the agreement between the calculated and measured distribution factors is acceptable.

An average maximum distribution factor of 33% (DF = 0.33) was determined from the controlled load tests (see Figure 5.26) for the interior beam with one lane loaded. For the exterior girder, a distribution factor of 0.63 was determined according to AASHTO 1965 (1) ($1.26/2 = 0.63$, see section 5.8.1) and 0.59 according to AASHTO 2010 (2) using the lever rule (see section 5.8.2). From the measured stresses during the single truck test in the left lane, a distribution factor of 12% (DF = 0.12) was determined for the exterior girder (Beam#12). However, during the controlled load test, the position of the truck was 8.75 feet away from the concrete parapet (see APPENDIX A–Drawing#9). Conversely, while determining the distribution factor according to AASHTO 2010 (2) for the exterior girder using the lever rule, the worst case scenario was chosen (5 inches away from the concrete parapet, directly above the exterior girder, see Figure 5.22). This is done in design for the extreme situations that may occur during the life of the bridge. Using the lever rule, according to AASHTO 2010 (2), for the exterior beam load distribution factor and considering the truck positioned 8.75 feet away from the concrete barrier (as in PARK_1.DAT) the distribution factor calculated this way would be DF = 0.17 or 17%. This would be closer to what was determined from the field measurements (DF = 0.12 or 12%).

The data presented in Figure 5.27, show the moments determined from measured stresses during the side-by-side trucks controlled load tests (see Table 5.15 for raw values). The graphs presented in Figure 5.28 show how the load was distributed among the girders during the side-by-side trucks controlled load tests.

Comparing the graphs in Figure 5.28, for single truck tests and side-by-side truck tests (Figure 5.25 and Figure 5.27), and using the moments summarized in Table 5.15, the load effects can be verified using superposition. For example the moments produced by the single truck in left lane (PARK_1.DAT) added with the moments produced by the single truck in the middle lane (PARK_2C.DAT) should be the same as the moments produced by the side-by-side trucks in the left and middle lane (PARK_3.DAT). Table 5.16 summarizes the superposition of loads for all the static controlled load tests.

From Table 5.16 it is observed that the moments from the side-by-side tests are very close to those obtained from superposition of single truck tests. There are mainly two (2) reasons for the small differences outlined in column eight (8) of the table. First, there are small differences between the test trucks like: geometry (axle, wheel spacing) and weight (gross weight, axle weight). Figure 4.2 and Figure 4.3 from Chapter 4 are diagrams of the tests trucks and outline these geometric and weight differences. This is important since only truck #63480 was used in the single truck tests. Second, the transverse positions of the truck(s) during the parked tests were not identical. For example, during the single truck test in the left lane (PARK_1.DAT) the

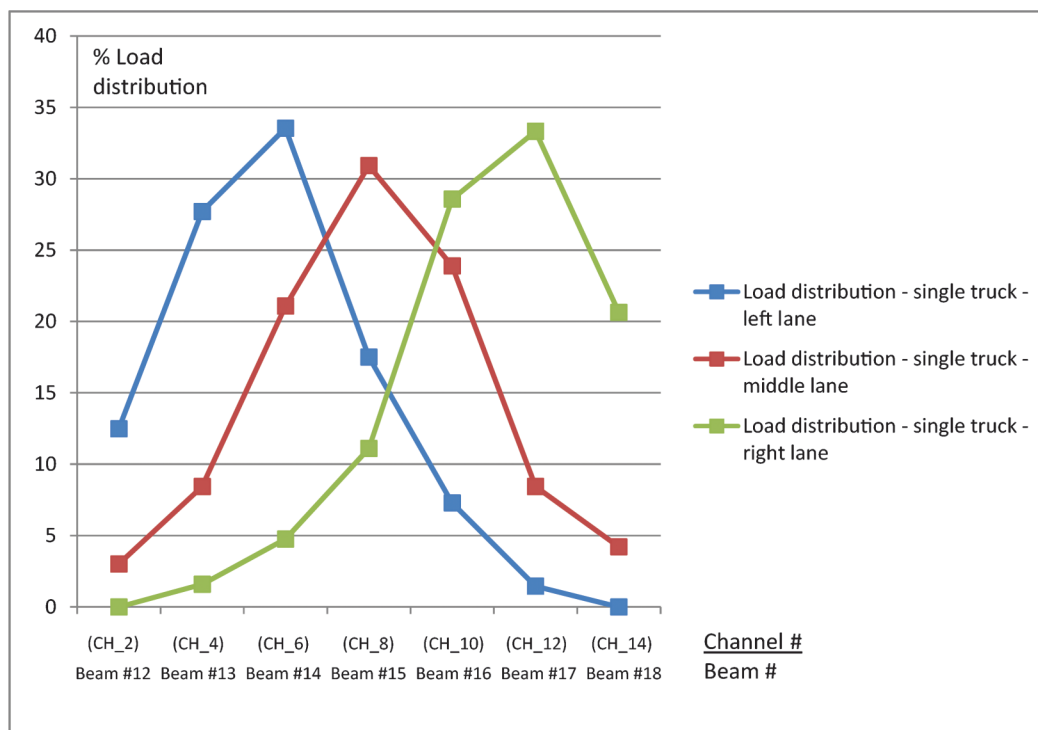


Figure 5.26 Load distribution between girders – single truck static tests.

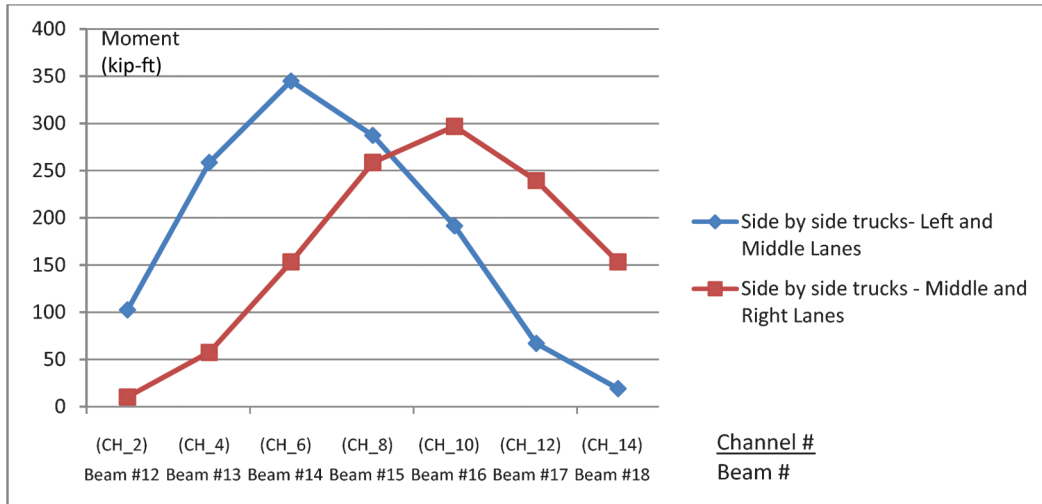


Figure 5.27 Moments determined from stresses recorded during side-by-side trucks static tests.

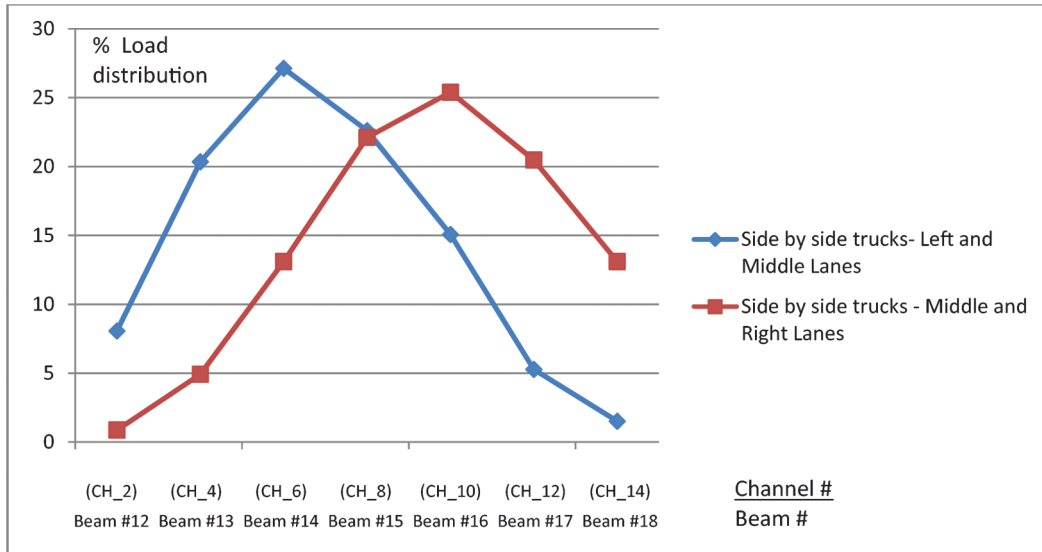


Figure 5.28 Load distribution between girders – trucks side-by-side static tests.

TABLE 5.16
Superposition of Loads Summary – Controlled Load Static Tests

Channel	Moments - single truck tests (kip-ft)			Moments determined from the superposition(kip-ft)		Moments - side-by-side trucks tests(kip-ft)		Difference (kip-ft)	
	PARK_1.DAT	PARK_2C.DAT	PARK_4.DAT	PARK_1.DAT & PARK_2C.DAT	PARK_2 C.DAT & PARK_4.DAT	PARK_3.DAT	PARK_5.DAT	Col. 4 & Col. 6	Col. 5 & Col. 7
	1	2	3	4	5	6	7	8	
CH_2	82.00	20.5	0.0	102.5	20.5	102.5	10.2	0	10.3
CH_4	182.0	57.5	9.6	239.5	67.1	258.6	57.5	19.1	9.6
CH_6	220.3	143.7	28.7	364.0	172.4	344.8	153.2	19.2	19.2
CH_8	114.9	210.7	67.0	325.7	277.7	287.3	258.6	38.4	19.1
CH_10	47.9	162.8	172.4	210.7	335.2	191.5	296.9	19.2	38.3
CH_12	9.6	57.5	201.1	67.1	258.6	67.0	239.4	0.1	19.2
CH_14	0.0	28.7	124.5	28.7	153.2	19.2	153.2	9.5	0

distance from the concrete parapet to test truck was 8.75 feet (see drawing #9 – Appendix A). During the side-by-side trucks test in the left and middle lanes (PARK_3.DAT), the distance from the concrete parapet to test truck in the left lane was only 7.00 feet (see drawing #11 – Appendix A). This can explain why the distribution is not exactly the same.

In conclusion, the steel superstructure of the bridge was not negatively affected by fire since composite action between deck and girders is present (see section 5.7) and there is excellent load distribution among the girders.

5.9 Response of Channels near Core Hole Locations

A total of four (4) strain gages were placed near locations where cores were cut for metallurgical investigation to monitor the stress levels during the long-term monitoring and controlled load testing. At these regions, the condition at the cored hole could be classified as an AASHTO Category D fatigue detail (CAFL = 7.0 ksi). Prior to cutting the cores the fatigue detail category at these locations was most likely Category B (CAFL = 16.0 ksi). Thus, the fatigue resistance at this location has been significantly reduced. However, this reduction in fatigue category may not be significant if the actual in-service live load stress ranges at these locations are low.

This section will be focused on the three (3) channels (CH_16, CH_17 and CH_18 - see Appendix A, Drawing #1 and Drawing# 4) that were installed near core holes on the eastbound bridge. Only one (1) strain gage (CH_15) was installed on the westbound bridge which will be covered in Chapter 6. Since there was no controlled load testing performed on the westbound bridge the response of this channel would not be valid. As-built instrumentation drawings that contain the specific location of all strain gages can be found in Appendix A. The response (maximum stress, minimum stress and stress range) of channels CH_16, CH_17 and CH_18 during the controlled load tests that were

discussed in sections 5.1 through 0 are summarized in Table 5.17.

The maximum stress range observed for these three (3) channels (CH_16, CH_17 and CH_18) during the controlled load tests was only 3.8 ksi (CH_18 in test CRL_3.DAT). This is well below Category D fatigue detail (CAFL = 7 ksi). Figure 5.29 shows the response of these three (3) channels as both test trucks passed side-by-side over the bridge in the left and middle lane in crawl test CRL_3.DAT. Further discussion on the fatigue resistance of these locations will follow in Chapter 6.

5.10 Controlled Load Testing – Summary

The response of the bridge during the controlled load tests was typical of a multi-span continuous composite steel bridge with good load distribution among the girders. The stress range recorded during the controlled load testing was well below the Category D fatigue detail (CAFL = 7 ksi) at the locations where coupons (cores) were retrieved for metallurgical investigation. Table 5.18 summarizes the stress ranges recorded in all the channels during the crawl tests.

6. LONG-TERM MONITORING

The long-term monitoring of the bridges was conducted from January 15, 2010 through May 04, 2010, for approximately 109 days. Long-term monitoring included all eighteen (18) strain gages originally installed. The monitoring consisted of collecting stress-range histograms and triggered time-history data. Table 6.1 shows a summary of the channels and monitoring period for each strain gage. The table also indicates whether triggered time history and/or stress-range histograms were developed.

Triggered time history data along with the stress-range histograms recorded during the monitoring phase gave an estimate of the magnitude of the stresses caused by the normal daily traffic. Stresses of higher magni-

TABLE 5.17
Response of CH_16, CH_17 and CH_18 during the Controlled Load Tests

Controlled Load Test	CH_16 (ksi)			CH_17 (ksi)			CH_18 (ksi)		
	σ_{max}	σ_{min}	$\Delta\sigma$	σ_{max}	σ_{min}	$\Delta\sigma$	σ_{max}	σ_{min}	$\Delta\sigma$
PARK_1.DAT	-0.4	-	-	-0.2	-	-	0.0	-	-
CRL_1.DAT	+0.2	-1.0	1.2	+0.1	-0.5	0.6	+0.2	-0.9	1.1
PARK_2C.DAT	-0.2	-	-	-0.3	-	-	-0.1	-	-
CRL_2.DAT	+0.2	-0.9	1.1	+0.5	-1.0	1.5	+1.3	-1.8	3.1
PARK_3.DAT	-0.6	-	-	-0.4	-	-	0.0	-	-
CRL_3.DAT	+0.3	-1.8	2.1	+0.4	-1.5	1.9	+1.2	-2.6	3.8
PARK_4.DAT	0.0	-	-	0.0	-	-	+0.2	-	-
CRL_4.DAT	0.0	-0.1	0.1	+0.1	-0.3	0.4	+0.2	-0.5	0.7
PARK_5.DAT	-0.2	-	-	-0.3	-	-	0.0	-	-
CRL_5.DAT	+0.2	-0.8	1.0	+0.6	-1.2	1.8	+1.5	-2.2	3.7

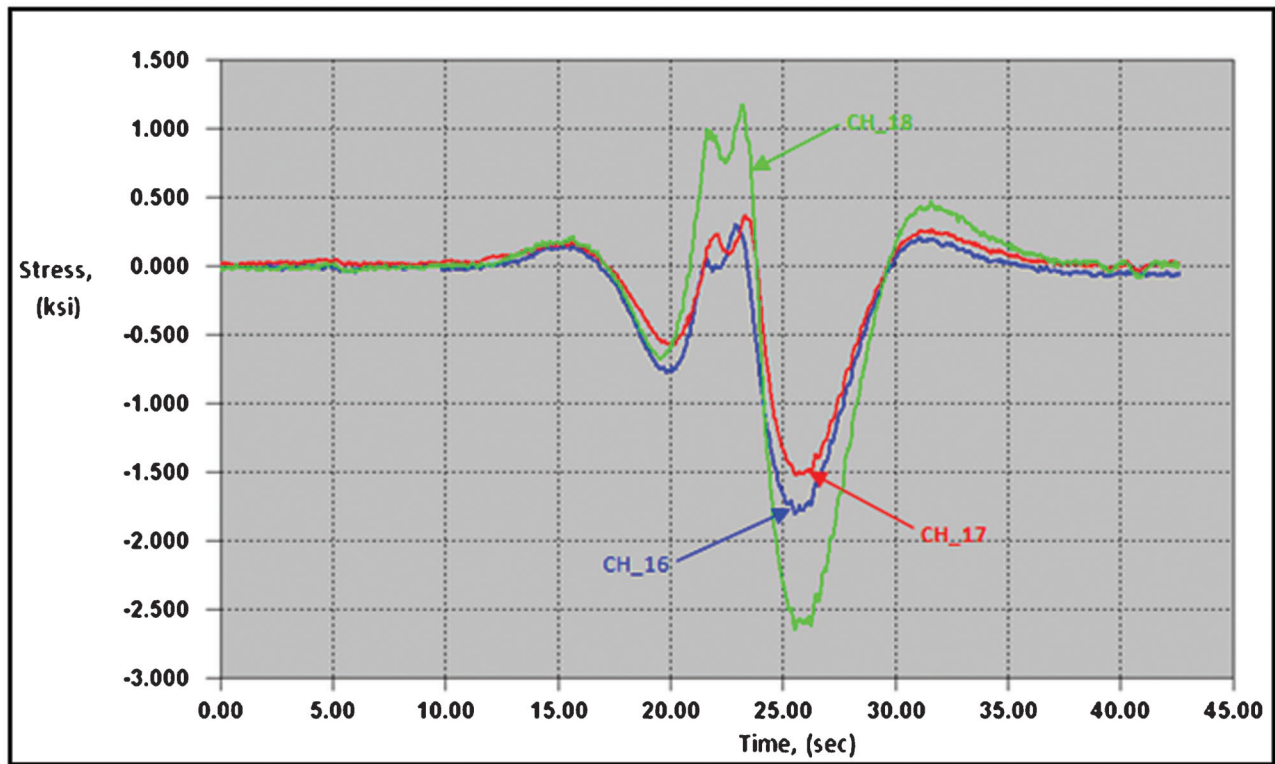


Figure 5.29 Response of CH_16, CH_17 and CH_18 - *Crawl test*: trucks side-by-side in left and middle lanes.

tude than those encountered during the controlled load testing (see section 5.10) were observed. This is not an uncommon observation since the normal daily traffic in that area includes many heavy trucks that cross the

bridges individually, side-by-side, or in tandem. These truck configurations are easily capable of producing larger stress cycles than those measured during the controlled load testing.

TABLE 5.18
Stresses in all Channels during the Single Truck and Side-by-Side Trucks Crawl Tests

Channel	Single truck in left lane (CRL_1.DAT)			Single truck in middle lane (CRL_2C.DAT)			Single truck in right lane (CRL_4.DAT)			Side-by-side trucks in left and middle lanes (CRL_3.DAT)			Side-by-side trucks in middle and right lanes (CRL_5.DAT)		
	σ_{mi} (ksi)	σ_{max} (ksi)	$\Delta\sigma$ (ksi)	σ_{min} (ksi)	σ_{max} (ksi)	$\Delta\sigma$ (ksi)	σ_{min} (ksi)	σ_{max} (ksi)	$\Delta\sigma$ (ksi)	σ_{min} (ksi)	σ_{max} (ksi)	$\Delta\sigma$ (ksi)	σ_{min} (ksi)	σ_{max} (ksi)	$\Delta\sigma$ (ksi)
CH_1	-0.1	+0.2	0.3	0.0	+0.1	0.1	0.0	0.0	0.0	-0.1	+0.2	0.3	0.0	+0.1	0.1
CH_2	-0.2	+1.0	1.2	-0.1	+0.2	0.3	0.0	0.0	0.0	-0.3	+1.0	1.3	-0.1	+0.2	0.3
CH_3	-0.1	+0.4	0.5	0.0	+0.1	0.1	0.0	0.0	0.0	0.0	+0.5	0.5	0.0	0.0	0.0
CH_4	-0.3	+2.2	2.5	-0.2	+0.8	1.0	0.0	0.0	0.0	-0.5	+2.6	3.1	-0.3	+0.6	0.9
CH_5	-0.1	+0.3	0.4	0.0	+0.1	0.1	0.0	0.0	0.0	-0.1	+0.4	0.5	0.0	+0.1	0.1
CH_6	-0.3	+2.0	2.3	-0.3	+1.9	2.2	-0.1	+0.2	0.3	-0.6	+3.6	4.2	-0.4	+1.6	2.0
CH_7	0.0	+0.1	0.1	0.0	+0.3	0.3	0.0	0.0	0.0	0.0	+0.3	0.3	0.0	+0.3	0.3
CH_8	-0.3	+0.9	1.2	-0.4	+2.4	2.8	-0.2	+0.6	0.8	-0.6	+3.0	3.6	-0.5	+2.8	3.3
CH_9	0.0	+0.1	0.1	0.0	+0.1	0.1	0.0	+0.1	0.1	0.0	+0.2	0.2	-0.1	+0.3	0.4
CH_10	-0.2	+0.4	0.6	-0.3	+1.5	1.8	-0.3	+1.4	1.7	-0.5	+2.1	2.6	-0.6	+3.2	3.8
CH_11	0.0	0.0	0.0	0.0	0.0	0.0	0.0	+0.2	0.2	0.0	0.0	0.0	0.0	+0.3	0.3
CH_12	0.0	+0.3	0.3	-0.2	+0.6	0.8	-0.3	+2.0	2.3	-0.2	+0.8	1.0	-0.5	+2.6	3.1
CH_13	0.0	+0.0	0.0	0.0	0.0	0.0	0.0	+0.1	0.1	0.0	0.0	0.0	0.0	+0.1	0.1
CH_14	-0.1	+0.2	0.3	-0.1	+0.2	0.3	-0.3	+1.5	1.8	-0.1	+0.3	0.4	-0.4	+1.6	2.0
CH_15	0.0	0.0	0.0	0.0	0.0	0.0	0.0	+0.1	0.1	0.0	0.0	0.0	0.0	0.0	0.0
CH_16	+0.2	-1.0	1.2	-0.9	0.2	1.1	0.0	0.0	0.0	-1.8	+0.3	2.1	-0.8	+0.2	1.0
CH_17	0.1	-0.5	0.6	-1.0	+0.5	1.5	-0.3	+0.1	0.4	-1.5	+0.4	1.9	-1.2	+0.6	1.8
CH_18	+0.1	-1.0	1.1	-1.8	1.3	3.1	-0.5	+0.1	0.6	-2.6	+1.2	4.2	-2.2	+1.5	3.7

TABLE 6.1
Summary of the Channels Included in the Long-Term Monitoring

Channel Number	Monitoring Period (Days)	COMMENTS
CH_1	108.51	Triggered Time History
CH_2	108.51	Triggered Time History / Stress-range histograms
CH_3	108.51	Triggered Time History
CH_4	108.51	Triggered Time History / Stress-range histograms
CH_5	108.51	Triggered Time History
CH_6	108.51	Triggered Time History / Stress-range histograms
CH_7	108.51	Triggered Time History
CH_8	108.51	Triggered Time History / Stress-range histograms
CH_9	108.51	Triggered Time History
CH_10	108.51	Triggered Time History / Stress-range histograms
CH_11	108.51	Triggered Time History
CH_12	108.51	Triggered Time History / Stress-range histograms
CH_13	108.51	Triggered Time History
CH_14	108.51	Triggered Time History / Stress-range histograms
CH_15	108.51	Triggered Time History / Stress-range histograms
CH_16	108.51	Triggered Time History / Stress-range histograms
CH_17	108.51	Triggered Time History / Stress-range histograms
CH_18	108.51	Triggered Time History / Stress-range histograms

6.1 Triggered Time-History Data

6.1.1 Background

The duration of the trigger event and all trigger stress levels were established by the Research Team based on a preliminary review of data collected over the first month of monitoring (December 17, 2009 through January 15, 2010). Recording of the data in all channels was triggered when a predefined stress value was measured in CH_4, CH_8 or CH_12. Data was then recorded for a defined period of time before and after the trigger event. These channels were placed on the bottom flanges of beams located under the left, middle and right lanes respectively. For every trigger event, three (3) seconds of data prior to the event and three (3) seconds of data after the event were recorded. This was done to ensure the entire loading event was captured. All the trigger channels (CH_4, CH_8 and CH_12) were located on the eastbound bridge. As-built instrumentation drawings that contain the specific location of all strain gages can be found in Appendix A. Table 6.2 explains the trigger channels and levels used for data collection.

TABLE 6.2
Trigger Channels and the Corresponding Trigger Stress Levels

Trigger Channel	Lane	Trigger Stress Level(ksi)
CH_4	Left	1.75
CH_8	Middle	2.5
CH_12	Right	2.5

6.1.2 Typical Trigger Event

A typical trigger event is shown in Figure 6.1. The figure presents measured stresses from strain gages located at midspan of the girders beneath the middle and right lanes of mainline I-465. During this event two (2) semi tractor trailers were crossing the eastbound bridge side-by-side in the middle and right lanes. Using the response from strain gages installed on the top flange of the girders (blue and green traces), the type (number of axles) and number of vehicle(s) can be identified. Another typical trigger event is shown in Figure 6.2. This figure presents measured stresses from strain gages located at midspan of a girder beneath the middle lane as a semi tractor trailer was crossing the eastbound bridge in the middle lane. Most of the triggered events recorded were single semi tractor trailers or single tandem-axle (or tri-axle) trucks that were crossing the bridge in the right or middle lane.

6.1.3 Maximum Trigger Events

MATLAB routines were created to search through the triggered data files and identify the maximum stress ranges for channels of interest. Table 6.3 summarizes these findings for the channels of interest located on the eastbound bridge. Figure 6.3 shows the maximum stress range event recorded by CH_2 on February 6, 2010. This event occurred while a tandem-axle truck crossed the bridge in the left lane. Plots of the maximum stress range events from triggered data for the remaining channels presented in Table 6.3 can be found in Appendix D.

6.2 Stress-Range Histograms

6.2.1 Stresses in Girder Bottom Flange Cover Plate at Midspan – Fatigue Life Determination

Seven (7) strain gages, CH_2 through CH_14 (even channels labels), were installed on the bottom flange cover plate of Beams #12 through #18 at the location of maximum moment (see Appendix A for as-built instrumentation plans). The detail category for these locations can be classified as Category B (CAFL = 16 ksi) per the AASHTO Specification.

Throughout the duration of monitoring no stress range cycles greater than the Category B CAFL (16 ksi)

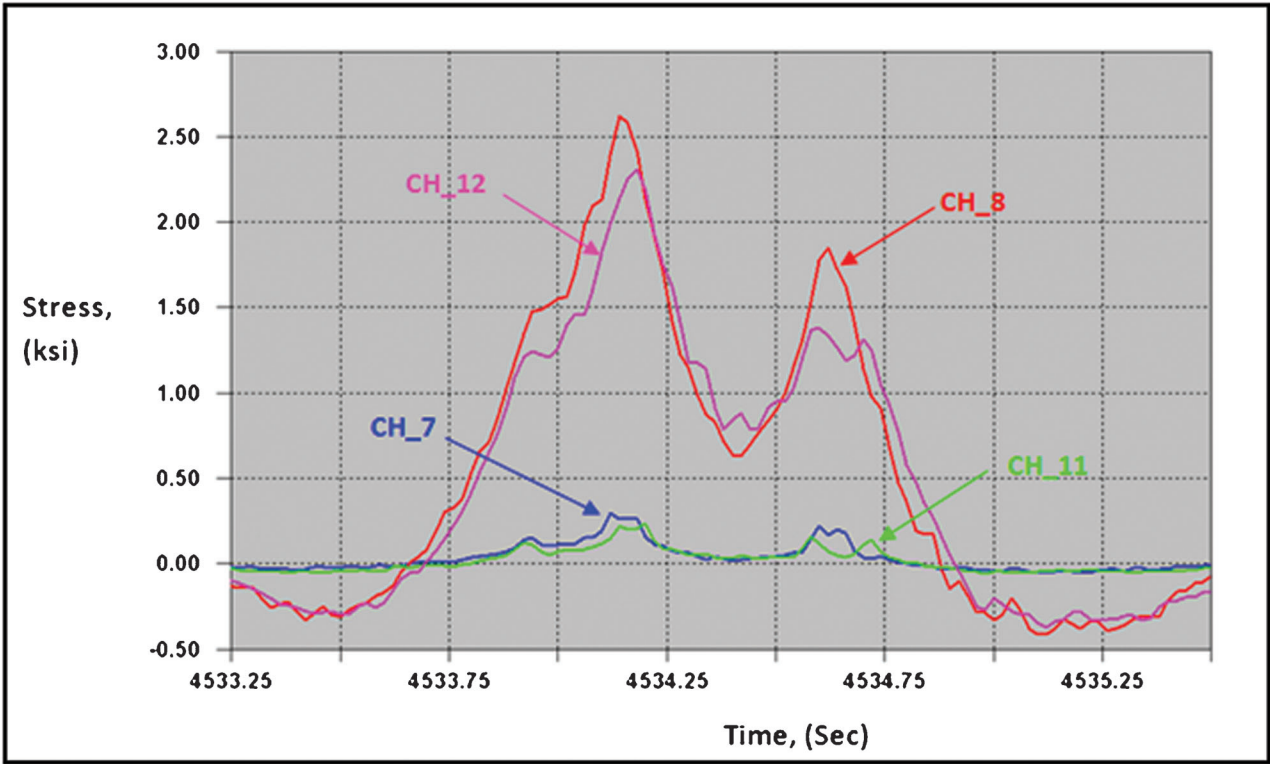


Figure 6.1 Typical trigger event: Two semi tractor trailers side-by-side in the middle and right lanes.

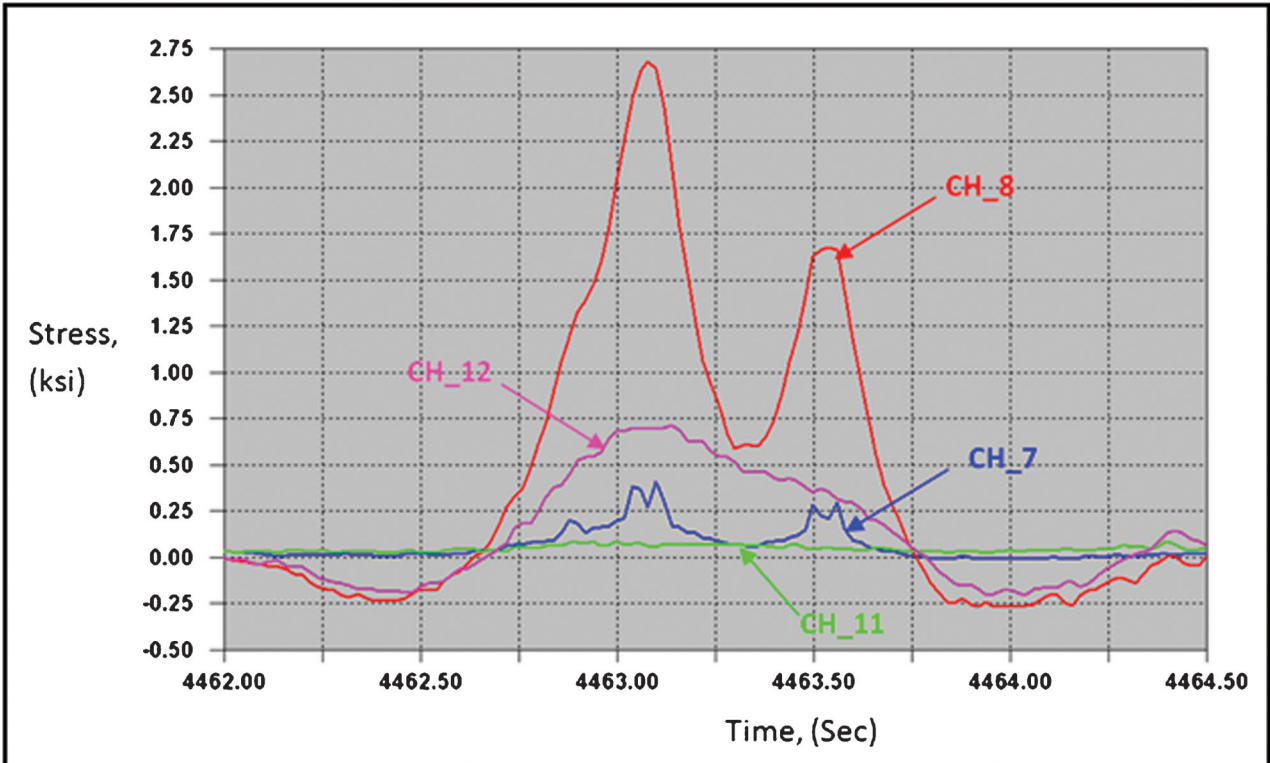


Figure 6.2 Typical trigger event: Semi tractor trailer in the middle lane.

TABLE 6.3
Maximum Stress Ranges Determined from Triggered Data Files

Channel	Truck(s) Type	Truck(s) Location	Stress range (ksi)	Date / Time
CH_2	Tandem-axle truck	Left Lane	1.7	02/06/2010 2:45 AM
CH_4	Two tractor-semi trailers	Left and Middle Lanes – side-by-side	2.9	01/22/2010 1:05 PM
CH_6	Tractor-semi trailer	Middle Lane	4.7	02/26/2010 12:46 AM
CH_8	Tractor-semi trailer	Middle Lane	6.1	02/26/2010 12:46 AM
CH_10	Tractor-semi trailer	Right Lane	5.2	04/02/2010 1:13 PM
CH_12	Tractor-semi trailer	Right Lane	5.5	04/05/2010 04:38 PM
CH_14	Tractor-semi trailer	Right Lane	4.8	04/05/2010 4:38 PM
CH_16	Tractor-semi trailer	Middle Lane	2.3	02/26/2010 12:46 AM
CH_17	Tractor-semi trailer	Middle Lane	3.7	03/08/2010 8:47 AM
CH_18	Tractor-semi trailer	Middle Lane	6.9	03/08/2010 8:47 AM

were measured at any of the instrumented locations. The maximum stress range measured was 6.8 ksi at CH_8, which was installed on Beam # 15. Table 6.4 shows the stress-range histogram for the channels installed on the bottom flange cover plate of the main girders at midspan. This data was collected over the period from January 15, 2010 to May 4, 2010.

A summary of the magnitude of the maximum stress range, effective stress range, number of cycles measured per day, and the estimated remaining fatigue life for the details is presented in Table 6.5. As can be seen from the table, the fatigue life calculations indicate an infinite remaining life for all seven (7) instrumented bottom flange cover plate locations. Calculations on how the

remaining fatigue life was determined in Table 6.5 can be found in Appendix B.

6.2.2 Stresses Near Core Holes Locations – Fatigue Life Determination

Four (4) strain gages, CH_15 through CH_18, were installed near core holes locations to monitor the stresses. Most of the strain gages were installed on the eastbound bridge on Beams #14 and #15. Only one channel (CH_15) was placed on the westbound bridge on the exterior girder (Beam #11). As built instrumentation plans can be found in Appendix A. The detail category for these

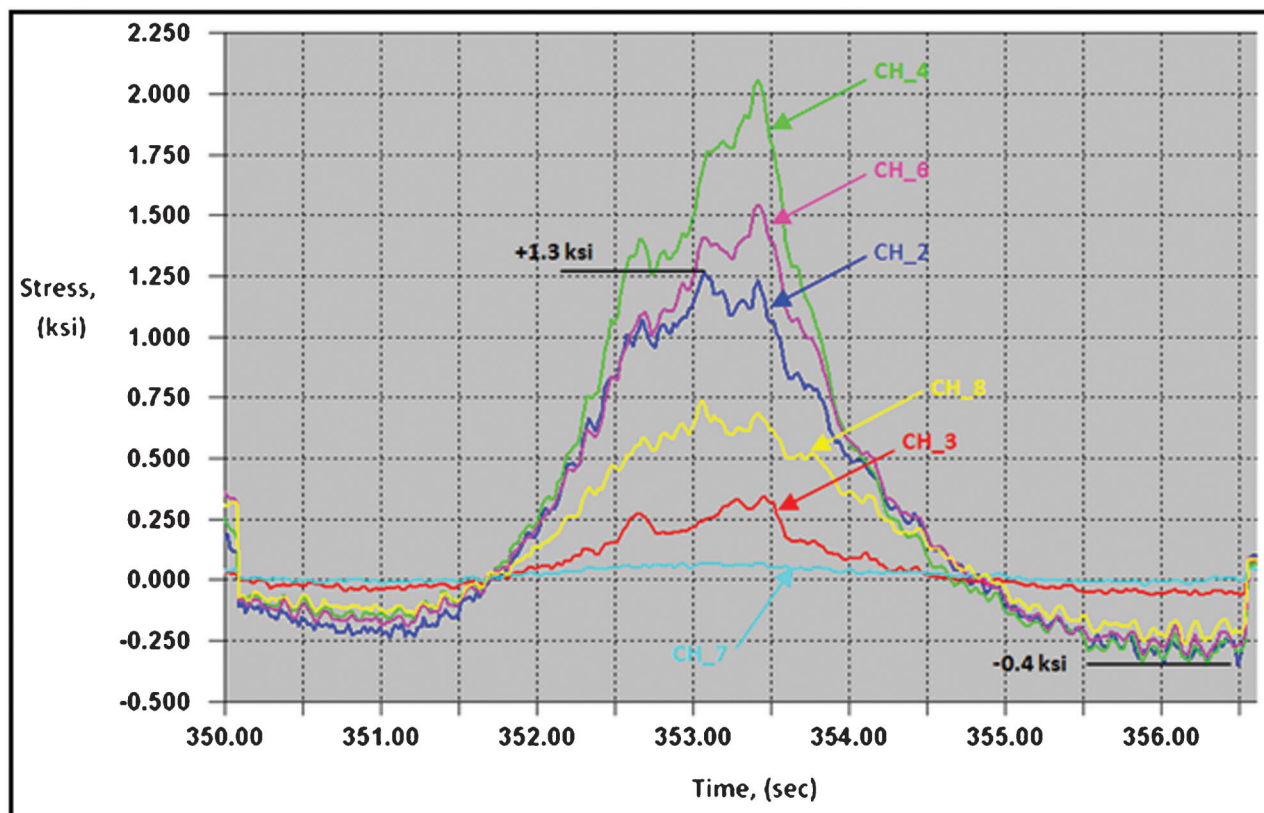


Figure 6.3 Maximum stress range recorded in CH_2 from triggered data.

TABLE 6.4
Stress-Range Histograms for CH_2, CH_4, CH_6, CH_8, CH_10, CH_12 and CH_14 from 01/15/2010 to 05/04/2010

Stress Range Bin Size (ksi)			Number of Cycles /Channel/ Bin Size 01/15/2010 – 05/04/2010						
S _{rmin}	S _{rmax}	S _{ravg}	CH_2	CH_4	CH_6	CH_8	CH_10	CH_12	CH_14
0.25	0.5	0.375	67945	497436	895209	1138643	1248915	1228375	564581
0.5	1.0	0.75	2202	116046	154368	282005	328669	287110	168743
1.0	1.5	1.25	74	2176	80398	114720	132045	115770	75194
1.5	2.0	1.75	2	569	24047	41937	111411	46458	27578
2.0	2.5	2.25	1	235	1378	48356	28326	45343	1578
2.5	3.0	2.75	1	18	466	13333	3462	6560	811
3.0	3.5	3.25	0	3	73	884	1402	808	115
3.5	4.0	3.75	0	0	21	303	269	792	15
4.0	4.5	4.25	0	0	1	117	59	186	3
4.5	5.0	4.75	0	0	1	16	17	30	1
5.0	5.5	5.25	0	0	2	15	4	8	0
5.5	6.0	5.75	0	0	0	10	0	1	0
6.0	6.5	6.25	0	0	0	1	0	0	0
6.5	7.0	6.75	0	0	0	1	0	0	0
7.0	7.5	7.25	0	0	0	0	0	0	0

locations can be classified as Category D (CAFL = 7 ksi) per the AASHTO Specification. No stress range cycles greater than the Category D CAFL (7 ksi) for this detail were measured at any of the four instrumented locations. The maximum stress range measured was 6.8 ksi by CH_18, which was installed

on Beam #15. Table 6.6 shows the stress-range histogram for the channels mentioned above. This data was collected over the period from January 15, 2010 to May 4, 2010.

A summary of the maximum stress range, effective stress range, number of cycles measured per day, and

TABLE 6.5
Summary of Fatigue Life Calculations for CH_2, CH_4, CH_6, CH_8, CH_10, CH_12 and CH_14

Channel	S _{rmax} (ksi)	Cycles > CAFL		S _{reff} ¹ (ksi)	Cycles / Day ²	Monitoring Period (Days)	Remaining Life (Years) ³	Detail Category	Location 2 nd Span (Midspan)
		#	%						
		CH_2	2.75						
CH_4	3.25	0	0	0.79	1097	108.51	Infinite	B	Bottom Flange CP Beam #13 EB Bridge
CH_6	5.25	0	0	1.13	980	108.51	Infinite	B	Bottom Flange CP Beam #14 EB Bridge
CH_8	6.75	0	0	1.42	2025	108.51	Infinite	B	Bottom Flange CP Beam #15 EB Bridge
CH_10	5.25	0	0	1.33	2553	108.51	Infinite	B	Bottom Flange CP Beam #16 EB Bridge
CH_12	5.75	0	0	1.36	1990	108.51	Infinite	B	Bottom Flange CP Beam #17 EB Bridge
CH_14	4.75	0	0	1.14	2525	108.51	Infinite	B	Bottom Flange CP Beam #18 EB Bridge

NOTES:

1. The effective stress range calculations ignore cycles less than 0.5 ksi.
2. The number of cycles per day were estimated for vehicles over 20 kips, using the stresses recorded during the controlled load tests (see Table 5.12) and number of cycles/bin size (see Table 6.4).
3. The remaining fatigue life calculations are from 2010 forward and assume current traffic represents past traffic.

TABLE 6.6
Stress-Range Histograms for CH_15, CH_16, CH_17 and CH_18

Stress Range Bin Size (ksi)			Number of Cycles/Channel/Bin Size			
S _{rmin}	S _{rmax}	S _{ravg}	CH_15	CH_16	CH_17	CH_18
0.25	0.5	0.375	2591	182296	422341	1545558
0.5	1.0	0.75	266	141812	200135	398837
1.0	1.5	1.25	15	10208	82970	82523
1.5	2.0	1.75	9	454	35996	85742
2.0	2.5	2.25	8	17	796	42954
2.5	3.0	2.75	4	1	168	39753
3.0	3.5	3.25	2	1	16	20533
3.5	4.0	3.75	0	0	1	1691
4.0	4.5	4.25	0	0	0	299
4.5	5.0	4.75	0	0	0	233
5.0	5.5	5.25	0	0	0	117
5.5	6.0	5.75	0	0	0	32
6.0	6.5	6.25	0	0	0	14
6.5	7.0	6.75	0	0	0	6
7.0	7.5	7.25	0	0	0	0

the estimated remaining fatigue life for the details is presented in Table 6.7. As can be seen from the table, the fatigue life calculations indicate an infinite remaining life for all four (4) details. Calculations on how the remaining fatigue life was determined in Table 6.7 can be found in Appendix B.

7. SUMMARY AND CONCLUSION

The following section provides a summary of the project and the results of the controlled load testing and

long-term monitoring conducted on the I-465 Bridges in Indianapolis, Indiana.

Laboratory Testing

1. Immediately after the accident, samples of the structural steel (from the web and cover plate of the girders) and HS bolts were removed from both bridges and sent to independent testing laboratories. A set of samples taken from an area protected by the embankment on the westbound bridge were used as control data set.

TABLE 6.7
Summary of Fatigue Life Calculations for CH_15, CH_16, CH_17 and CH_18

Fatigue Life Calculation Summary									
Channel	S _{rmax} (ksi)	Cycles > CAFL		S _{reff} (ksi)	Cycles / Day	Monitoring Period (Days)	Remaining Life (Years) ³	Detail Category	Location 2 nd Span
		#	%						
CH_15	2.75	0	0	1.12	27	108.51	Infinite	D	Bottom Flange CP Beam #11 6'-3" E of Bent #2 WB Bridge
CH_16	3.25	0	0	0.81	1405	108.51	Infinite	D	Bottom Flange CP Beam #14 5'-10" W of Bent #3 EB Bridge
CH_17	5.25	0	0	1.12	2950	108.51	Infinite	D	Bottom Flange CP Beam #15 6'-3" W of Bent #3 EB Bridge
CH_18	6.75	0	0	1.61	1764	108.51	Infinite	D	Bottom Flange CP Beam #15 7'-9" W of Bent #3 EB Bridge

NOTES:

1. The effective stress range calculations ignore cycles less than 0.5 ksi.
2. The number of cycles per day were estimated for vehicles over 20 kips, using the stresses recorded during the controlled load tests (see Table 5.17) and number of cycles/bin size (see Table 6.6).
3. The remaining fatigue life calculations are from 2010 forward and assume current traffic represents past traffic.

2. Based on the hardness test results it is the opinion of the Purdue Research Team that the fire did not have any effect on the ultimate strength (F_u) of the structural steel in the bridges.
3. Charpy V-notch impact tests were performed on CVN specimens obtained from the web and cover plate cores samples. The notch, for the web CVN specimens, was oriented transverse to the longitudinal axis of the girder. For the cover plate CVN specimens, the notch was oriented parallel to the longitudinal axis (provides a conservative lower bound of the longitudinal mechanical properties). Based on the measured data and the orientation of the CVN specimens, it is the opinion of the Purdue Research Team that the CVN impact energy data are adequate for these bridges.
4. A total of eight (8) bolts and eight (8) nuts were removed from various web and flange splices for hardness, proof load and wedge tension testing. Considering there was no physical damage/evidence of fire on the bolts (i.e. no heat or damaged paint) and based on the test results, it is the opinion of Purdue Research Team that there was no measurable fire damage to the bolts. Additionally the hardness test results of the nuts, also suggest the fire did not have negative effect on the integrity of these nuts.

Instrumentation Plan

1. Instrumentation consisted of eighteen (18) uniaxial resistance-type strain gages installed on the two bridges: seventeen (17) strain gages were installed on the east-bound structure and

2. The primary intent of the monitoring was to capture live load stress ranges in predetermined areas of interest: location of maximum moment as well as the locations where core samples were removed for metallurgical testing.

Controlled Load Testing

1. The results of the controlled load tests showed good load distribution between the girders. The maximum response in the instrumented girders was observed when the test truck was directly located over the instrumented detail, as expected.
2. The response of the bridge was typical of a multi-span continuous composite steel bridge. The concrete deck and girders behave compositely, as designed.

Long-Term Monitoring

1. The maximum stress range cycles observed during the remote long-term monitoring program were all below the CAFL of instrumented details.
2. Infinite fatigue life was estimated for all the instrumented details

REFERENCES

1. AASHTO. *Standard Specifications for Highway Bridges*, ed. 9. American Association of State Highway Officials, Washington, D.C., 1965.
2. AASHTO. *AASHTO LRFD Bridge Design Specifications*, ed. 5. American Association of State Highway and Transportation Officials, Washington, D.C., 2010.

APPENDIX A. INSTRUMENTATION PLANS

<http://docs.lib.purdue.edu/cgi/viewcontent.cgi?filename=0&article=3022&context=jtrp&type=additional>

APPENDIX B. DEVELOPMENT OF STRESS-RANGE HISTOGRAMS USED TO CALCULATE FATIGUE DAMAGE

<http://docs.lib.purdue.edu/cgi/viewcontent.cgi?filename=1&article=3022&context=jtrp&type=additional>

APPENDIX C. REPORT LETTERS

<http://docs.lib.purdue.edu/cgi/viewcontent.cgi?filename=2&article=3022&context=jtrp&type=additional>

APPENDIX D. MAXIMUM STRESS RANGES FIGURES – TRIGGERED DATA FILES

<http://docs.lib.purdue.edu/cgi/viewcontent.cgi?filename=3&article=3022&context=jtrp&type=additional>